molecular pharmaceutics

pubs.acs.org/molecularpharmaceutics

Article

Acid-Sensitive Surfactants Enhance the Delivery of Nucleic Acids

Joachim Justad Røise, Hesong Han, Jie Li, D. Lucas Kerr, Chung Taing, Kamyar Behrouzi, Maomao He, Emily Ruan, Lienna Y. Chan, Eli M. Espinoza, Sören Reinhard, Kanav Thakker, Justin Kwon, Mohammad R. K. Mofrad, and Niren Murthy*

Cite This: *Mol. Pharmaceutics* 2022, 19, 67−79

Read Online

ACCESS | Metrics & More | Article Recommendations | Supporting Information

ABSTRACT: The development of endosomal disruptive agents is a major challenge in the field of drug delivery and pharmaceutical chemistry. Current endosomal disruptive agents are composed of polymers, peptides, and nanoparticles and have had limited clinical impact. Alternatives to traditional endosomal disruptive agents are therefore greatly needed. In this report, we introduce a new class of low molecular weight endosomal disruptive agents, termed caged surfactants, that selectively disrupt endosomes via reversible PEGylation under acidic endosomal conditions. The caged surfactants have the potential to address several of the limitations hindering the development of current endosomal disruptive agents, such as high toxicity and low excretion, and are amenable to traditional medicinal chemistry approaches for optimization. In this report, we synthesized three generations of caged surfactants and demonstrated that they can enhance the ability of cationic lipids to deliver mRNA into primary cells. We also show that caged surfactants can deliver siRNA into cells when modified with the RNA-binding dye thiazole orange. We anticipate that the caged surfactants will have numerous applications in pharmaceutical chemistry and drug delivery given their versatility.

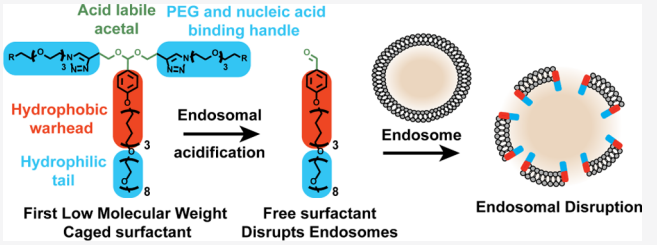

KEYWORDS: *drug delivery, endosomal disruption, nucleic acids, surfactants, transfection*

INTRODUCTION

The lysosomal degradation of endocytosed nucleic acid therapeutics is a central problem in drug delivery and limits the development of a wide range of experimental therapeutics.[1,2] For example, the percentage of endocytosed nucleic acid/cationic lipid complexes that reach the cytoplasm is only between 1 and 5%,[3,4] and is similarly low for a variety of other delivery vehicles. There is consequently an urgent need to develop strategies for enhancing the endosomal release of nucleic acid therapeutics. The endosomal membrane is a lipid bilayer, similar to the plasma membrane, and strategies to enhance endosomal release require the development of compounds that can selectively disrupt the endosomal lipid bilayer, while maintaining the integrity of the plasma membrane lipid bilayer. The pH of the endosome is between 5 and 6, which is lower than the pH of the extracellular fluid.[5] This difference has been widely exploited to develop agents that can selectively disrupt endosomes, termed endosomal disruptive agents.[6,7]

Three classes of pH-sensitive triggers have been developed to engineer pH-sensitive membrane disruption, based upon (i) the protonation of a carboxyl group, (ii) the hydrolysis of an acid degradable linkage, and (iii) the protonation of ionizable lipids. The two former strategies both function by increasing the hydrophobicity of the endosomal disruptive agent under acidic conditions, enabling membrane insertion at pH 5.0 but not at pH 7.4, while ionizable lipids destabilize the endosomal membrane through a change in the lipid structure upon protonation and subsequent fusion with the endosomal membrane.[4] Lipid nanoparticles (LNPs) that contain ionizable lipids have seen great clinical success, most recently in the development of vaccines against the SARS-CoV-2 virus,[4,8] and have demonstrated the tremendous benefits of efficient endosomal disruption.

The earliest endosomal disruptive agents were based upon the protonation of carboxylic acid groups. Carboxylic acids are found in a variety of peptides, proteins, and polymers and undergo a significant change in hydrophobicity upon protonation, and hence, they are ideal for designing endosomal disruptive agents and have found numerous applications.[6,7,9] For example, glutamic acid-containing peptides, such as the GALA peptide,[10] are protonated in the acidic endosome, causing an increase in hydrophobicity followed by insertion and disruption of the endosomal membrane. These endosomal disruptive peptides were capable of enhancing DNA, mRNA,

Received: July 19, 2021
Revised: November 12, 2021
Accepted: November 19, 2021
Published: December 21, 2021

https://doi.org/10.1021/acs.molpharmaceut.1c00579
Mol. Pharmaceutics 2022, 19, 67−79

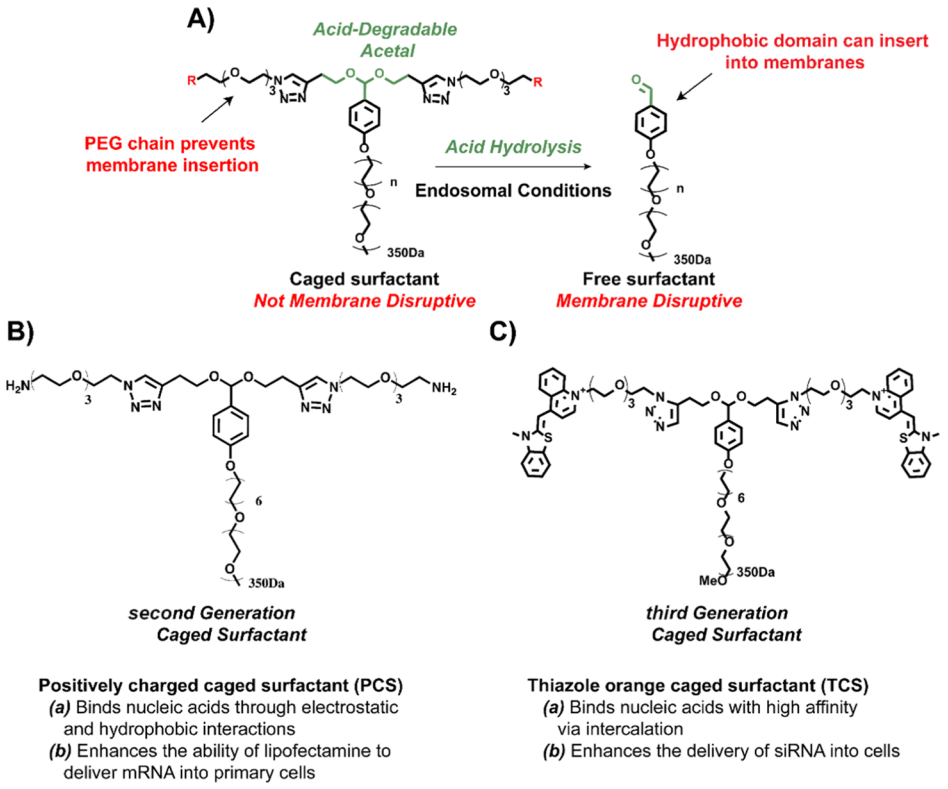

Figure 1. Caged surfactants: low molecular weight endosomal disruptive agents that can enhance the delivery of mRNA and siRNA. (A) Caged surfactants composed of a surfactant that has been reversibly masked with PEG chains. The caged surfactants are not membrane-disruptive at pH 7.4. However, after endocytosis, the acidic pH of the endosome hydrolyzes their acetal linkage, unmasking their hydrophobic domains which can then disrupt endosomes. The caged surfactants are efficient pH-sensitive membrane disruptive agents, despite their low molecular weight. In this report, we synthesized second generation and third generation caged surfactants, which were able to enhance the delivery of mRNA and siRNA into cells. (B) Second generation caged surfactants: a PCS that complexes nucleic acids via electrostatic and hydrophobic forces was synthesized. The PCS was able to enhance the ability of lipofectamine to transfect mRNA into hard-to-transfect primary cell cultures. (C) Third generation caged surfactants: a caged surfactant that contains the RNA binding dye thiazole orange (TO) (TCS) was synthesized. TCS was able to enhance the delivery of siRNA into cells.

and siRNA delivery into cells[11−13] and demonstrated that endosomal disruptive agents could have a significant impact on nucleic acid delivery. Endosomal disruptive agents based upon synthetic polymers, such as poly(propyl acrylic acid), have also been developed,[14] which undergo large changes in hydrophobicity in acidic environments and are capable of significantly enhancing the delivery of nucleic acids to cells and *in vivo*.

While endosomal disruptive agents based upon the carboxyl trigger have had some initial successes in cell culture and even animal models, this class of endosomal disruptive agents has had some downsides such as having low uptake efficiencies.[15] An alternative strategy achieves pH-sensitive membrane disruption based upon reversible PEGylation, where PEG is conjugated to a hydrophobic membrane disruptive polymer through an acid labile linkage.[16,17] The PEG chains prevent the hydrophobic backbone from partitioning into the lipid bilayer; however, after endocytosis, the linkage between the PEG and polymer hydrolyzes and the polymer can then insert into the membrane and disrupt it. This strategy has tremendous versatility because PEG can be conjugated to a variety of endosomal disruptive agents, such as cationic polymers, liposomes, and nanoparticles.[16−19] In addition, because the size of the PEG can be easily varied, this strategy allows for the robust chemical optimization of endosomal disruptive agents.

Despite the wide investigation on endosomal disruptive agents, state-of-the-art approaches for nucleic acid delivery, such as LNPs, still only achieve a 1−5% cytosolic delivery of endocytosed cargo.[3,4] In addition, polymer-based approaches such as polyethyleneimine and poly-lysine also cause significant toxicity due to their concentrated cationic charges.[20] These downfalls have contributed to the delayed incorporation of endosomal disruptive agents in clinical therapy. An alternative to the common LNP and polymer-based approaches is found in small molecule endosomal disruptors. We hypothesized that small molecules have the potential to address several drawbacks of polymer-based delivery strategies. In particular, smaller molecules are well defined, can easily be characterized by NMR, and are excretable without the need for incorporating biodegradable linkers.

However, despite their potential, the development of low molecular weight endosomal disruptive agents has been challenging. At present, the only strategy available for disrupting endosomes with low molecular weight molecules is via the proton sponge effect, based on molecules such as chloroquine, which selectively partitions into endosomes. However, chloroquine requires high concentrations and incubation times of 10−12 h to efficiently promote nucleic acid delivery, which in addition to its toxicity severely limits its use as an endosomal disruptive agent.[21,22] Developing endosomal disruptive agents based upon the proton sponge

https://doi.org/10.1021/acs.molpharmaceut.1c00579
Mol. Pharmaceutics 2022, 19, 67−79

effect will be challenging, given the high concentrations needed, and consequently, additional strategies for disrupting endosomes with low molecular weight molecules are necessary.

Surfactants have great potential as platforms for developing endosomal disruptive agents due to their low molecular weight, synthetic accessibility, high membrane disruptive efficiency, and low immunogenicity. For example, surfactants such as Triton X have a generic structure of PEG-hydrocarbon chain and have a membrane-disruptive efficiency comparable to ED peptides,[23] lack antigenicity, are small enough to be excreted from the kidneys, and have been used extensively as excipients in a wide variety of medical products. However, Triton X lacks pH-sensitive membrane disruptive properties, leading to high toxicity, and consequently cannot be used directly as an endosomal disruptor.

In this report, we demonstrate that Triton X-like surfactants can be converted into pH-sensitive membrane disruptive agents via reversible PEGylation. This new class of endosomal disruptors are termed caged surfactants and are the first example of low molecular weight pH-sensitive membrane disruptive agents. They have a base structure of $(PEG)_2$-acetal-hydrocarbon-PEG, as shown in Figure 1A. The hydrocarbon-PEG fragment of the caged surfactants is modeled after common membrane disruptive surfactants such as Triton X and Nonoxynol-9, which disrupt cells through membrane insertion and destabilization. However, the caged surfactants are not membrane-disruptive in their intact form because their $(PEG)_2$ chains prevent their hydrophobic domains from inserting into the membrane. In contrast, after endosomal uptake, the acidic pH in the endosome hydrolyzes the acetal linkage connecting the caging PEG to the hydrocarbon-PEG domain, and this allows the hydrophobic domain of the caged surfactant to penetrate the membrane and trigger endosomal disruption.

In order to optimize their efficacy, we performed a structure−activity analysis of the caged surfactants and identified that a C12 chain was the optimal hydrophobic length for efficient membrane disruption. The C12 caged surfactant was able to disrupt red blood cell (RBC) membranes at a concentration of 24 μM at pH 5.5, with no disruption at pH 7.4. This is similar to the working concentrations of the GALA peptide[7,12] and ionizable lipids such as DLin-MC3-DMA,[24] which are both in the 5−10 μM range. For the caged surfactants to be able to deliver nucleic acids, they must have some affinity to bind DNA and RNA. We therefore synthesized second and third generation caged surfactants, which had either amine moieties or RNA-binding dyes conjugated to the distal ends of their PEG chains (Figure 1B,C). The second generation caged surfactants bind nucleic acids via a combination of electrostatic and hydrophobic forces[25−27] and are able to significantly improve the ability of lipofectamine to deliver mRNA into HUVECs, a primary cell culture that is challenging to transfect.

A limitation of the second generation caged surfactants is that they bind nucleic acids with relatively weak affinity, and we therefore further optimized them by replacing their amines with RNA binding dyes, which bind nucleic acids with much higher affinity than positive charges. The third generation caged surfactants (termed TCS) bound nucleic acids with a $K_b = 9 \times 10^7\ M^{-1}$. We investigated if the TCS could enhance the delivery of siRNA. TCS bound siRNA and formed 55 nm sized complexes with siRNA; in addition, TCS was able to significantly enhance their delivery into cells. Collectively, these results suggest that reversible PEGylation has great potential for the design and synthesis of new low molecular weight endosomal disruptive agents and demonstrate that the caged surfactants can be easily engineered for diverse biomedical applications.

EXPERIMENTAL METHODS

Reagents and Methods. All compounds were purchased from Sigma-Aldrich (St. Louis, MO, USA), Fisher Scientific (Hampton, NH, USA), or VWR (Radnor, PA, USA). THF was purchased from Fisher Scientific (Hampton, NH, USA) and distilled from solid sodium and benzophenone before using in acetal formation reactions. siSTABLE Luc-knockdown siRNA (sense strand; GAU UAU GUC CGG UUA UGU AUU) was purchased from Horizon Discovery Biosciences Limited (Cambridge, UK). Compound purity was assessed by ^{1}H NMR spectroscopy. HPLC was not utilized due to the instability of acetal-containing compounds in standard 0.1% TFA HPLC mobile phases. NMR spectra were collected on either a Bruker AVANCE 400 console with Oxford Instruments 9.4 T magnet, a Bruker AVANCE 500 console with Bruker 11.7 T magnet, or a Bruker AVANCE III 600 console with Bruker 14 T magnet instrument at the College of Chemistry NMR Facility at UC Berkeley. Additionally, low-mass ^{13}C NMR spectra were collected on a Bruker 900 MHz NMR spectrometer. Aldehydes and acetals were visualized on thin-layer chromatography (TLC) plates with a 2,4-dinitrophenylhydrazine solution. Mass spectra were collected at the QB3/Chemistry Mass Spectrometry Facility at UC Berkeley. Absorbance was measured on a Tecan infinite M200 plate reader (Männedorf, Switzerland). Fluorescent microscopy images were taken on an Invitrogen Evos M5000 instrument (Carlsbad, CA, USA). UV vis spectra were collected on a Shimadzu UV-2600 spectrophotometer with a Shimadzu TCC-100 temperature-controlled cell holder. Flow cytometry was collected on an Invitrogen Attune NxT flow cytometer. Gels were imaged using a Bio-Rad ChemiDoc MP Imaging System using 1:1000 SYBR Safe (Thermo Fischer Scientific) as the intercalating imaging agent. Dynamic light scattering (DLS) measurements were done on a Zetasizer Nano ZS with backscatter detection (Malvern Instruments). CleanCap eGFP mRNA was purchased from Trilink Biotechnologies (San Diego, CA).

Hemolysis. *Preparation of 2% RBC Solution.* Defibrinated RBCs (Hemostat Laboratories, Dixon CA, USA) were diluted in PBS at the desired pH (1:10), and the suspension was centrifuged at 4 °C (750*g*, 10 min), followed by the removal of the supernatant. This was repeated three additional times, diluting with PBS (1:50) each time. After the last centrifugation, 200 μL of the collected RBCs were diluted with 9.8 mL of PBS at the desired pH to create a 2% RBC solution.

Hemolysis Assay. Caged surfactants were dissolved in PBS at the desired pH at various concentrations, and 100 μL was added to 200 μL centrifuge tubes, which were capped and allowed to stand for 1 h at room temperature for hydrolysis to occur. Then, to each tube was added 50 μL of the prepared 2% RBC solution, and the tubes were incubated for 30 min at 37 °C, followed by centrifugation at 2,000*g* for 10 min. A spectrophotometer was used to measure the hemoglobin content of the supernatant at 546 nm. All hemolysis experiments were performed in triplicate.

https://doi.org/10.1021/acs.molpharmaceut.1c00579
Mol. Pharmaceutics 2022, 19, 67−79

Preparation of Positive Control. Positive control (100% hemolysis) was prepared by adding 50 μL of the prepared RBC solution to 100 μL of DI H_2O. The solution was then frozen and thawed three times, leading to complete disruption of the blood cells.

Hydrolysis Kinetics. *Preparation of Buffer.* Buffers were prepared by making an aqueous solution of 0.1 M citric acid and 0.2 M Na_2HPO_4, followed by adjusting the pH with 0.1 M HCl to give citrate buffers at a pH range of 3.5−7.4.

Measurement of Hydrolysis Kinetics. The caged surfactants were dissolved in PBS (pH 7.4) to make a stock solution of 1 mg/mL. The stock solution was diluted in the appropriate citrate buffer to a final concentration of 50 μg/mL and immediately placed in a UV spectrometer. The hydrolysis of the acetal gives rise to a peak at 286 nm, corresponding to the formation of the benzaldehyde. Absorbance was therefore measured at 286 nm to monitor the acid-dependent hydrolysis kinetics of the acetal in the caged surfactants. The rate constant for acetal hydrolysis shows second-order kinetics and is first order in acetal concentration and first order in hydronium ion concentration.[45] The hydronium ion concentration was kept constant in our hydrolysis experiments, and the hydrolysis rate remained constant at constant pH, giving a pseudo-first-order rate constant k_{obs}, which is related to the second-order rate constant by $k_{obs} = k_{2nd} \times [H_3O^+]$. The k_{2nd} for each caged surfactant was determined by plotting k_{obs} over $[H_3O^+]$ and determining the slope, which gave k_{2nd}. The hydrolysis kinetics of **CS12** and **CS16** were measured at pH 3.5, 4.0, and 4.5.

HUVEC mRNA Transfection Assays with PCS. HUVEC cells were transfected by first adding **PCS** (2 μg/mL) to CleanCap eGFP mRNA (0.5 μg/mL) (Trilink Biotechnologies, San Diego, CA), followed by incubation for 30 min at room temperature. Then, lipofectamine 2000 was added at different amounts followed by an additional 30 min incubation. The resulting mixture was then added to HUVEC cells in a 96-well plate in OptiMEM media. The cells were incubated for 24 h before eGFP expression was measured by flow cytometry. The transfection was expressed as the percentage of positive cells/total cells. This also takes into consideration the toxicity that is caused by lipofectamine and is a better measurement of the total efficiency of the system.

Toxicity of mRNA/Lipo/PCS was measured on HUVEC cells by keeping the PCS concentration constant at 2 μg/mL, while varying the lipofectamine 2000 concentration. Toxicity was then determined as the number of dead cells as seen by flow cytometry. The protocol is the same as for transfection. Briefly, eGFP-expressing mRNA (0.5 μg/mL) was mixed with PCS (2 μg/mL) and incubated for 30 min, followed by the addition of lipofectamine. After an additional 30 min incubation, the complexes were added to HUVEC cells in a 96-well plate (100 μL/well) in OptiMEM media. After a 24 h incubation, flow cytometry was performed to determine cell toxicity.

siRNA Binding Constants. To 100 μL of siRNA (1 μM in DEPC-treated water) was added increasing amounts of TCS (25 μM in DMSO) in 1 μL intervals until saturation was observed. From the resulting graph, binding constants were measured and calculated according to published procedures.[46]

DLS Measurements of siRNA/TCS. Average sizes were measured using DLS. Luc-siRNA stocks were prepared in DEPC-treated water to a concentration of 10 μM, and TCS was dissolved in DMSO to a concentration of 0.5 mg/mL. In a cuvette, 50 μL of siRNA and 1 μL of TCS were added and left to complex for 15 min before size measurement (n = 3). siRNA alone was added 1 μL of DMSO instead of TCS solution, and TCS alone was added 50 μL of DEPC-treated water instead of the siRNA mixture.

siRNA Transfection with TCS. Luc-siRNA (100 μM in DEPC-treated water) was mixed with TCS (1 mg/mL in DMSO) and allowed to complex for 1 h at room temperature. The siRNA/TCS mixture was then added to Luciferase-expressing Hela cells, with a final concentration of 10 μg/mL TCS and 25 nM/100 nM Luc-siRNA. The final DMSO concentration was 1%. The cells were allowed to incubate for 24 h before cell lysis and luciferase addition according to standard procedures. Chemiluminescence was then measured, and the results were given in % inhibition. Cells with 1% DMSO were used as a reference for 0% inhibition.

Cell Toxicity of TCS. TCS (20 mg/mL in DMSO) was added to Hela cells at increasing amounts and allowed to incubate for 24 h. Cell toxicity was then investigated using a standard resazurin assay, and results were reported in % cell survival.

Synthetic Protocols. *4-(Bis(but-3-yn-1-yloxy)methyl)-phenyl Acetate (**2**).* To a mixture of 4-formylphenyl acetate (5.0033 g, 30.5 mmol, 1 equiv) in THF (30 mL, distilled from sodium using benzophenone as an indicator) was added but-3-yn-1-ol (13.9 mL, 12.8 g, 0.183 mol, 6 equiv) and 5 Å molecular sieves (roughly 1/2 of THF volume). Then, toluenesulfonic acid (0.834 g, 4.87 mmol, 0.16 equiv, anhydrous, dried in a Dean Stark trap) was added, and the reaction was allowed to stir overnight. The reaction was then quenched with TEA (6 mL), and the mixture was concentrated by rotary evaporation. The crude product was purified by silica column chromatography (EtOAc/Hex/TEA; 10:90:0.1) to yield a white solid (4.982 g, 57% yield). ^{1}H NMR (400 MHz, chloroform-d): δ 7.51 (d, J = 8.6 Hz, 2H), 7.09 (d, J = 8.6 Hz, 2H), 5.65 (s, 1H), 3.73−3.57 (m, 4H), 2.50 (td, J = 6.8, 2.7 Hz, 4H), 2.30 (s, 3H), 1.99 (t, J = 2.7 Hz, 2H). ^{13}C NMR (101 MHz, $CDCl_3$): δ 169.49, 150.86, 135.60, 128.04, 121.49, 100.81, 81.42, 69.53, 63.34, 21.28, 20.02. HRMS (EI^+); found, 286.1203 m/z: calcd 286.1205 m/z for $[C_{17}H_{18}O_4]^+$.

*4-(Bis(but-3-yn-1-yloxy)methyl)phenyl Alkylbromides (**3a-3e**).* To a suspension of K_2CO_3 (2 equiv) in acetone (0.1 M to **2**) was added **2** (1 equiv) and dibromoalkane (3 equiv) under a flow of nitrogen. A solution of NaOMe (30% in MeOH, 1 equiv) was added to the solution, and it was allowed to stir at room temperature overnight, after which the reaction was added TEA and concentrated by rotary evaporation. The crude mixtures were then purified by silica flash chromatography (EtOAc/HEX/TEA; 5:95:0.1 to 10:90:0.1).

*1-(Bis(but-3-yn-1-yloxy)methyl)-4-((8-bromooctyl)oxy)-benzene (**3a**).* ^{1}H NMR (400 MHz, chloroform-d): δ 7.39 (d, J = 8.5 Hz, 2H), 6.87 (d, J = 8.8 Hz, 2H), 5.61 (s, 1H), 3.95 (t, J = 6.5 Hz, 2H), 3.64 (qt, J = 9.5, 6.9 Hz, 4H), 3.41 (t, J = 6.8 Hz, 2H), 2.49 (td, J = 6.9, 2.7 Hz, 4H), 1.98 (t, J = 2.7 Hz, 2H), 1.90−1.81 (m, 2H), 1.81−1.74 (m, 2H), 1.51−1.31 (m, 8H). ^{13}C NMR (101 MHz, $CDCl_3$): δ 159.42, 130.09, 128.05, 114.25, 101.35, 81.53, 69.44, 68.05, 63.30, 34.13, 32.91, 29.34, 29.32, 28.82, 28.23, 26.09, 20.07. HRMS (EI^+); found, 434.1453 m/z: calcd 434.1457 m/z for $[C_{23}H_{31}O_3Br]^+$.

*1-(Bis(but-3-yn-1-yloxy)methyl)-4-((10-bromodecyl)oxy)-benzene (**3b**).* ^{1}H NMR (400 MHz, chloroform-d): δ 7.39 (d, J = 8.6 Hz, 2H), 6.87 (d, J = 8.7 Hz, 2H), 5.61 (s, 1H), 3.95 (t, J = 6.5 Hz, 2H), 3.64 (qt, J = 9.5, 6.9 Hz, 4H), 3.41 (t, J = 6.9 Hz, 2H), 2.49 (td, J = 6.9, 2.7 Hz, 4H), 1.98 (t, J = 2.7 Hz,

https://doi.org/10.1021/acs.molpharmaceut.1c00579
Mol. Pharmaceutics 2022, 19, 67−79

2H), 1.93−1.69 (m, 4H), 1.49−1.28 (m, 12H). ^{13}C NMR (101 MHz, $CDCl_3$): δ 159.42, 130.04, 128.03, 114.24, 101.33, 81.53, 69.44, 68.09, 63.28, 34.19, 32.94, 29.56, 29.48, 29.37, 28.87, 28.29, 26.15, 20.05. HRMS (EI^+); found, 462.1758 *m/z*: calcd 462.1770 *m/z* for $[C_{25}H_{35}O_3Br]^+$.

*1-(Bis(but-3-yn-1-yloxy)methyl)-4-((12-bromododecyl)-oxy)benzene (**3c**).* ^{1}H NMR (400 MHz, chloroform-*d*): δ 7.39 (d, *J* = 8.7 Hz, 2H), 6.87 (d, *J* = 8.6 Hz, 2H), 5.61 (s, 1H), 3.95 (t, *J* = 6.5 Hz, 2H), 3.64 (qt, *J* = 9.3, 6.8 Hz, 4H), 3.40 (t, *J* = 6.8 Hz, 2H), 2.49 (td, *J* = 6.9, 2.7 Hz, 4H), 1.98 (t, *J* = 2.7 Hz, 2H), 1.93−1.71 (m, 4H), 1.49−1.26 (m, 16H). ^{13}C NMR (101 MHz, $CDCl_3$): δ 159.42, 130.01, 128.02, 114.22, 101.32, 81.52, 69.44, 68.11, 63.26, 34.22, 32.95, 29.65, 29.55, 29.51, 29.37, 28.88, 28.30, 26.16, 20.04. HRMS (EI^+); found, 490.2074 *m/z*: calcd 490.2083 *m/z* for $[C_{27}H_{39}O_3Br]^+$.

*1-(Bis(but-3-yn-1-yloxy)methyl)-4-((14-bromotetradecyl)-oxy)benzene (**3d**).* ^{1}H NMR (400 MHz, chloroform-*d*): δ 7.39 (d, *J* = 8.6 Hz, 2H), 6.88 (d, *J* = 8.8 Hz, 2H), 5.61 (s, 1H), 3.95 (t, *J* = 6.4 Hz, 2H), 3.64 (tdd, *J* = 9.5, 7.0, 2.7 Hz, 4H), 3.41 (t, *J* = 6.8 Hz, 2H), 2.49 (td, *J* = 6.9, 2.7 Hz, 4H), 1.98 (t, *J* = 2.7 Hz, 2H), 1.92−1.72 (m, 4H), 1.44 (dt, *J* = 10.7, 6.0 Hz, 4H), 1.37−1.23 (m, 16H). ^{13}C NMR (101 MHz, $CDCl_3$): δ 159.48, 130.07, 128.05, 114.28, 101.39, 81.54, 69.44, 68.17, 63.33, 34.20, 32.99, 29.74, 29.68, 29.54, 29.41, 28.92, 28.33, 26.20, 20.08. HRMS (EI^+); found, 518.2399 *m/z*: calcd 518.2396 *m/z* for $[C_{29}H_{43}O_3Br]^+$.

*1-(Bis(but-3-yn-1-yloxy)methyl)-4-((16-bromohexadecyl)-oxy)benzene (**3e**).* ^{1}H NMR (400 MHz, chloroform-*d*): δ 7.39 (d, *J* = 8.7 Hz, 2H), 6.87 (d, *J* = 8.7 Hz, 2H), 5.61 (s, 1H), 3.95 (t, *J* = 6.6 Hz, 2H), 3.64 (qt, *J* = 9.4, 6.9 Hz, 4H), 3.40 (t, *J* = 6.9 Hz, 2H), 2.49 (td, *J* = 6.9, 2.7 Hz, 4H), 1.98 (t, *J* = 2.6 Hz, 2H), 1.85 (dt, *J* = 14.5, 7.0 Hz, 2H), 1.81−1.73 (m, 2H), 1.47−1.38 (m, 4H), 1.35−1.24 (m, 20H). ^{13}C NMR (101 MHz, $CDCl_3$): δ 159.46, 130.04, 128.03, 114.26, 101.36, 81.53, 77.37, 69.44, 68.16, 63.30, 34.21, 32.98, 29.79, 29.73, 29.68, 29.58, 29.40, 28.91, 28.32, 26.19, 20.06. HRMS (EI^+); found, 546.2701 *m/z*: calcd 546.2709 *m/z* for $[C_{31}H_{47}O_3Br]^+$.

*4-(Bis(but-3-yn-1-yloxy)methyl)phenyl Alkyl-PEG350Da (**4a−4e**).* To a mixture of HO-PEG_{350Da}-OMe (2 equiv) in THF (0.7 M) at 0 °C was added NaH (60% in mineral oil, 2 equiv). The suspension was allowed to stir for 30 min before **3n** (1 equiv) in THF (0.5 M) was added dropwise. The mixture was then left to stir overnight, before some TEA was added for stability, and the solvent was removed by rotary evaporation. The crude was then purified by silica flash chromatography (MeOH/DCM/TEA; 1:99:0.1 to 4:96:0.1), and the PEG-containing fractions were collected to yield a mixture of **4a−4e** and excess HO-PEG350-OMe. These fractions were used directly in the next step.

*1-(Bis(but-3-yn-1-yloxy)methyl)-4-((8-PEG_{350Da}octyl)oxy)-benzene (**4a**).* HRMS (ESI^+); Found, 761.4448 *m/z*: calcd 761.4446 *m/z* for $[C_{40}H_{66}O_{12}Na]^+$.

*1-(Bis(but-3-yn-1-yloxy)methyl)-4-((10-PEG_{350Da}decyl)-oxy)benzene (**4b**).* HRMS (ESI^+); found, 789.4760 *m/z*: calcd 789.4759 *m/z* for $[C_{42}H_{70}O_{12}Na]^+$.

*1-(bis(but-3-yn-1-yloxy)methyl)-4-((12-PEG_{350Da}dodecyl)-oxy)benzene (**4c**).* HRMS (ESI^+); found, 817.5068 *m/z*: calcd 817.5072 *m/z* for $[C_{44}H_{74}O_{12}Na]^+$.

*1-(Bis(but-3-yn-1-yloxy)methyl)-4-((14-PEG_{350Da}tetradecyl)oxy)benzene (**4d**).* HRMS (ESI^+); found, 845.5384 *m/z*: calcd 845.5385 *m/z* for $[C_{46}H_{78}O_{12}Na]^+$.

*1-(Bis(but-3-yn-1-yloxy)methyl)-4-((16-PEG_{350Da}hexadecyl)oxy)benzene (**4e**).* HRMS (ESI^+); found, 873.5695 *m/z*: calcd 873.5699 *m/z* for $[C_{48}H_{82}O_{12}Na]^+$.

*First Generation Caged surfactants (**CS8−CS16**).* To dry DMF (6 mL) was added DIPEA (1 equiv), **4a−e** (1 equiv), tetraethylene glycol azide (4 equiv), and lastly CuI (0.2 equiv). The reaction was allowed to stir at RT for 48 h. TEA was added to the crude reaction to stabilize the acetal, and the majority of the DMF was removed by co-evaporation with toluene. The resulting crude product was purified by flash chromatography (90:10:0.1 EtOAc/MeOH/TEA to 20:80:0.1 MeOH/DCM/TEA) to yield **CS8−CS16**.

CS8. ^{1}H NMR (500 MHz, methanol-d_4): δ 7.80 (s, 2H), 7.27 (d, *J* = 8.4 Hz, 2H), 6.86 (d, *J* = 8.8 Hz, 2H), 5.49 (s, 1H), 4.53 (t, *J* = 5.2 Hz, 4H), 3.96 (t, *J* = 6.5 Hz, 2H), 3.86 (t, *J* = 5.1 Hz, 4H), 3.77−3.68 (m, 2H), 3.68−3.51 (m, 69H), 3.47 (t, *J* = 6.5 Hz, 3H), 3.35 (s, 3H), 2.94 (t, *J* = 6.6 Hz, 4H), 1.82−1.71 (m, 2H), 1.57 (d, *J* = 7.0 Hz, 2H), 1.48 (d, *J* = 7.8 Hz, 2H), 1.37 (s, 8H). ^{13}C NMR (151 MHz, $CDCl_3$): δ 145.00, 127.94, 123.10, 114.25, 101.86, 72.65, 71.65, 70.72, 70.65, 70.58, 70.44, 69.74, 68.15, 64.67, 61.79, 59.19, 50.23, 29.78, 29.57, 29.42, 26.67, 26.20. HRMS (ESI^+); found, 1199.6918 *m/z*: calcd 1199.6885 *m/z* for $[C_{56}H_{100}O_{20}N_6Na]^+$.

CS10. ^{1}H NMR (400 MHz, methanol-d_4): δ 7.80 (s, 2H), 7.27 (d, *J* = 8.7 Hz, 2H), 6.87 (d, *J* = 8.7 Hz, 2H), 5.49 (s, 1H), 4.53 (t, *J* = 5.0 Hz, 4H), 3.96 (t, *J* = 6.4 Hz, 3H), 3.85 (t, *J* = 5.1 Hz, 4H), 3.74−3.70 (m, 2H), 3.68−3.51 (m, 61H), 3.47 (t, *J* = 6.6 Hz, 3H), 3.35 (s, 3H), 2.94 (t, *J* = 6.5 Hz, 4H), 1.77 (t, *J* = 7.3 Hz, 2H), 1.57 (t, *J* = 6.8 Hz, 2H), 1.47 (d, *J* = 7.2 Hz, 2H), 1.34 (s, 12H). ^{13}C NMR (101 MHz, MeOD): δ 160.73, 146.15, 131.87, 129.02, 124.84, 115.10, 103.04, 73.68, 72.98, 72.36, 71.58, 71.49, 71.41, 71.37, 71.19, 70.44, 69.03, 65.55, 62.23, 59.10, 51.32, 47.41, 30.74, 30.67, 30.56, 30.42, 27.22, 10.24. HRMS (ESI^+); found, 1227.7228 *m/z*: calcd 1227.7198 *m/z* for $[C_{58}H_{104}O_{20}N_6Na]^+$.

CS12. ^{1}H NMR (400 MHz, methanol-d_4): δ 7.81 (s, 2H), 7.27 (d, *J* = 8.6 Hz, 2H), 6.87 (d, *J* = 8.6 Hz, 2H), 5.49 (s, 1H), 4.54 (m, 4H), 3.96 (t, *J* = 6.4 Hz, 2H), 3.87 (m, 4H), 3.83−3.77 (m, 2H), 3.76−3.50 (m, 71H), 3.47 (t, *J* = 6.6 Hz, 3H), 3.35 (s, 3H), 3.00−2.92 (m, 4H), 1.83−1.72 (m, 2H), 1.61−1.54 (m, 2H), 1.52−1.45 (m, 2H), 1.32 (b, 16H). ^{13}C NMR (101 MHz, MeOD): δ 160.74, 146.14, 129.02, 124.84, 115.10, 103.04, 73.68, 72.99, 72.37, 71.58, 71.49, 71.42, 71.37, 71.19, 70.44, 69.04, 65.57, 62.23, 59.10, 51.32, 47.43, 30.73, 30.60, 30.58, 30.53, 30.43, 27.23, 10.27. HRMS (ESI^+); found, 1255.7510 *m/z*: calcd 1255.7511 *m/z* for $[C_{60}H_{108}O_{20}N_6Na]^+$.

CS14. ^{1}H NMR (400 MHz, methanol-d_4): δ 7.85 (s, 2H), 7.32 (d, *J* = 8.6 Hz, 2H), 6.89 (d, *J* = 8.8 Hz, 2H), 5.31 (s, 1H), 4.58−4.52 (m, 4H), 3.97 (t, *J* = 6.4 Hz, 2H), 3.88 (dd, *J* = 5.6, 4.6 Hz, 4H), 3.80 (t, *J* = 6.1 Hz, 4H), 3.62 (d, *J* = 7.7 Hz, 53H), 3.46 (t, *J* = 6.6 Hz, 2H), 3.35 (s, 3H), 2.90 (t, *J* = 6.7 Hz, 4H), 1.76 (dq, *J* = 8.2, 6.5 Hz, 2H), 1.56 (q, *J* = 6.9 Hz, 2H), 1.51−1.44 (m, 2H), 1.36−1.28 (m, 20H). ^{13}C NMR (101 MHz, MeOD): δ 160.76, 131.54, 128.99, 124.77, 115.06, 104.56, 73.66, 72.97, 72.36, 71.57, 71.48, 71.41, 71.37, 71.17, 70.41, 68.99, 62.21, 62.13, 59.10, 51.31, 47.94, 30.73, 30.69, 30.58, 30.49, 30.40, 29.93, 27.21, 27.16, 9.22. HRMS (ESI^+); found, 1283.7853 *m/z*: calcd 1283.7824 *m/z* for $[C_{62}H_{112}O_{20}N_6Na]^+$.

CS16. ^{1}H NMR (400 MHz, methanol-d_4): δ 7.81 (s, 2H), 7.27 (d, *J* = 8.7 Hz, 2H), 6.86 (d, *J* = 8.7 Hz, 2H), 5.49 (s, 1H), 4.53 (t, *J* = 5.1 Hz, 4H), 3.96 (t, *J* = 6.5 Hz, 2H), 3.85 (t, *J* = 5.1 Hz, 4H), 3.69−3.49 (m, 59H), 3.46 (t, *J* = 6.6 Hz, 2H),

https://doi.org/10.1021/acs.molpharmaceut.1c00579
Mol. Pharmaceutics 2022, 19, 67−79

3.35 (s, 3H), 1.81−1.71 (m, 2H), 1.56 (q, J = 6.8 Hz, 2H), 1.46 (d, J = 7.9 Hz, 2H), 1.31 (d, J = 8.0 Hz, 22H). ^{13}C NMR (101 MHz, MeOD): δ 160.73, 146.14, 131.86, 129.01, 124.85, 115.09, 103.03, 73.67, 72.97, 72.37, 71.56, 71.48, 71.41, 71.17, 70.44, 69.04, 65.55, 62.22, 59.10, 51.32, 47.50, 30.76, 30.59, 30.53, 30.43, 27.23, 10.09. HRMS (ESI$^+$); found, 1311.8137 m/z: calcd 13.11.8137 m/z for $[C_{64}H_{116}O_{20}N_6Na]^+$.

PCS. **PCS** was prepared fresh from **CS12-DITFAA** (see Supporting Information) 1−2 days before its use and kept at −80 °C. It was prepared by adding **CS12-DITFAA** (2.6 mg) to a solution of NaOH (aq., 6 M, 4.3 μL). The mixture was stirred for 5 min before the addition of 22 μL 1,4-dioxane. The mixture was allowed to sit at room temperature for 2 h before the addition of phosphate buffer (233.7 μL, 0.2 M at pH 8.3) to yield a 10 mg/mL stock solution, which was used directly in all subsequent assays. The formation of PCS was confirmed by TLC and HRMS. HRMS (ESI$^+$); found, 1143.7493 m/z: calcd 1143.7487 m/z for $[C_{56}H_{103}O_{16}N_8]^+$ (n = 6).

TCS. A mixture of **4c** (10.3 mg, 0.014 mmol, 1 equiv) in DMF (200 μL) and DIPEA (6.3 μL, 4.6 mg, 0.036 mmol, 2.5 equiv) was added to a round bottomed flask, and the solution was purged with nitrogen gas. The solution was then added to **TO-PEG4-N3** (see Supporting Information) (33 mg, 0.07 mmol, 5 equiv) and CuI (cat. amount), and the mixture was allowed to stir at room temperature for 48 h. The reaction mixture was added to toluene (50 mL), and the solution was concentrated by rotary evaporation, and the residue was purified by neutral alumina flash chromatography (2−4% MeOH in DCM + 0.1% TEA) to yield **TCS** as a red tar (9 mg, 0.005 mmol, 38% yield). TCS was stored in the presence of TEA. ^{1}H NMR (900 MHz, MeOD): δ 8.52 (d, J = 8.4 Hz, 2H), 8.29 (d, J = 7.1 Hz, 2H), 7.96 (d, J = 8.6 Hz, 2H), 7.85 (t, J = 7.7 Hz, 2H), 7.79 (d, J = 7.8 Hz, 2H), 7.69 (s, 2H), 7.66 (t, J = 7.5 Hz, 2H), 7.54−7.47 (m, 2H), 7.32 (t, J = 7.1 Hz, 2H), 7.22 (d, J = 7.0 Hz, 2H), 7.13 (d, J = 8.0 Hz, 2H), 6.72 (d, J = 8.2 Hz, 2H), 6.70 (s, 2H), 5.50 (s, 1H), 4.65 (d, J = 6.0 Hz, 4H), 4.43 (t, J = 5.1 Hz, 4H), 3.90 (t, J = 4.9 Hz, 4H), 3.87 (s, 6H), 3.80 (t, J = 6.4 Hz, 2H), 3.77 (t, J = 5.1 Hz, 4H), 3.65−3.43 (m, 55H), 2.80 (t, J = 6.5 Hz, 4H), 1.65 (p, J = 6.6 Hz, 2H), 1.54 (p, J = 6.8 Hz, 2H).

^{13}C NMR (226 MHz, MeOD): δ 161.91, 150.61, 146.29, 146.10, 141.86, 138.91, 134.48, 129.62, 129.10, 128.25, 126.72, 126.02, 125.76, 124.81, 123.84, 119.07, 115.17, 113.84, 109.28, 103.09, 89.29, 78.36, 73.13, 72.51, 71.94, 71.73, 71.65, 71.55, 71.50, 71.34, 70.49, 69.45, 69.12, 65.71, 59.25, 56.40, 55.70, 53.75, 51.38, 34.36, 30.90, 30.84, 30.74, 30.64, 30.51, 27.38, 27.32, 7.77. HRMS (ESI$^+$); found, 889.9699 m/z: calcd 889.9671 m/z for $[C_{96}H_{134}N_{10}O_{18}S_2]^{2+}$ for n = 8 (PEG chain length).

RESULTS AND DISCUSSION

Caged Surfactants: Molecular Design and Synthesis.

Surfactants like Triton X have the general structure PEG-hydrocarbon chain and disrupt membranes by inserting their hydrophobic domain into the lipid bilayer. Triton X-like surfactants are not pH-sensitive, and this prevents them from being used as endosomal disruptive agents. We therefore investigated if Triton X-like surfactants could be converted into pH-sensitive membrane disruptive agents by conjugating short PEG chains to their hydrophobic domain, via acid degradable acetal linkages. The presence of the PEG chains was hypothesized to prevent the hydrophobic domain from inserting into membranes. This was further corroborated through a molecular dynamics simulation of the caged surfactant **CS12**, shown in Figures 2A and S2, which shows

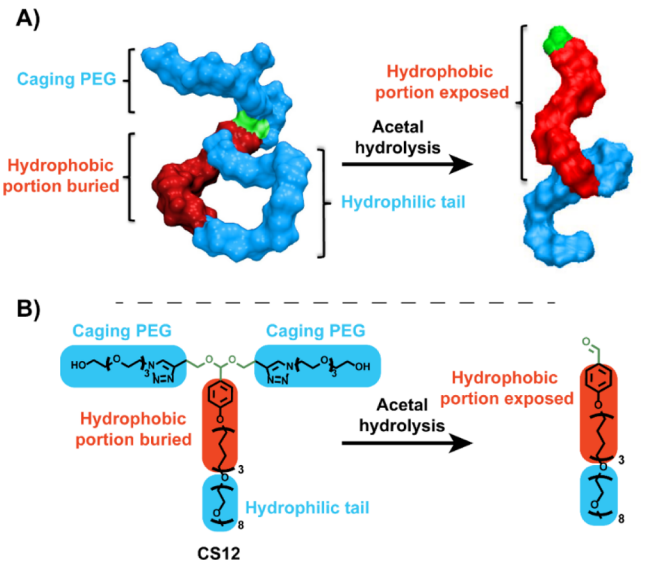

Figure 2. Molecular dynamics simulations of the caged surfactants indicate that they will be pH-sensitive membrane disruptive agents. (A) Molecular dynamics simulation of the caged surfactant CS12 reveals that in its intact form (pH 7.4), it cannot adopt a conformation that allows for membrane penetration because its hydrophobic domain (red) is flanked by PEG chains (blue). However, at acidic pHs, the PEG chains of CS12 are hydrolyzed off, exposing a large hydrophobic area, which should be able to penetrate membranes. (B) Chemical structure of CS12 in its intact and hydrolyzed form. Blue portions represent PEG chains, red represents hydrophobic moieties, while green represents the acetal linker.

that the hydrophobic region of the caged surfactants is shielded by the branching PEG chains. However, upon hydrolysis, the hydrophobic portion is exposed, which should allow for it to insert into the endosomal membrane.

Reversible PEGylation has never been applied to low molecular weight surfactants, and consequently, it is unknown what the optimal hydrophobic/hydrophilic balance will be for the caged surfactants. The membrane partitioning and the membrane disruptive efficiency of Triton X-like surfactants scale with the length of their hydrophobic domains, and consequently, a large hydrophobic domain is desirable. However, if the hydrophobic domain was made too prominent, the intact caged surfactant may itself cause membrane disruption at pH 7.4, causing high levels of toxicity.

We synthesized a variety of caged surfactants, which had hydrophobic domains composed of a benzaldehyde followed by an 8 to 16-carbon alkyl chain, and measured their pH-dependent membrane disruptive efficiency to determine the hydrophobic chain length that most efficiently disrupted membranes at pH 5.5 with minimal membrane disruptive activity at pH 7.4.

The synthetic strategy used to generate the five caged surfactants (**CS8**−**CS16**) is shown in Figure 3A. These caged surfactants contain a $(HO\text{-}PEG)_2$-masking group to simplify their syntheses. The caged surfactants contain an unstable alkoxy acetal, which makes multistep synthetic procedures challenging. To circumvent this challenge, we developed a synthetic protocol that introduces the alkoxy group late in the synthesis and allows the acetal to be formed on an aldehyde

https://doi.org/10.1021/acs.molpharmaceut.1c00579
Mol. Pharmaceutics 2022, 19, 67−79

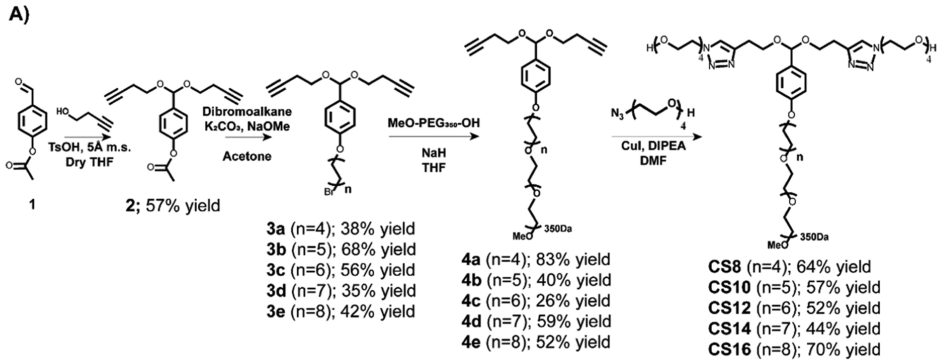

B)

Molecule	Hydrophobic Chain Length	$Hemo_{50\%}$ (mM) pH 7.4	$Hemo_{50\%}$ (mM) pH 5.5
CS8	8	>8.7*	0.98
CS10	10	>8.5*	0.093
CS12	12	>8.3*	0.024
CS14	14	>0.81*	0.026
CS16	16	>0.80*	0.029

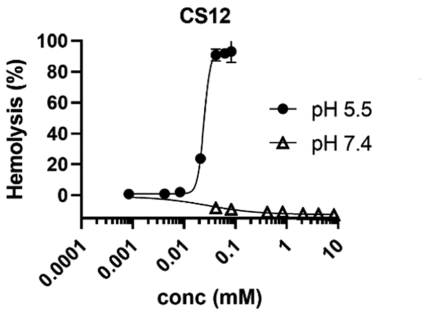

Figure 3. Caged surfactants are pH-sensitive membrane disruptive agents. (A) Synthesis of five different caged surfactants, CS8−CS16. (B) Concentration of CS at which 50% hemolysis is achieved at either pH 7.4 or 5.5. $Hemo_{50\%}$ values at pH 7.4 represent the highest concentration tested, and no hemolysis was observed for any of the caged surfactants at pH 7.4 at the tested concentrations. Several of the caged surfactants, in particular, CS12, CS14, and CS16, are remarkably efficient at performing membrane disruption and have $Hemo_{50\%}$ in the micromolar range. (C) Representative hemolysis curves for compound CS12 at pH 5.5 and pH 7.4.

that has an ester substituent, as opposed to an alkoxy substituent. A benzylic acetal with an ester group in the para position (σ_{para} = 0.31) is significantly more stable compared to an acetal with a methoxy group in the para position (σ_{para} = −0.27).[28] In short, treatment of aldehyde **1** with 1-butyn-4-ol under acidic conditions gave the acetal 2 with a yield of 57%. Compound **2** was then treated with NaOMe in the presence of a dibromo-alkyl compound with 8, 10, 12, 14, or 16 carbons, yielding compounds **3a−e**, respectively. These compounds were then added to a solution of MeO-PEG_{350}-OH pretreated with NaH, followed by stirring overnight to yield compounds **4a−e**. Finally, the caged surfactants **CS8−CS16** were synthesized through copper-click cycloaddition with tetraethyleneglycol monoazide. The removal of copper was confirmed by ICP-OES (Figure S3).

Caged Surfactants are pH-Sensitive Membrane Disruptive Agents−Structure−Activity Relationship. The caged surfactants are designed to function as pH-sensitive membrane disruptive agents. A hemolysis assay was utilized to measure the ability of the caged surfactants **CS8−CS16** to disrupt RBC membranes at pH 7.4 and 5.5 (Figure 3B).[6] The results of the caged surfactant hemolysis assay are presented in Figure 3B in terms of the concentration needed to generate 50% hemolysis at either pH 5.5 or 7.4 ($Hemo_{50}$). All the caged surfactants showed pH-sensitive membrane disruptive ability. For example, the caged surfactant **CS12** had a $Hemo_{50}$ of 24 μM at pH 5.5 and generated no hemolysis at pH 7.4 at concentrations up to 8.3 mM, the highest concentration measured (Figure 3B). Interestingly, **CS16**, which bears the longest hydrocarbon chain, also shows no hemolysis at pH 7.4 despite having the largest hydrophobic surface. The hydrolyzed aldehyde corresponding to **CS8** was independently synthesized and showed no pH dependency (Figure S1). This confirms that the pH-sensitive membrane disruptive property of the caged surfactants is due to the masking PEG chains. These results demonstrate that the branched $(HO\text{-}PEG)_2$-structure is remarkably efficient at preventing membrane insertion of long hydrophobic domains even though it consists of only short PEG chains.

Figure 3B demonstrates that the membrane disruptive efficiency of the caged surfactants increases with their hydrocarbon chain length. For example, **CS12** was approximately 37 times more efficient at disrupting membranes than **CS8**, with $Hemo_{50}$ values of 900 and 24 μM at pH 5.5 for **CS8** and **CS12**, respectively. The increased membrane disruptive activity of **CS12** over **CS8** is not surprising because Triton X-like surfactants, which share structural similarities with the hydrolyzed caged surfactants, also show an increase in membrane disruptive efficiency with larger hydrophobic domains.[29] Importantly, the membrane disruptive activity of the caged surfactant **CS12** (Figure 3C) is similar to endosomal disruptive polymers such as poly(ethyl-acrylic acid), despite being only 10% of the molecular weight.[30] Conjugation of short PEG chains to Triton X-like surfactants consequently has the potential to generate highly efficient low molecular weight endosomal disruptive agents.

Caged Surfactants Have pH-Sensitive Hydrolysis Kinetics. The membrane disruptive activity of the caged surfactants is triggered by the hydrolysis of the acetal linkage. The hydrolysis kinetics of the acetal linkage in the caged surfactants is therefore a key parameter for their efficacy, as it establishes a timeline of their membrane disruptive abilities. Upon endosomal uptake, biomolecules are trafficked to lysosomes within 30 min where they are broken down by

https://doi.org/10.1021/acs.molpharmaceut.1c00579
Mol. Pharmaceutics 2022, 19, 67−79

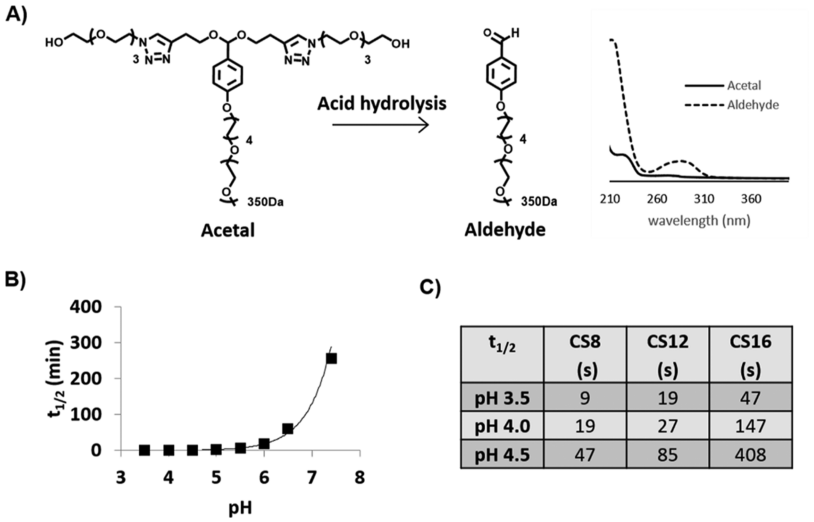

$t_{1/2}$	CS8 (s)	CS12 (s)	CS16 (s)
pH 3.5	9	19	47
pH 4.0	19	27	147
pH 4.5	47	85	408

Figure 4. Caged surfactants exhibit pH-dependent hydrolysis. (A) Caged surfactants hydrolyze in acid and give free aldehyde. Generation of the aldehyde causes the appearance of an absorption peak with λ_{max} = 286 nm. (B) Plot of hydrolysis half-life of CS8 at a range of pH conditions at 37 °C. (C) Hydrolysis half-lives for CS8, CS12, and CS16 at pH 3.5, 4.0, and 4.5 at 37 °C.

lysosomal enzymes.[31] Consequently, the caged surfactants need to hydrolyze with a half-life of <30 min in endosomal conditions to ensure that endosomal disruption occurs before lysosomal degradation. In addition, the caged surfactants need to be stable at pH 7.4 for several hours to allow for sufficient time for uptake into cells and to prevent toxicity due to uncontrolled release of the surfactant. The acetal linkages hydrolyze in proportion to the hydronium ion concentration and will consequently hydrolyze roughly 250-fold faster at pH 5.0 than at pH 7.4.

We measured the hydrolysis kinetics of the caged surfactants **CS8**, **CS12**, and **CS16** via absorption spectroscopy (λ = 286 nm) at a 50 μg/mL concentration at 37 °C. Figure 4 demonstrates that the caged surfactants hydrolyze rapidly at pH 5.0. For example, **CS8** had a k_{2nd} = 261 s^{-1} M^{-1}, which corresponds to a hydrolysis half-life of 2.5 min at pH 5.0 and over 4 h at pH 7.4. The hydrolysis kinetics of **CS12** and **CS16** show similar pH-sensitive hydrolysis, but overall, longer hydrocarbon chains lead to slower hydrolysis rates. For example, hydrolysis rates at pH 4.5 for **CS8**, **CS12**, and **CS16** were found to be 0.8, 1.4, and 6.8 min, respectively (Figure 4C).

The hemolytic efficiencies of the **CS12**, **CS14**, and **CS16** caged surfactants are similar; however, the hydrolysis half-life increases with hydrophobicity, shown by the hydrolysis of **CS16** being roughly five times slower than that of **CS12**. We anticipate that this factor makes **CS12** preferable over **CS14** and **CS16**, as endosomal contents need to be released from endosomes before they are degraded in lysosomes. We therefore selected the C12 caged surfactants for further studies due to their rapid hydrolysis kinetics in comparison to the C14 and C16 caged surfactants.

PCS—Design and Synthesis. The caged surfactants need to complex nucleic acids in order to enhance their cytoplasmic delivery. We consequently synthesized a second generation caged surfactant, which contained two primary amines conjugated to the distal ends of the (PEG)2 chains, termed positively charged caged surfactants (PCS). The chemical structure of the PCS is shown in Figure 5A. The PCS is designed to bind nucleic acids via a combination of electrostatic forces and hydrophobic forces, similar to cationic

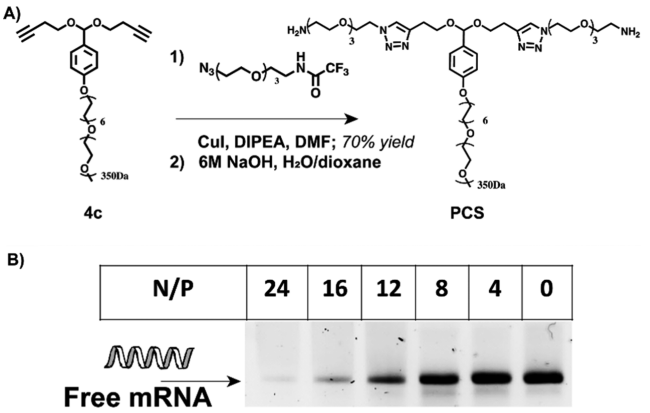

Figure 5. PCS binds nucleic acids. (A) Synthetic scheme for PCS. (B) PCS binds mRNA: PCS was mixed with mRNA at various ratios and run on an agarose gel. 50% retention is reached at roughly N/P = 11. The full gel is shown in Figure S4.

surfactants (Figure 5B). However, after endocytosis, the PCS will hydrolyze, generating individual positive charges and hydrophobic domains, which independently will not bind nucleic acids tightly, leading to efficient release of nucleic acids. The synthesis of the PCS is shown in Figure 5A, and it follows a strategy similar to the first generation caged surfactants, as shown in Figure 3A. Briefly, a trifluoroacetamide-protected amine was used for the click reaction with the alkyne acetal **4c**, and this reaction gave a 70% yield of the trifluoroaceto-protected intermediate, which was deprotected *in situ* to generate the amine (see Supporting Information).

The ability of the PCS to bind nucleic acids was tested by mixing it with mRNA at various ratios and measuring its retention on an agarose gel. The degree of PCS binding to mRNA was quantified by performing densitometry analysis of the mRNA band; in particular, we determined how much PCS was needed to reduce the mRNA band intensity by 50%. Figure 5B shows that the PCS binds mRNA with a retention efficiency of 50% at an N/P ratio of 11. The relatively weak complexation between the PCS and nucleic acids is expected based upon their molecular structure, given that single-chained

https://doi.org/10.1021/acs.molpharmaceut.1c00579
Mol. Pharmaceutics 2022, 19, 67−79

cationic surfactants also bind nucleic acids with a similar N/P ratio.[32] We also investigated if the PCS released nucleic acids after acid hydrolysis, due to separation of the two positive charges from the surfactant domain. For these experiments, plasmid DNA (pDNA) was used because it has a higher stability under acidic conditions. Figure S5 shows that acid hydrolysis of PCS + pDNA leads to pDNA release even at an N/P ratio of 110. These results suggest that the PCS will release complexed nucleic acids in endosomes following acid hydrolysis, which should allow for efficient transcription and translation. DLS was used to determine the sizes of the PCS/nucleic acid complexes (Figure S6).

PCS Can Enhance Lipofectamine-Based mRNA Delivery into HUVECs. We investigated if the PCS could enhance the ability of lipofectamine to deliver eGFP-expressing mRNA into HUVECs (Figure 6B). The PCS by itself was unable to deliver mRNA into cells (data not shown), and we consequently focused on determining if the PCS could enhance the delivery of commonly used transfection reagents. We selected lipofectamine 2000, a mixture of a cationic and a zwitterionic lipid,[33] for transfection studies because it is one of the most widely used transfection agents for nucleic acids, which greatly outperformed the commercially available transfection agents X-tremeGENE 360 and TurboFect in Hela cells (Figure S7). In addition, despite its widespread use, lipofectamine has issues with toxicity in sensitive cell lines,[34] and consequently, adjuvants that can enhance its transfection efficiency can potentially have a significant biomedical impact. Lipofectamine consists of a mixture of two positively charged lipids, which disrupt endosomes through membrane fusion or the proton sponge effect, following endosomal entrapment.[35,36] The caged surfactants, however, disrupt endosomes through membrane insertion and destabilization and should complement lipofectamine's ability to disrupt endosomes.

We selected primary cells as a testbed for these studies because they are challenging to transfect due to their sensitivity to cationic reagents and because of their biomedical importance. In particular, primary cells are the basis of a wide number of cell therapies and are also being intensely investigated as platforms for screening drugs. There is consequently great interest in developing reagents that can transfect primary cells with high efficiencies. HUVECs, like most primary cells, are challenging to transfect, for example, HUVEC transfection with cationic reagents rarely exceeds 45% and frequently causes high levels of toxicity.[37] Consequently, an endosomal disruptive agent that can increase the efficiency of lipofectamine has the potential to impact multiple areas of biotechnology.

We therefore performed experiments to determine if the PCS (Figure 6A) could enhance the ability of lipofectamine to deliver mRNA to HUVECs. We first determined the cell toxicity of lipofectamine + PCS + mRNA and lipofectamine + mRNA. Figure 6C indicates that the PCS does not increase the toxicity of lipofectamine and that lipofectamine causes <20% toxicity at 1 μL/mL. We set <80% survival as an acceptable level of toxicity and therefore used 1 μL/mL of lipofectamine for future cell transfection studies.

We investigated if lipofectamine + PCS could increase the delivery of mRNA into HUVECs, following the protocol described above (Figure 6B). The results, shown in Figure 6D, demonstrates that the PCS can significantly enhance the delivery of mRNA into HUVECs. For example, at a 0.2 μL/mL concentration of lipofectamine, no cells were transfected with

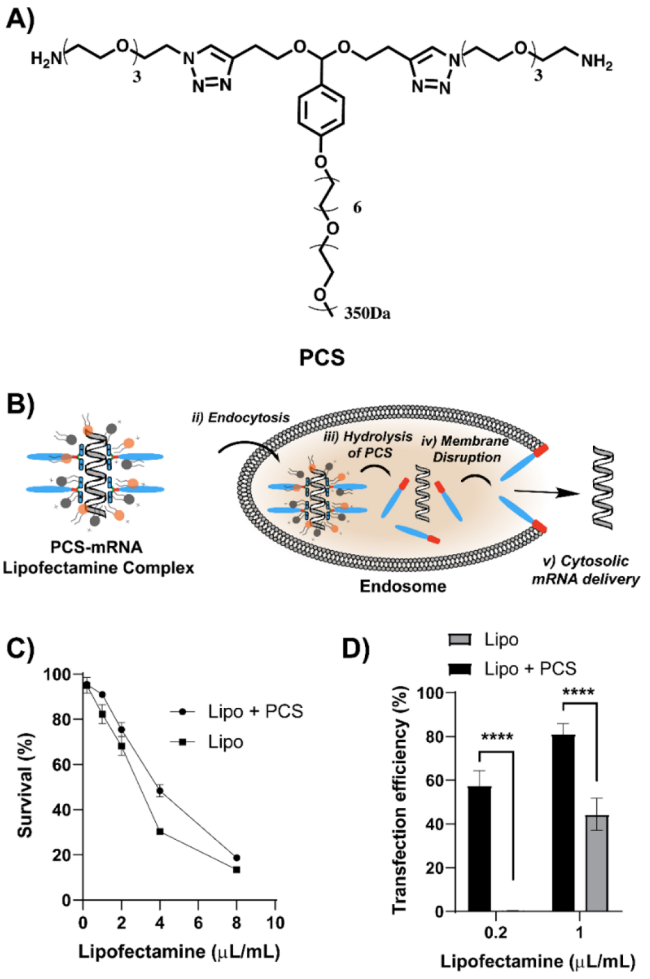

Figure 6. PCS increases the mRNA transfection efficiency of lipofectamine in HUVECs. (A) Chemical structure of the PCS. (B) Summary of the experiment. eGFP-expressing mRNA (0.5 μg/mL) was mixed with the PCS (2.0 μg/mL) and incubated for 30 min followed by the addition of lipofectamine 2000. The resulting complex was added to HUVEC cells, and the expression of eGFP was measured by flow cytometry. (C) Toxicity data for lipofectamine alone as well as lipofectamine/PCS. The PCS does not increase the toxicity of lipofectamine. (D) PCS increases the transfection efficiency of lipofectamine in HUVEC cells. Lipofectamine/PCS had an 81% transfection efficiency, whereas the maximum transfection efficiency of lipofectamine alone was 40%. In all cases, the concentrations of the PCS (2 μg/mL) and mRNA (500 ng/mL) were kept constant. ****P < 0.0001, **P < 0.01, *P < 0.05 (unpaired two-tailed t-test).

mRNA, whereas lipofectamine + PCS transfected approximately 58% of the cells. Similarly, at a 1 μL/mL concentration of lipofectamine, 40% of the cells was transfected with lipofectamine, whereas 80% of the cells was transfected with lipofectamine + PCS. These results suggest that the caged surfactants are disrupting endosomes in cells; however, they may also be increasing the lipofectamine transfection rate by increasing endocytosis. This however would be unlikely, due to PEG coatings generally leading to lower levels of cell uptake.[38] The overall delivery mechanism of lipofectamine + mRNA also does not appear to be altered upon PCS addition (Figure S8). These experiments were repeated in Hela cells to further illustrate the ability of the PCS to increase mRNA delivery to cells (Figure S7 for transfection results and Figure S13 for toxicity data).

https://doi.org/10.1021/acs.molpharmaceut.1c00579
Mol. Pharmaceutics 2022, 19, 67−79

Caged Surfactants Conjugated to RNA-Binding Dyes Enhance the Delivery of siRNA. A limitation of the PCS is its relatively weak affinity for nucleic acids, which may limit its applications. Nucleic acid-binding dyes have great potential as scaffolds for increasing the binding affinity of delivery vectors to nucleic acids because they bind nucleic acids with much higher affinity than individual positive charges. For example, the DNA binding dye acridine has an apparent binding constant on the order of 10^4 M^{-1} for DNA, whereas individual positive charges bind DNA with K_a < 10 M^{-1}.[39] Nucleic acid binding dyes have been used to develop DNA and mRNA delivery vehicles. The Rice group demonstrated that by introducing 4−6 acridine moieties to a polylysine-PEG block copolymer,[40,41] they could successfully deliver luciferase-expressing mRNA to cells. We therefore designed and synthesized a third generation caged surfactant, which used RNA binding dyes for nucleic acid complexation, instead of positive charges. We selected TO as our nucleic acid binding group, as it has binding affinities on the order of 10^6 M^{-1}, significantly higher than that of acridine.[42] The third generation caged surfactant has the RNA binding dye TO conjugated to the distal ends of its PEG chains and is termed the TO caged surfactant (TCS). The TCS was synthesized according to the scheme shown in Figure 7A. Briefly, the intermediate **4c** was reacted with TO-PEG_4-azide in the presence of CuI and DIPEA to yield the final TCS (see Supporting Information).

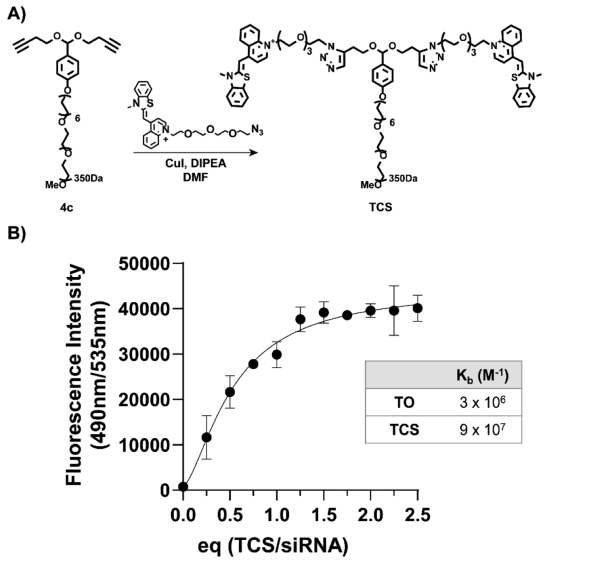

Figure 7. TCS can bind siRNA with high efficiency. (A) Synthesis of the TCS. (B) Binding of the TCS to siRNA causes an increase in fluorescence. The TCS was mixed with siRNA at various mole ratios, and the increase in fluorescence was measured. A 23 base siRNA can bind 2 TCS molecules. Table: TCS binds siRNA with a K_b of 9×10^7 M^{-1}, compared to 3×10^6 M^{-1} for TO, which is in line with previously reported values.[42]

The TCS has the potential to enhance the delivery of a variety of nucleic acid therapeutics. We selected siRNA as an initial drug for TCS-mediated delivery because of its importance in biomedicine and because of its double stranded nature, which should enable efficient complexation with the TCS. The binding constant of the TCS with siRNA was determined as $K_b = 9 \times 10^7$ (Figure 7B). In addition, we determined the size of TCS-siRNA complexes, which were approximately 55 nm in size (see Figure 8C).

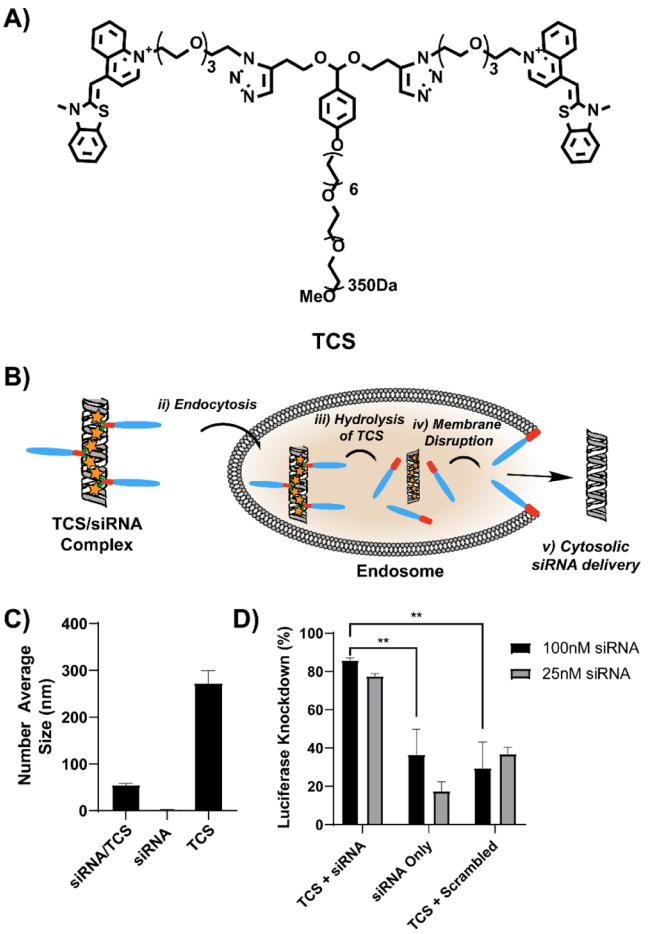

Figure 8. TCS can enhance the delivery of siRNA into cells. (A) Chemical structure of the TCS. (B) Schematic showing intracellular delivery of siRNA by the TCS. The TCS binds siRNA and hydrolyzes in the endosome, triggering endosomal release. (C) TCS forming 55 nm sized particles with siRNA. The particle size was determined via DLS. (D) TCS can enhance the delivery of siRNA into cells. TCS + siRNA (100 nM) caused 86% luciferase inhibition, whereas siRNA by itself caused only 37% inhibition. At 25 nM siRNA, these values were 78 and 18%, respectively. **P < 0.01 (unpaired two-tailed t-test).

The ability of the TCS (Figure 8A) to enhance the delivery of luciferase-siRNA to luciferase-expressing Hela cells was investigated. Luciferase-expressing Hela cells were selected as a test bed for the TCS because of their straightforward read-out for siRNA delivery efficiency. The toxicity of TCS to Hela cells was determined using the resazurin assay. As with the PCS experiments, the highest concentration of the TCS that caused <20% toxicity was used in subsequent cell studies, in this case, 10 μg/mL of TCS (Figure S15). We investigated siRNA concentrations of 25 and 100 nM, based on previous studies.[43] Luciferase knockdown siRNA (sense strand; GAU UAU GUC CGG UUA UGU AUU) was complexed with the TCS and incubated with luciferase-expressing Hela cells in serum-containing media for 24 h followed by cell lysis and addition of luciferin and measurement of chemiluminescence (Figure 8B). As shown in Figure 8D, the TCS was able to significantly enhance the delivery of siRNA into Hela cells. For example, at a 25 nM concentration of siRNA, siRNA by itself caused only

https://doi.org/10.1021/acs.molpharmaceut.1c00579
Mol. Pharmaceutics 2022, 19, 67−79

an 18% knockdown of luciferase, whereas siRNA complexed to the TCS caused a 78% inhibition of luciferase. Knockout of luciferase caused by siRNA alone most likely arises due to the stability of the modified siRNA that was utilized, allowing for a degree of self-delivery. In addition, siRNA is prone to off-target effects, which can cause unexpected knockdown for scrambled siRNA. Similar enhancements in siRNA delivery with the TCS were also seen at a 100 nM concentration of siRNA, with 37% inhibition by siRNA alone and 86% with TCS and siRNA. The TCS complexed with scrambled siRNA was used as a control. The amount of the TCS used to deliver siRNA is comparable to the amount of ionizable lipid used to achieve efficient *in vitro* transfection of siRNA, as in a study by Kulkarni et al., where >85 μM of lipid and N/P ratios of 1−3 were used to successfully transfect Luc-siRNA and GFP-siRNA to human prostate carcinoma cells and neurons, respectively.[44] We also tested delivery efficiency using lipofectamine and found that we needed to use 200 nM of siRNA for efficient luciferase knockdown under the same conditions as for the TCS (Figure S16).

In this report, we demonstrated that Triton X-like surfactants can be converted into pH-sensitive membrane disruptive agents via reversible PEGylation. Interestingly, short PEG chains, 4 units in length, were able to prevent large hydrophobic domains as large as 23 carbons in length, hexadecane and a benzaldehyde, from disrupting membranes. This result suggests that reversible PEGylation enables the design and synthesis of a wide variety of new low molecular weight endosomal disruptive agents. A key benefit of low molecular weight endosomal disruptive agents is their well-defined chemical structure, which makes them easily amenable to chemical optimization, allowing for great versatility. In this report, we demonstrated that by introducing amine functionalities to the caged surfactant, the PCS was able to enhance the ability of lipofectamine to deliver mRNA and allowed for lowering of the lipofectamine dose required to achieve efficient transfection in sensitive cell lines. We also showed that caged surfactants that contained two TO moieties were able to successfully deliver siRNA to Hela cells. Collectively, these results show that the caged surfactants are a versatile class of endosomal disruptors and that reversible PEGylation of surfactants has the potential to generate new classes of endosomal disruptive agents.

■ ASSOCIATED CONTENT

Supporting Information

The Supporting Information is available free of charge at https://pubs.acs.org/doi/10.1021/acs.molpharmaceut.1c00579.

Data on the pH-independent hemolysis of an isolated surfactant, molecular dynamics data, ICP measurements, full gels, DLS data, transfection efficiencies with additional transfection agents and with endocytosis inhibitors, flow cytometry histograms, full toxicity information, and NMR spectra (PDF)

■ AUTHOR INFORMATION

Corresponding Author

Niren Murthy − *Department of Bioengineering, University of California, Berkeley, Berkeley, California 94720, United States; Innovative Genomics Institute (IGI), Berkeley, California 94704, United States*; Email: nmurthy@berkeley.edu

Authors

Joachim Justad Røise − *Department of Chemistry and Department of Bioengineering, University of California, Berkeley, Berkeley, California 94720, United States*; orcid.org/0000-0002-1794-7570

Hesong Han − *Department of Bioengineering, University of California, Berkeley, Berkeley, California 94720, United States*

Jie Li − *Department of Bioengineering, University of California, Berkeley, Berkeley, California 94720, United States*; orcid.org/0000-0003-0189-2787

D. Lucas Kerr − *Department of Chemistry and Department of Bioengineering, University of California, Berkeley, Berkeley, California 94720, United States*

Chung Taing − *Department of Chemistry and Department of Bioengineering, University of California, Berkeley, Berkeley, California 94720, United States*

Kamyar Behrouzi − *Department of Bioengineering and Department of Mechanical Engineering, University of California, Berkeley, Berkeley, California 94720, United States*

Maomao He − *Department of Bioengineering, University of California, Berkeley, Berkeley, California 94720, United States*

Emily Ruan − *Department of Chemistry and Department of Chemical and Biomolecular Engineering, University of California, Berkeley, Berkeley, California 94720, United States*

Lienna Y. Chan − *Department of Bioengineering, University of California, Berkeley, Berkeley, California 94720, United States*

Eli M. Espinoza − *Department of Bioengineering, University of California, Berkeley, Berkeley, California 94720, United States*; orcid.org/0000-0002-0134-2833

Sören Reinhard − *Department of Bioengineering, University of California, Berkeley, Berkeley, California 94720, United States*

Kanav Thakker − *Department of Chemical and Biomolecular Engineering, University of California, Berkeley, Berkeley, California 94720, United States*

Justin Kwon − *Department of Bioengineering, University of California, Berkeley, Berkeley, California 94720, United States*

Mohammad R. K. Mofrad − *Department of Bioengineering and Department of Mechanical Engineering, University of California, Berkeley, Berkeley, California 94720, United States; Molecular Biophysics and Integrative Bioimaging Division, Lawrence Berkeley National Lab, Berkeley, California 94720, United States*; orcid.org/0000-0001-7004-4859

Complete contact information is available at: https://pubs.acs.org/10.1021/acs.molpharmaceut.1c00579

Author Contributions

Authors J.J.R. and H.H. contributed equally. N.M. and J.J.R. conceived of and presented the idea. J.J.R., D.L.K., C.T., E.R., K.T., and J.K. performed the synthesis. J.J.R., C.T., D.L.K, M.H., E.M.E., S.R., and L.Y.C. carried out the characterization studies including hemolysis and kinetics measurements. H.H.

https://doi.org/10.1021/acs.molpharmaceut.1c00579
Mol. Pharmaceutics 2022, 19, 67−79

and J.L. performed the cell culture studies. K.B. and M.R.K.M. carried out the computational studies.

Notes

The authors declare no competing financial interest.

■ ACKNOWLEDGMENTS

The authors acknowledge funding support from the National Institutes of Health (grant nos. R01AI117064, R33AI119115-01, NIH R61DA048444-01, RO1EB029320-01A1, RO1EB023776, NIH UG3NS115599, and U24HG010423). This work was also funded by the Innovative Genomics Institute. We thank Dr. Jeffrey Pelton at the QB3 NMR Facility for help with the 900 MHz NMR (funded by NIH grant GM68933). We acknowledge the NMR facility at UC Berkeley (funded by NIH grant S10OD024998). We thank Dr. Wenbo Yang for help with the ICP measurements.

■ REFERENCES

(1) Stewart, M. P.; Langer, R.; Jensen, K. F. Intracellular Delivery by Membrane Disruption: Mechanisms, Strategies, and Concepts. *Chem. Rev.* **2018**, *118*, 7409−7531.
(2) Varkouhi, A. K.; Scholte, M.; Storm, G.; Haisma, H. J. Endosomal Escape Pathways for Delivery of Biologicals. *J. Control. Release* **2011**, *151*, 220−228.
(3) Cohen, R. N.; van der Aa, M. A. E. M.; Macaraeg, N.; Lee, A. P.; Szoka, F. C. Quantification of Plasmid DNA Copies in the Nucleus after Lipoplex and Polyplex Transfection. *J. Control. Release* **2009**, *135*, 166−174.
(4) Schlich, M.; Palomba, R.; Costabile, G.; Mizrahy, S.; Pannuzzo, M.; Peer, D.; Decuzzi, P. Cytosolic Delivery of Nucleic Acids: The Case of Ionizable Lipid Nanoparticles. *Bioeng. Transl. Med.* **2021**, *6*, No. e10213.
(5) Mellman, I.; Fuchs, R.; Helenius, A. Acidification of the Endocytic and Exocytic Pathways. *Annu. Rev. Biochem.* **1986**, *55*, 663−700.
(6) Li, J.; Røise, J. J.; Zhang, J.; Yang, J.; Kerr, D. L.; Han, H.; Murthy, N. A Novel Fluorescent Surfactant Enhances the Delivery of the Cas9 Ribonucleoprotein and Enables the Identification of Edited Cells. *Chem. Commun.* **2019**, *55*, 4562−4565.
(7) Akishiba, M.; Takeuchi, T.; Kawaguchi, Y.; Sakamoto, K.; Yu, H.-H.; Nakase, I.; Takatani-Nakase, T.; Madani, F.; Gräslund, A.; Futaki, S. Cytosolic Antibody Delivery by Lipid-Sensitive Endosomolytic Peptide. *Nat. Chem.* **2017**, *9*, 751−761.
(8) Samaridou, E.; Heyes, J.; Lutwyche, P. Lipid Nanoparticles for Nucleic Acid Delivery: Current Perspectives. *Adv. Drug Deliv. Rev.* **2020**, *154*−*155*, 37−63.
(9) Khadsai, S.; Seeja, N.; Deepuppha, N.; Rutnakornpituk, M.; Vilaivan, T.; Nakkuntod, M.; Rutnakornpituk, B. Poly(Acrylic Acid)-Grafted Magnetite Nanoparticle Conjugated with Pyrrolidinyl Peptide Nucleic Acid for Specific Adsorption with Real DNA. *Colloids Surf., B* **2018**, *165*, 243−251.
(10) Nakase, I.; Kobayashi, S.; Futaki, S. Endosome-Disruptive Peptides for Improving Cytosolic Delivery of Bioactive Macromolecules. *Pept. Sci.* **2010**, *94*, 763−770.
(11) Hatakeyama, H.; Ito, E.; Akita, H.; Oishi, M.; Nagasaki, Y.; Futaki, S.; Harashima, H. A PH-Sensitive Fusogenic Peptide Facilitates Endosomal Escape and Greatly Enhances the Gene Silencing of SiRNA-Containing Nanoparticles in Vitro and in Vivo. *J. Controlled Release* **2009**, *139*, 127−132.
(12) Kakudo, T.; Chaki, S.; Futaki, S.; Nakase, I.; Akaji, K.; Kawakami, T.; Maruyama, K.; Kamiya, H.; Harashima, H. Transferrin-Modified Liposomes Equipped with a PH-Sensitive Fusogenic Peptide: An Artificial Viral-like Delivery System. *Biochemistry* **2004**, *43*, 5618−5628.
(13) Lou, B.; De Koker, S.; Lau, C. Y. J.; Hennink, W. E.; Mastrobattista, E. MRNA Polyplexes with Post-Conjugated GALA Peptides Efficiently Target, Transfect, and Activate Antigen Presenting Cells. *Bioconjugate Chem.* **2019**, *30*, 461−475.
(14) Murthy, N.; Robichaud, J. R.; Tirrell, D. A.; Stayton, P. S.; Hoffman, A. S. The Design and Synthesis of Polymers for Eukaryotic Membrane Disruption. *J. Controlled Release* **1999**, *61*, 137−143.
(15) Kobayashi, S.; Nakase, I.; Kawabata, N.; Yu, H.-H.; Pujals, S.; Imanishi, M.; Giralt, E.; Futaki, S. Cytosolic Targeting of Macromolecules Using a PH-Dependent Fusogenic Peptide in Combination with Cationic Liposomes. *Bioconjugate Chem.* **2009**, *20*, 953−959.
(16) Murthy, N.; Campbell, J.; Fausto, N.; Hoffman, A. S.; Stayton, P. S. Design and Synthesis of PH-Responsive Polymeric Carriers That Target Uptake and Enhance the Intracellular Delivery of Oligonucleotides. *J. Control. Release* **2003**, *89*, 365−374.
(17) Nie, Y.; Günther, M.; Gu, Z.; Wagner, E. Pyridylhydrazone-Based PEGylation for PH-Reversible Lipopolyplex Shielding. *Biomaterials* **2011**, *32*, 858−869.
(18) Zhu, J.; Qiao, M.; Wang, Q.; Ye, Y.; Ba, S.; Ma, J.; Hu, H.; Zhao, X.; Chen, D. Dual-Responsive Polyplexes with Enhanced Disassembly and Endosomal Escape for Efficient Delivery of SiRNA. *Biomaterials* **2018**, *162*, 47−59.
(19) Chan, C.-L.; Majzoub, R. N.; Shirazi, R. S.; Ewert, K. K.; Chen, Y.-J.; Liang, K. S.; Safinya, C. R. Endosomal escape and transfection efficiency of PEGylated cationic liposome-DNA complexes prepared with an acid-labile PEG-lipid. *Biomaterials* **2012**, *33*, 4928−4935.
(20) Yuan, W.; Li, H. Polymer-Based Nanocarriers for Therapeutic Nucleic Acids Delivery. In *Nanostructures for Drug Delivery*; Andronescu, E., Grumezescu, A. M., Eds.; Micro and Nano Technologies; Elsevier, 2017; Chapter 14, pp 445−460.
(21) Collins, L.; Sawyer, G. J.; Zhang, X.-h.; Gustafsson, K.; Fabre, J. W. In Vitro Investigation of Factors Important for the Delivery of an Integrin-targeted Nonviral Dna Vector in Organ Transplantation1. *Transplantation* **2000**, *69*, 1168−1176.
(22) Zhang, X.; Sawyer, G. J.; Dong, X.; Qiu, Y.; Collins, L.; Fabre, J. W. Thein vivo use of chloroquine to promote non-viral gene delivery to the liver via the portal vein and bile duct. *J. Genet. Med.* **2003**, *5*, 209−218.
(23) Ciobanasu, C.; Siebrasse, J. P.; Kubitscheck, U. Cell-Penetrating HIV1 TAT Peptides Can Generate Pores in Model Membranes. *Biophys. J.* **2010**, *99*, 153−162.
(24) Gilleron, J.; Querbes, W.; Zeigerer, A.; Borodovsky, A.; Marsico, G.; Schubert, U.; Manygoats, K.; Seifert, S.; Andree, C.; Stöter, M.; Epstein-Barash, H.; Zhang, L.; Koteliansky, V.; Fitzgerald, K.; Fava, E.; Bickle, M.; Kalaidzidis, Y.; Akinc, A.; Maier, M.; Zerial, M. Image-based analysis of lipid nanoparticle-mediated siRNA delivery, intracellular trafficking and endosomal escape. *Nat. Biotechnol.* **2013**, *31*, 638−646.
(25) Görl, D.; Würthner, F. Entropically Driven Self-Assembly of Bolaamphiphilic Perylene Dyes in Water. *Angew. Chem., Int. Ed.* **2016**, *55*, 12094−12098.
(26) Wang, T.; Li, Y.; Liu, M. Gelation and self-assembly of glutamate bolaamphiphiles with hybrid linkers: effect of the aromatic ring and alkyl spacers. *Soft Matter* **2009**, *5*, 1066−1073.
(27) Matulis, D.; Rouzina, I.; Bloomfield, V. A. Thermodynamics of Cationic Lipid Binding to DNA and DNA Condensation: Roles of Electrostatics and Hydrophobicity. *J. Am. Chem. Soc.* **2002**, *124*, 7331−7342.
(28) Ritchie, C. D.; Sager, W. F. An Examination of Structure-Reactivity Relationships. In *Progress in Physical Organic Chemistry*; Wiley, 1964; Vol. *2*, pp 323−456.
(29) Naka, K.; Sadownik, A.; Regen, S. L. Molecular Harpoons. Membrane-Disruptive Surfactants That Can Recognize Osmotic Stress in Phospholipid Bilayers. *J. Am. Chem. Soc.* **1993**, *115*, 2278−2286.
(30) Kusonwiriyawong, C.; van de Wetering, P.; Hubbell, J. A.; Merkle, H. P.; Walter, E. Evaluation of PH-Dependent Membrane-Disruptive Properties of Poly(Acrylic Acid) Derived Polymers. *Eur. J. Pharm. Biopharm* **2003**, *56*, 237−246.
(31) Thyberg, J.; Hedin, U.; Stenseth, K. Endocytic Pathways and Time Sequence of Lysosomal Transfer of Macromolecules in

Cultured Mouse Peritoneal Macrophages. *Cell Tissue Res.* **1985**, *241*, 299−303.
(32) von Groll, A.; Levin, Y.; Barbosa, M. C.; Ravazzolo, A. P. Linear DNA Low Efficiency Transfection by Liposome Can Be Improved by the Use of Cationic Lipid as Charge Neutralizer. *Biotechnol. Prog.* **2006**, *22*, 1220−1224.
(33) Buck, J.; Grossen, P.; Cullis, P. R.; Huwyler, J.; Witzigmann, D. Lipid-Based DNA Therapeutics: Hallmarks of Non-Viral Gene Delivery. *ACS Nano* **2019**, *13*, 3754−3782.
(34) Müller, K.; Nahde, T.; Fahr, A.; Müller, R.; Brüsselbach, S. Highly Efficient Transduction of Endothelial Cells by Targeted Artificial Virus-like Particles. *Cancer Gene Ther.* **2001**, *8*, 107−117.
(35) Cardarelli, F.; Digiacomo, L.; Marchini, C.; Amici, A.; Salomone, F.; Fiume, G.; Rossetta, A.; Gratton, E.; Pozzi, D.; Caracciolo, G. The Intracellular Trafficking Mechanism of Lipofectamine-Based Transfection Reagents and Its Implication for Gene Delivery. *Sci. Rep.* **2016**, *6*, 25879.
(36) Rehman, Z. u.; Hoekstra, D.; Zuhorn, I. S. Mechanism of Polyplex- and Lipoplex-Mediated Delivery of Nucleic Acids: Real-Time Visualization of Transient Membrane Destabilization without Endosomal Lysis. *ACS Nano* **2013**, *7*, 3767−3777.
(37) Hunt, M. A.; Currie, M. J.; Robinson, B. A.; Dachs, G. U. Optimizing Transfection of Primary Human Umbilical Vein Endothelial Cells Using Commercially Available Chemical Transfection Reagents. *J. Biomol. Tech.* **2010**, *21*, 66−72.
(38) Song, L. Y.; Ahkong, Q. F.; Rong, Q.; Wang, Z.; Ansell, S.; Hope, M. J.; Mui, B. Characterization of the Inhibitory Effect of PEG-Lipid Conjugates on the Intracellular Delivery of Plasmid and Antisense DNA Mediated by Cationic Lipid Liposomes. *Biochim. Biophys. Acta, Biomembr.* **2002**, *1558*, 1−13.
(39) Gaugain, B.; Markovits, J.; Le Pecq, J.-B.; Roques, B. P. DNA Polyintercalation: Comparison of DNA Binding Properties of an Acridine Dimer and Trimer. *FEBS Lett.* **1984**, *169*, 123−126.
(40) Poliskey, J. A.; Crowley, S. T.; Ramanathan, R.; White, C. W.; Mathew, B.; Rice, K. G. Metabolically Stabilized Double-Stranded MRNA Polyplexes. *Gene Ther.* **2018**, *25*, 473−484.
(41) Kizzire, K.; Khargharia, S.; Rice, K. G. High-Affinity PEGylated Polyacridine Peptide Polyplexes Mediate Potent in Vivo Gene Expression. *Gene Ther.* **2013**, *20*, 407−416.
(42) Bowen, B. P.; Woodbury, N. W. TOTO Binding Affinity Analysis Using Single-molecule Fluorescence Spectroscopy. *Photochem. Photobiol.* **2003**, *78*, 582−586.
(43) Kohata, A.; Hashim, P. K.; Okuro, K.; Aida, T. Transferrin-Appended Nanocaplet for Transcellular SiRNA Delivery into Deep Tissues. *J. Am. Chem. Soc.* **2019**, *141*, 2862−2866.
(44) Kulkarni, J. A.; Thomson, S. B.; Zaifman, J.; Leung, J.; Wagner, P. K.; Hill, A.; Tam, Y. Y. C.; Cullis, P. R.; Petkau, T. L.; Leavitt, B. R. Spontaneous, Solvent-Free Entrapment of SiRNA within Lipid Nanoparticles. *Nanoscale* **2020**, *12*, 23959−23966.
(45) Huggins, M. J.; Kubler, D. G. Kinetics of Hydrolysis of Acetals of Ketones. *J. Org. Chem.* **1975**, *40*, 2813−2815.
(46) Boger, D. L.; Fink, B. E.; Brunette, S. R.; Tse, W. C.; Hedrick, M. P. A Simple, High-Resolution Method for Establishing DNA Binding Affinity and Sequence Selectivity. *J. Am. Chem. Soc.* **2001**, *123*, 5878−5891.

https://doi.org/10.1021/acs.molpharmaceut.1c00579
Mol. Pharmaceutics 2022, 19, 67−79

Supporting Information

Acid-Sensitive Surfactants Enhance the Delivery of Nucleic Acids

Joachim Justad Røise[ab‡], Hesong Han[b‡], Jie Li[b], D. Lucas Kerr[ab], Chung Taing[ab], Kamyar Behrouzi[bc], Maomao He[b], Emily Ruan[ad], Lienna Y. Chan[b], Eli M. Espinoza[b], Sören Reinhard[b], Kanav Thakker[d], Justin Kwon[b], Mohammad R. K. Mofrad[bce] & Niren Murthy[bf*]

a) Department of Chemistry, University of California, Berkeley, Berkeley, CA 94720, USA
b) Department of Bioengineering, University of California, Berkeley, Berkeley, CA 94720, USA
c) Department of Mechanical Engineering, University of California, Berkeley, Berkeley, CA 94720, USA
d) Department of Chemical and Biomolecular Engineering, University of California, Berkeley, Berkeley, CA 94720, USA
e) Molecular Biophysics and Integrative Bioimaging Division, Lawrence Berkeley National Lab, Berkeley, CA 94720
f) Innovative Genomics Institute (IGI), 2151 Berkeley Way, Berkeley, CA 94704, USA
‡ These authors contributed equally

Table of Contents

1. pH-independent hemolytic efficiency of Ald-C8-PEG

Ald-C8-PEG was synthesized (see *Section 12*) in order to confirm that the pH dependency of the caged surfactants is due to the caging PEG chains, as opposed to a pH dependent destabilization of RBC membranes. The hemolytic efficiency was measured at pH 7.5 and 5.5.

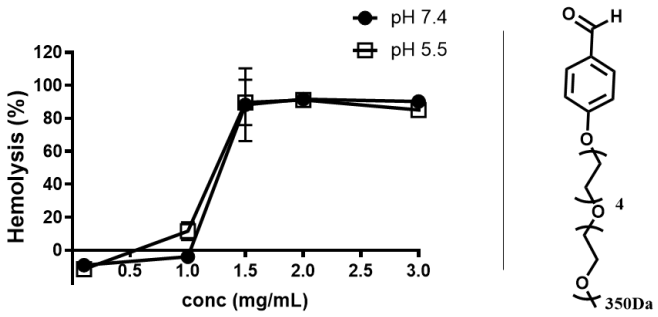

Figure S1: ***Ald-C8-PEG*** *shows pH-independent hemolytic properties.*

2. Molecular dynamics of CS12

Molecular Dynamic (MD) simulations were performed to determine the behavior of **CS12** in physiological conditions. The chemical structure of **CS12** was drawn using MARVIN[1]. As the proposed surfactant is new, we used the CHARMM forcefield database through the CGENFF interface to set the coefficients.[2–5] To prepare input files for the CHARMM database, we used OPENBABEL and PyMOL software.[6,7] After preparing the necessary input files for performing MD, we started to solvate **CS12** inside the water box with a periodic boundary condition in the GROMACS environment. Then, we neutralized our box with Na^+ and Cl^- and equilibrated our system at 300 K and 1 atm by using a modified Berendsen thermostat and Berendsen pressure coupling[8]. Finally, we let **CS12** find its structure freely after 10 ns, with 2 fs timesteps, under physiological conditions. It should be noted, that during 10 ns simulation, the pressure coupling was performed by using a Parrinello-Rahman barostat[9], whereas the Berendsen method was used during equilibration, since the Berendsen method is useful for sudden pressure changes in the system[8]. Finally, we used VMD[10] for molecular visualization and Adobe Photoshop for removing the background and making **Figure S2**.

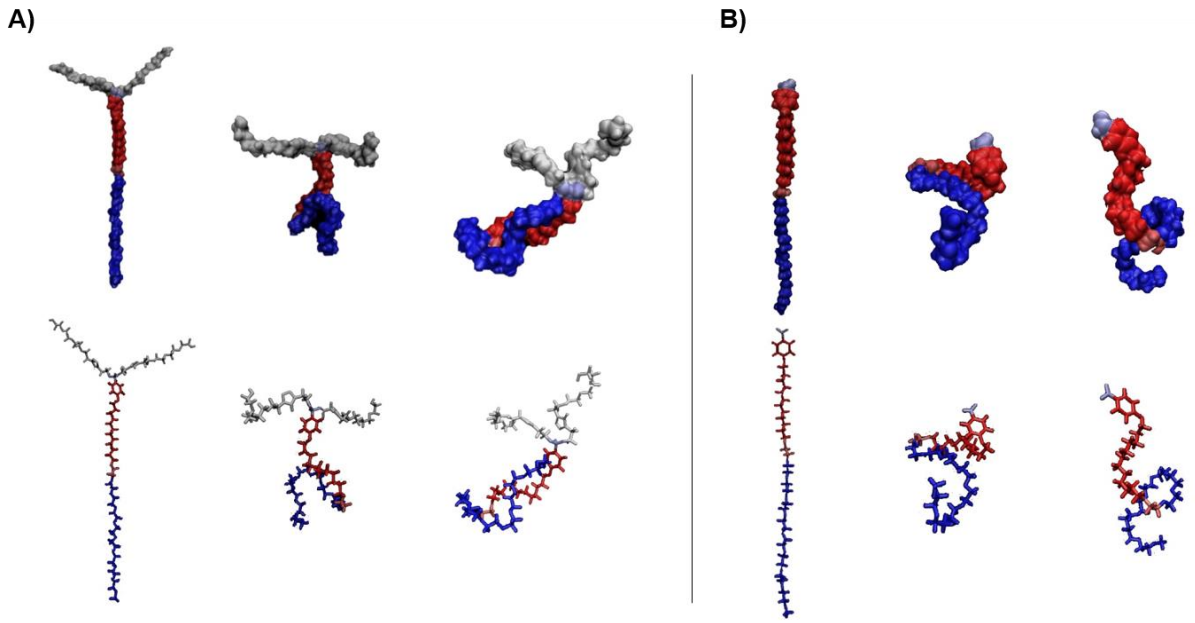

Figure S2: ***Molecular dynamics simulation to obtain molecular structures of CS12 in its intact and hydrolyzed form***. *(A) Molecular dynamics simulation of intact CS12 at* t_0*, after 1ns, and 10ns from left to right. (B) Structure of hydrolyzed* ***CS12*** *at* t_0*, after 1ns, and 10ns from left to right. At top, the surface structure of surfactant is shown and at bottom the licorice structure of caged surfactant has been depicted. Red refers to the hydrophobic domain and blue and white colors depict the hydrophilic (PEG) portions of the molecule.*

3. Measuring Copper content of CS12-DITFAA using ICP

Due to the cytotoxic nature of copper, the copper content of **CS12-DITFAA** was by ICP-OES on a Perkin Elmer 5300 DV optical emission ICP instrument. **CS12-DITFAA** (1mg) was added to 2.5mL of 2% nitric acid. A calibration curve (*Figure S3*) was established using copper standards ranging from 0.01 to 1000mg/L. When compared with the standard curve, the copper concentration was found to be 0.4mg/L in **CS12-DITFAA** stock. This equals roughly 1ppm of copper in **CS12-DITFAA**. This value is near the limit of detection for copper on this instrument.

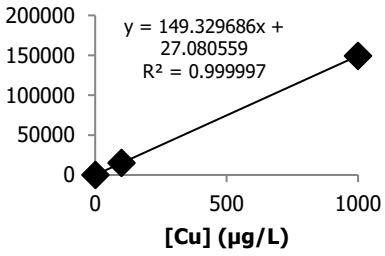

Figure S3: *Calibration curve for Cu content.*

4. Nucleic acid retention gel

mRNA retention by **PCS** was measured by adding **PCS** (6µL, various concentrations) to mRNA (eGFP encoding, 600ng in 2µL) followed by incubation for 1 hour before loading onto a 1% agarose gel. After running at 120V for 30 minutes, the gel was imaged using a Bio-Rad ChemiDoc MP Imaging System using 1:1000 SYBR™ Safe (Thermo Fischer Scientific) as the intercalating imaging agent.

pDNA retention was measured similarly to mRNA retention on an agarose gel (1%). eGFP-pDNA (250ng in 5µL) was added to 5uL of **PCS** at various concentrations. After incubating for 1 hour at room temperature, the gel was run at 120V, and retention was quantified based on the dominant band of free pDNA (*Figure S5*). The efficiency was shown to be 50% retention at roughly N/P=10, which is similar to that of mRNA with a 50% retention efficiency at N/P = 11. Full gels are shown in *Figure S4* (mRNA) and *Figure S5* (pDNA).

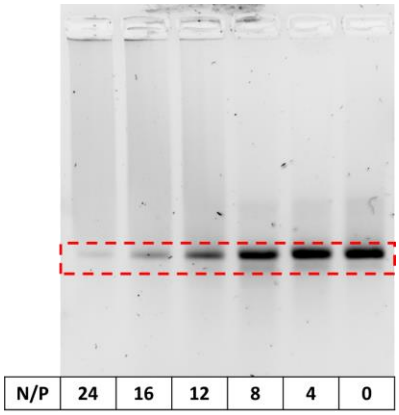

Figure S4: ***PCS retains mRNA on a gel.*** *A) Agarose gel showing retention of mRNA upon addition of PCS. The ratio is given as N/P, referencing the amount of amine groups per phosphate group. 50% retention is achieved at roughly N/P = 11.*

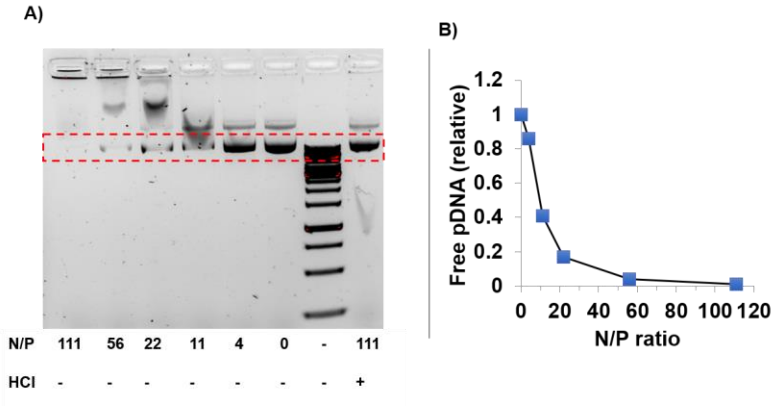

Figure S5: PCS retains pDNA on a gel. A) Agarose gel showing retention of pDNA. B) A plot showing degree of retention of pDNA. A retention efficiency of 50% is achieved around N/P=10. This is similar to the value found for mRNA of N/P=11.

5. Dynamic Light Scattering of PCS

DLS measurements were done by mixing 50 µL (50 µg/mL in PBS) of nucleic acid (mRNA) with 7.5µL of PCS (75 µg in PBS). The mixture was incubated for 30 minutes before adding 1 µL of Lipofectamine 2000. For the measurements of mRNA alone, as well as its complexes with PCS without Lipofectamine, the missing components were replaced with PBS. The measurements were done in triplicate. The complete data, including that of PCS alone, is given in Figure S6. Raw data and polydispersity indexes are given in Table S1.

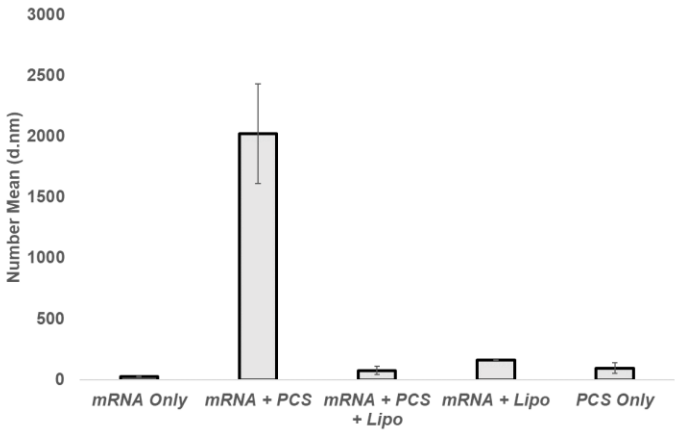

Figure S6: *DLS measurements of mRNA, mRNA+PCS, and mRNA+PCS in the presence of Lipofectamine. A) The data shows a clear dependence of Lipofectamine to achieve efficient packing of nucleic acids, with average size of 77nm for mRNA/PCS/Lipo complexes, compared to 2023nm and for mRNA/PCS complexes.*

Table S1: *Raw data for size and polydispersity indexes of mRNA, mRNA+PCS, mRNA+PCS+Lipo, mRNA+Lipo, and PCS only.*

	mRNA Only		mRNA + PCS		mRNA + PCS + Lipo		mRNA + Lipo		PCS Only	
	Number Mean (d.nm)	PDI	Number Mean (d.nm)	PDI	Number Mean (d.nm)	PDI	Number Mean (d.nm)	PDI	Number Mean (d.nm)	PDI
1	24.59	0.819	2398	0.194	42.94	0.99	166	0.261	100.4	0.599
2	28.44	0.811	1589	0.347	80.17	1	164.1	0.229	51.75	0.697
3	26.15	0.516	2082	0.3	107.4	0.873	160.3	0.229	136.3	0.644
Ave	26.39	0.72	2023.00	0.28	76.84	0.95	163.47	0.24	96.15	0.65

6. Dynamic Light Scattering of TCS

DLS data (size and PDI) was collected as stated in the methods section of the main manuscript. The raw data is found in Table S2.

Table 2: *Raw data for size and polydispersity indexes of siRNA, TCS, and siRNA+TCS.*

	siRNA		TCS		siRNA+TCS	
	Number Mean (d.nm)	PDI	Number Mean (d.nm)	PDI	Number Mean (d.nm)	PDI
1	2.511	0.482	325.4	0.152	61.26	0.667
2	3.322	0.462	248.3	0.527	48.34	0.679
3	1.36	0.467	243.3	0.412	54.53	0.8
Ave	2.40	0.47	272.33	0.36	54.71	0.72

7. Comparison of transfection agents

In addition to Lipofectamine 2000, two additional transfection agents were investigated for their ability to transfect Hela cells (Figure S7). Transfections were performed by mixing together mRNA (0.5µg/mL final concentration), PCS (2µg/mL final concentration) and X-tremeGene™ 360 (low: 0.2µL/mL), TurboFect™ (low: 0.3µL/mL), or Lipofectamine 2000 (low: 0.2 µL/mL). The complexes were added to Hela cells and incubated overnight in OptiMEM. This was compared to mRNA delivered at optimal delivery concentrations for X-tremeGene™ 360 (high: 2µL/mL), TurboFect™ (high: 3µL/mL), and Lipofectamine 2000 (high: 2 µL/mL). Neither X-tremeGene™ 360 or TurboFect™ achieved transfection levels comparable to that of Lipofectamine 2000, which saw roughly 80% transfection at optimal conditions. X-tremeGene™ 360 was the only control transfection reagent with high levels of transfection, which gave roughly 30% transfection, while low levels of transfection agent with PCS only gave around 10% transfection. For TurboFect™ these numbers were 40% for mRNA/transfection agent and 30% for mRNA/TurboFect™/PCS. For flow cytometry histograms for the Lipofectamine data see Figure S9-S12.

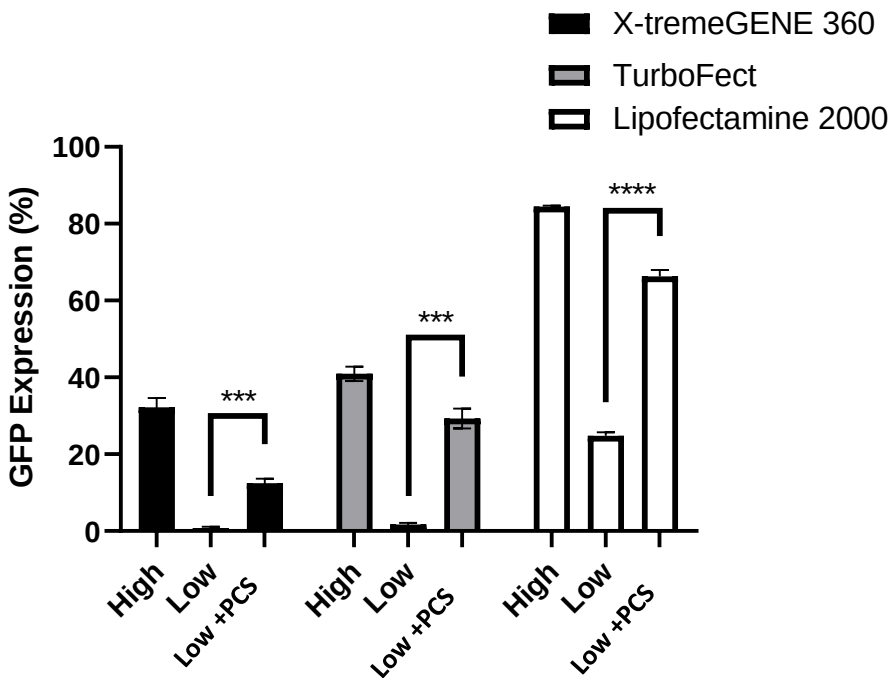

Figure S7: *PCS increases the transfection rate of low levels of both X-tremeGene™ 360 (0.2μL/mL), TurboFect™ (0.3μL/mL) and Lipofectamine 2000 (0.2μL/mL) respectively. High levels of X-tremeGene™ 360, TurboFect™, and Lipofectamine 2000 are 2μL/mL, 3μL/mL and 2μL/mL, respectively. ***P<0.001, ****P<0.0001 (unpaired two-tailed t-test).*

8. Endocytosis Assays

In order to investigate the mechanism of delivery for the mRNA/PCS/Lipo complexes, Hela cells were transfected in the presence of Wortmannin (0.15μg/mL), Chlorpromazine (1.5μg/mL), Genistein (5μg/mL) and methyl-β-cyclodextrin (7.5mg/mL). The inhibitors were incubated with Hela cells for 1hr before replacing the media. The mRNA/PCS/Lipo complexes were prepared by making a mixture of 2μg/mL PCS, 500ng/mL mRNA, and 2μL/mL Lipofectamine 2000. The complex was incubated for 30 minutes before being added to cells and incubated overnight in OptiMEM. A control was done by using only Lipofectamine 2000 for delivery to see if there were any significant changes in delivery mechanism. The inhibitors used and their inhibiting pathways are as follows[11]: (A) Wortmannin - Clathrin-dependent endocytosis (CDE), (B) Chlorpromazine – CDE, (C) Genistein – Clathrin-independent endocytosis (CIE), (D) Methyl-β-cyclodextrin (MβCD) – Cholesterol-dependent uptake mechanisms (CDE and CIE at used concentrations[12]). The results below show that the uptake of the mRNA/PCS/Lipo-complexes happens by a similar mechanism to that of mRNA/Lipo complexes (Figure S8). The uptake is dependent on both Clathrin-dependent and Clathrin-independent endocytosis, as seen in the knock-down in the presence of chlorpromazine and genistein, respectively. This is in agreement with previously reported data.[13] In addition, MβCD caused a total knockdown in transfection efficiency, while maintaining cell viability (data not shown). At high concentrations, MβCD can inhibit both Clathrin-dependent and independent pathways that

are dependent on cholesterol, specifically those that involve lipid raft domains.[14] These results confirm that endocytosis plays an important part in the delivery of mRNA complexed with PCS and Lipofectamine.

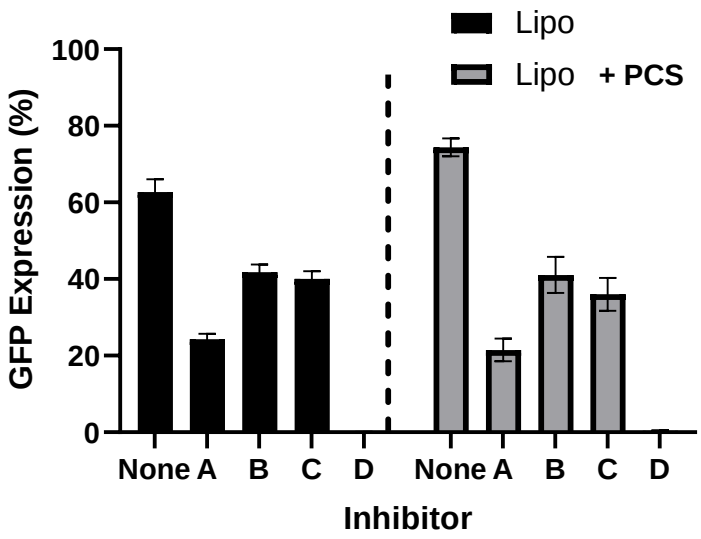

Figure S8: mRNA/PCS/Lipofectamine 2000 in endocytosed by a similar mechanism to Lipofectamine 2000-mediated delivery. The transfection efficiency is dependent on both Clathrin-dependent endocytosis (CDE) and Clathrin-independent endocytosis (CIE). *The following inhibitors were incubated with Hela cells before transfection: (A) Wortmannin - (CDE), (B) Chlorpromazine – CDE, (C) Genistein – (CIE), (D) Methyl-β-cyclodextrin (MβCD) – Cholesterol-dependent uptake mechanisms (CDE and CIE at the concentrations used[12]).*

9. Flow Cytometry Histograms - Hela cells

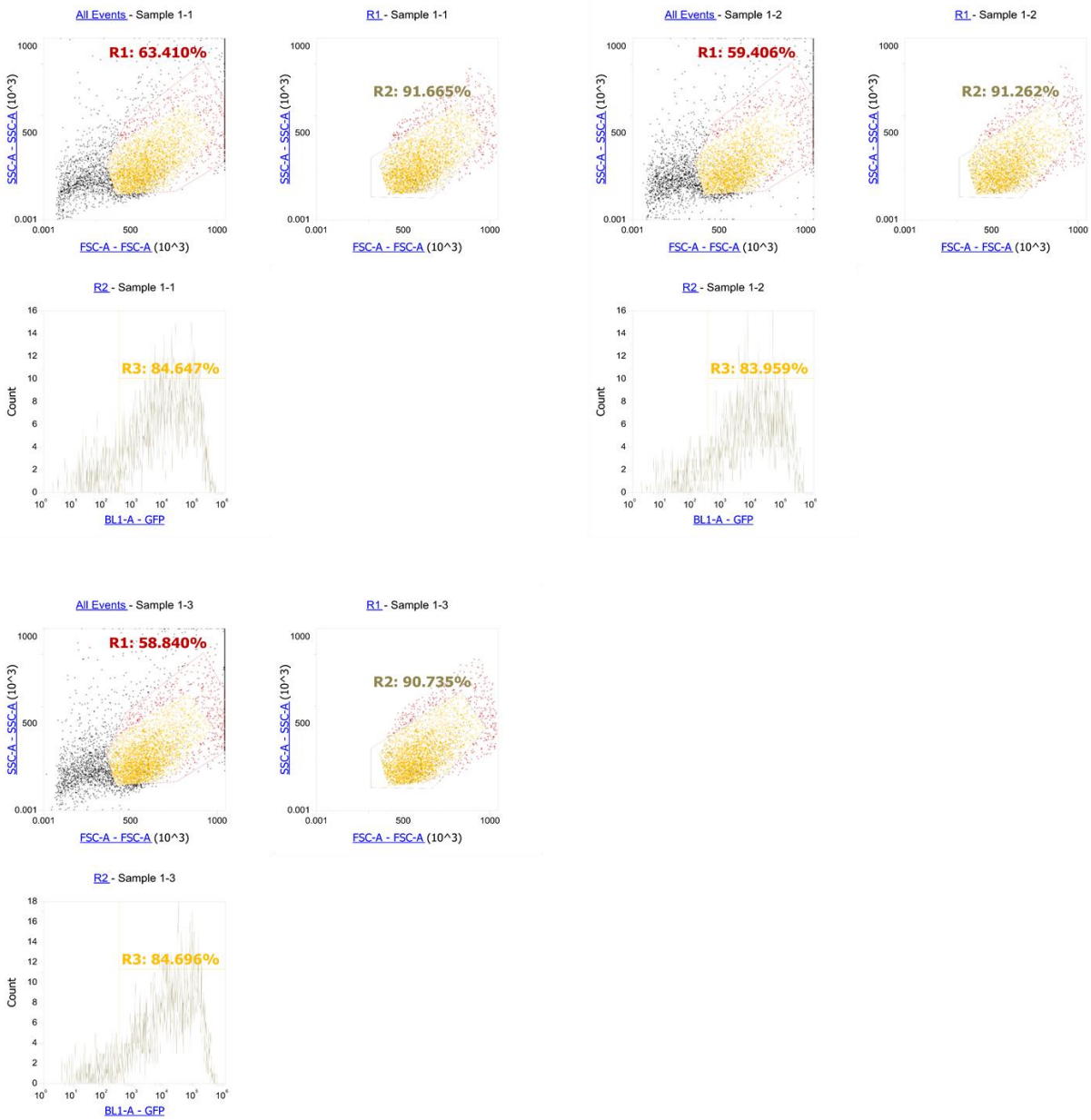

Figure S9: Flow Histograms for Hela cells transfected with GFP-expressing mRNA with Lipofectamine (2mL/mL).

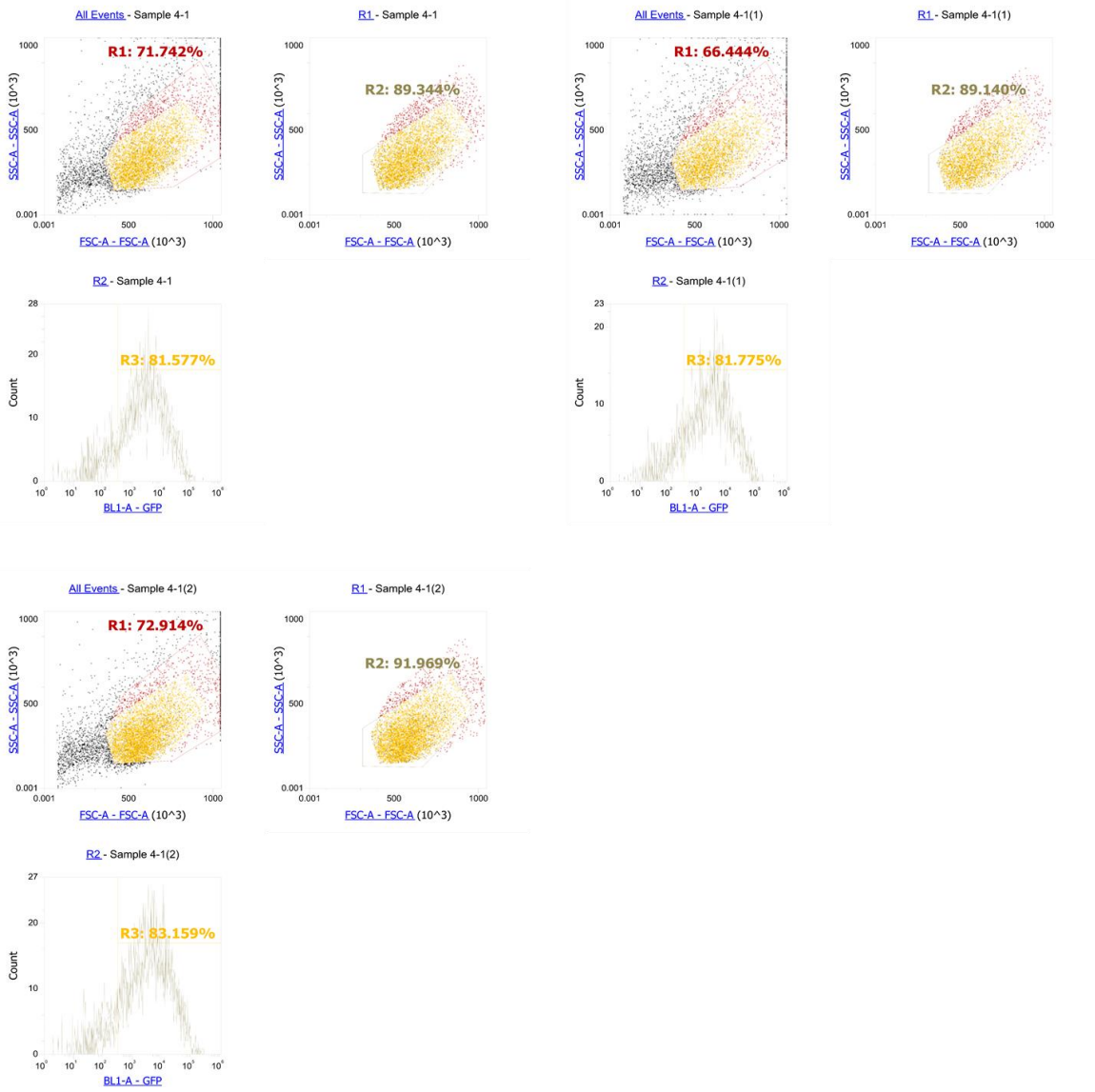

Figure S10: Flow Histograms for Hela cells transfected with GFP-expressing mRNA with Lipofectamine (2mL/mL) and PCS (2μg/mL).

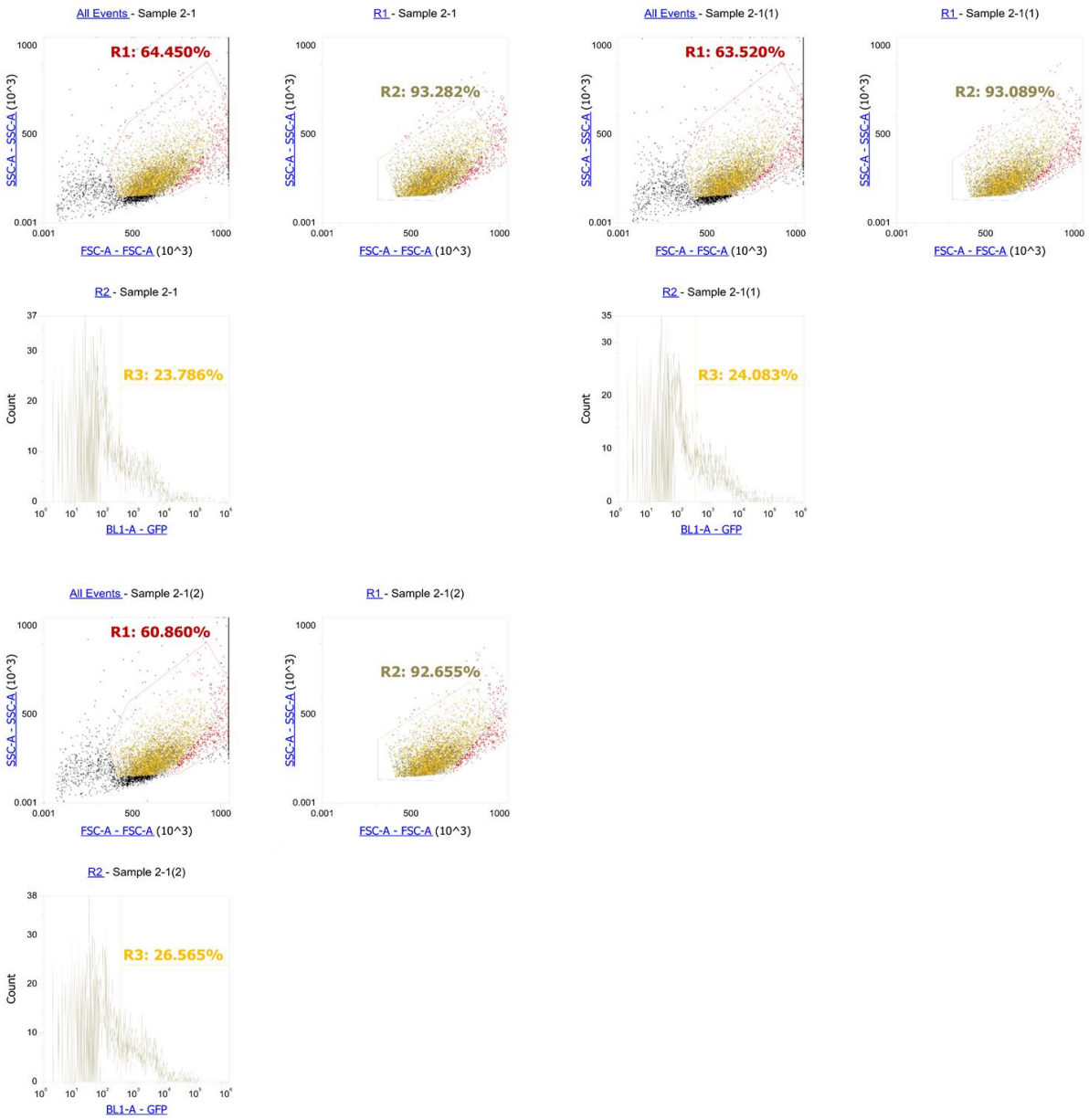

Figure S11: Histograms for Hela cells transfected with GFP-expressing mRNA with Lipofectamine (0.2μL/mL).

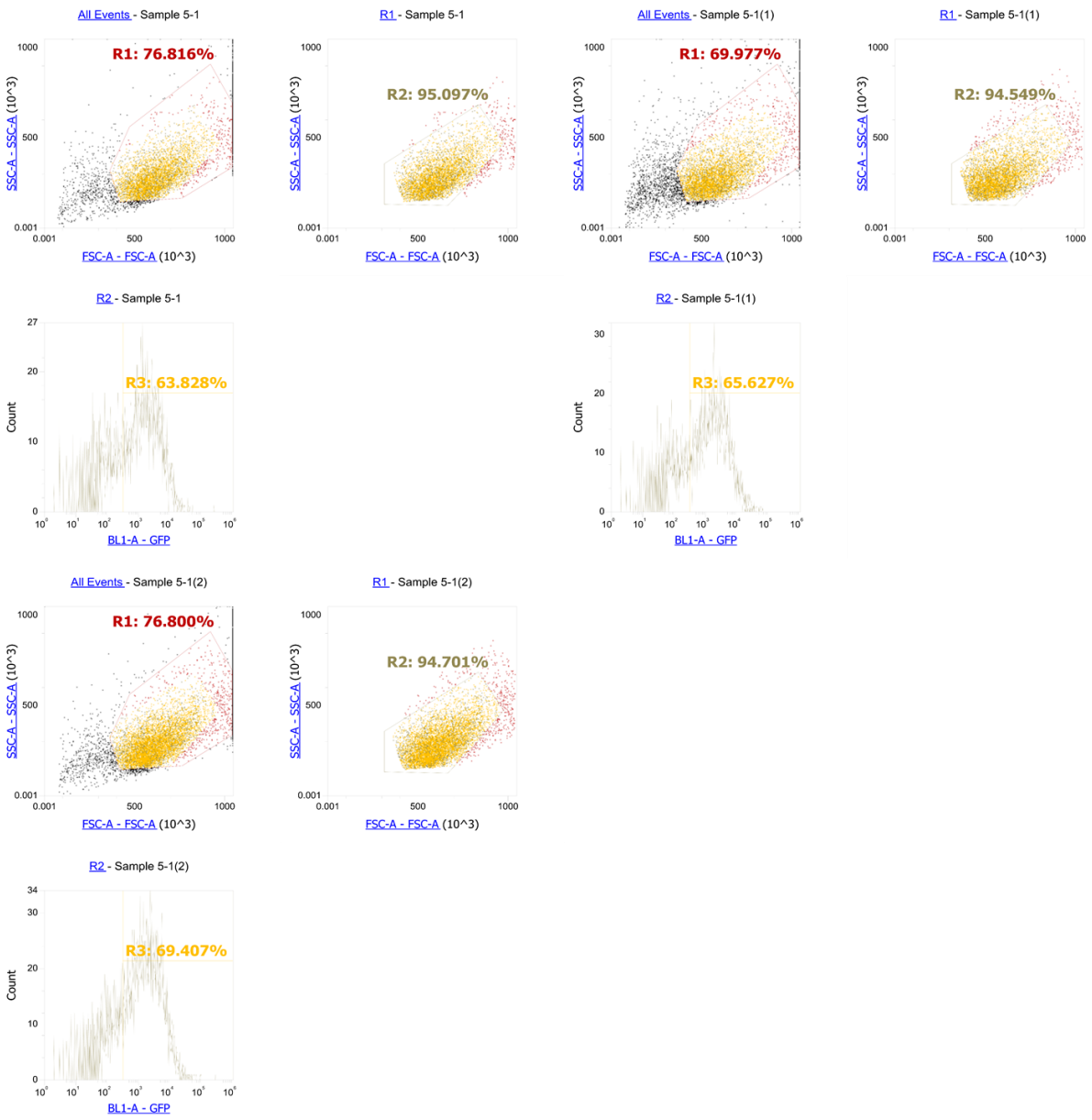

Figure S12: Histograms for Hela cells transfected with GFP-expressing mRNA with Lipofectamine (0.2μL/mL) and PCS (2μg/mL).

10. Hela PCS Cell Toxicity

Hela cells were transfected by first adding **PCS** (2μg/mL) to CleanCap® eGFP mRNA (0.5μg/mL) (Trilink Biotechnologies, San Diego, CA), followed by incubation for 30 minutes at room temperature. Then, Lipofectamine 2000 was added at different amounts followed by an additional 30-minute incubation. The resulting mixture was then added to Hela cells in a 96-well plate in OptiMEM media. The cells were incubated for 24 hours before eGFP expression was measured by flow cytometry. The toxicity of PCS alone was measured on Hela cells using a simple Resazurin assay. As seen in *Figure S13*, this showed a CC50% of roughly 50 μg/mL, which was significantly higher than the concentrations used for mRNA transfections, which was 2 μg/mL.

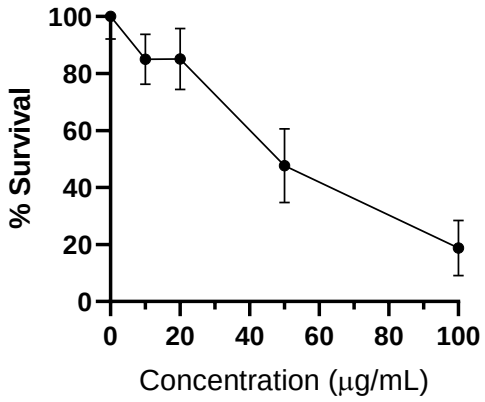

Figure S13: *PCS shows toxicity on Hela cells with a CC50% of roughly 50ug/mL. This is above the concentration used for transfection, which was 2 μg/mL for Hela cells.*

11.Flow Cytometry Histograms - HUVECs

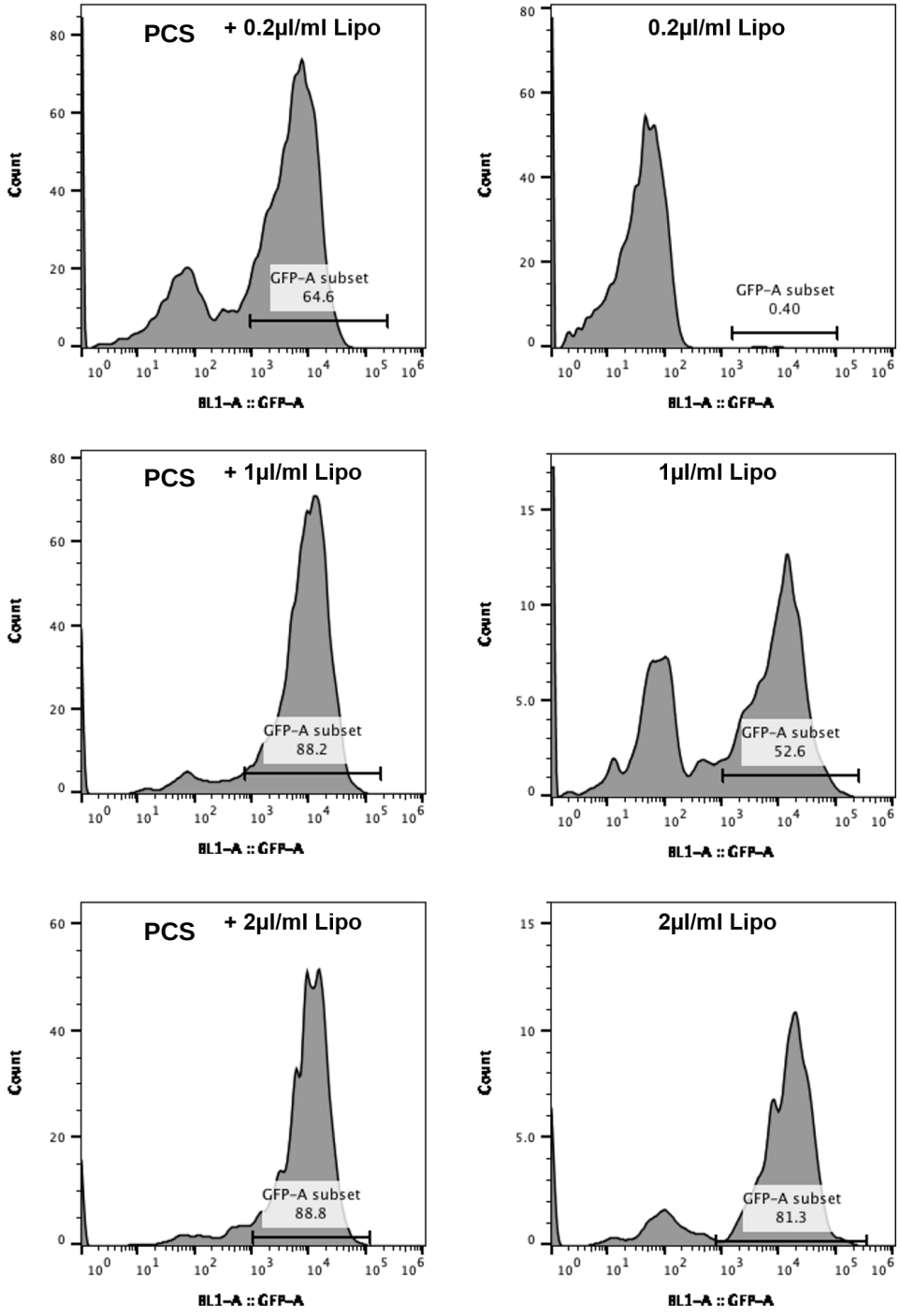

Figure S14: Representative flow cytometry histograms for transfection of HUVECs with PCS/Lipo and Lipofectamine 2000 alone at 0.2, 1, and 2 µL/mL of Lipofectamine. PCS concentrations are kept constant at 2µg/mL. The transfection was expressed as the percentage of positive cells/total cells. This also takes into consideration the toxicity that is caused by Lipofectamine 2000, and is a better measurement of the total efficiency of the system.

12. TCS Toxicity

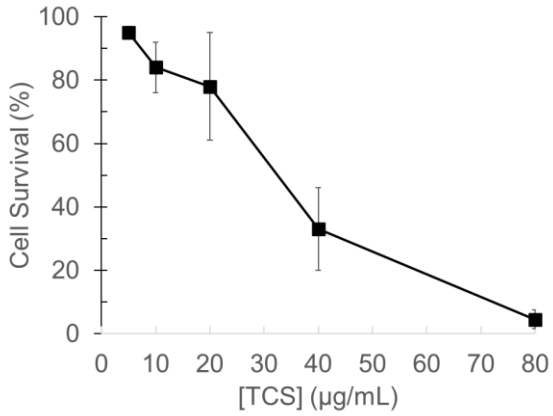

Figure S15: TCS toxicity to Hela cells. The lowest concentration that gave <20% toxicity was at 10µg/mL of TCS after a 24hr incubation and subsequent resazurin assay.

13. siRNA delivery by Lipofectamine

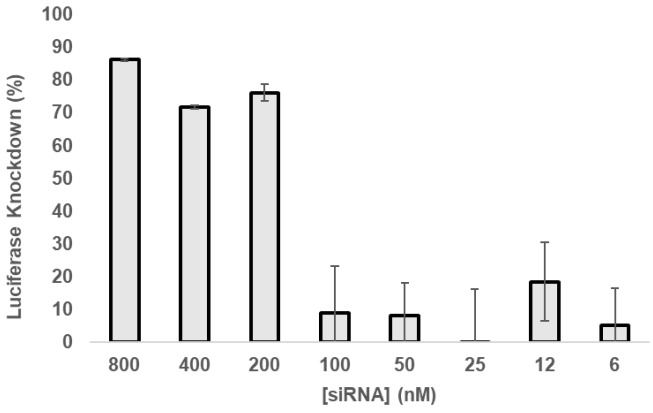

Figure S16: Lipofectamine needs 200nM of siRNA for efficient Luciferase knockdown at same conditions as TCS. In comparison, TCS efficiently delivered siRNA down to 25nM concentrations.

14.Synthesis and Characterization of HO-PEG$_4$-N$_3$

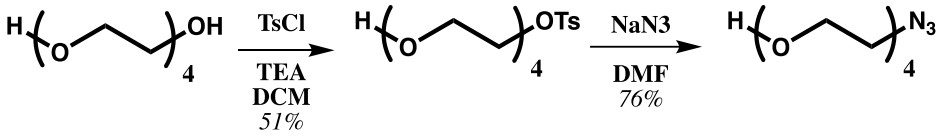

Scheme S1: *Synthetic scheme of HO-PEG4-N$_3$.*

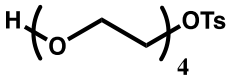

5

2-(2-(2-(2-hydroxyethoxy)ethoxy)ethoxy)ethyl 4-methylbenzenesulfonate (**5**): To a solution of tetraethylene glycol (26.7 mL, 154 mmol, 2 eq) in DCM (500 mL) was added TsCl (14.7 g, 77 mmol, 1 eq) and TEA (41.8 mL, 300 mmol, 3.9 eq). The mixture was stirred at room temperature for 22 hours. The reaction mixture was then washed with saturated ammonium chloride and extracted with additional DCM. The combined organic layers were dried and concentrated. The crude product was purified by flash chromatography (100% DCM) to afford a colorless oil (13.58 g, 62.8 mmol, 51% yield). ^{1}H NMR (600 MHz, Chloroform-d) δ 7.80 (d, J = 8.1 Hz, 2H), 7.34 (d, J = 8.0 Hz, 2H), 4.16 (t, J = 4.8 Hz, 2H), 3.86 – 3.57 (m, 14H), 2.45 (s, 3H), 2.27 (b, 1H). ^{13}C NMR (151 MHz, Chloroform-d) δ 144.94, 133.15, 129.97, 128.14, 72.58, 70.90, 70.82, 70.64, 70.50, 69.39, 68.87, 61.90, 21.80. HRMS (ESI+): Found: 371.1135m/z, Calc: 371.1135m/z for $[C_{15}H_{24}O_7SNa]^+$

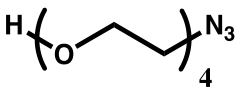

6

2-(2-(2-(2-azidoethoxy)ethoxy)ethoxy)ethan-1-ol (**6**): To a solution of **5** (994.5 mg, 2.85 mmol, 1 eq) in DMF (10 mL) was added sodium azide (986 mg, 15.17 mmol, 5 eq). The mixture was set to reflux at 60ºC for 5 hours, after which it was concentrated and resuspended in water. The mixture was extracted with DCM and washed with water and brine. The organic phase was dried with sodium sulfate, filtered, and concentrated. The resulting crude product was purified by flash chromatography (100% EtOAc to 1:19 MeOH:EtOAc) to yield a colorless oil (477.7 mg, 2.18 mmol, 76% yield). ^{1}H NMR (600 MHz, Chloroform-d) δ 3.73 (t, J = 4.5 Hz, 2H), 3.70 – 3.66 (m, 10H), 3.62 (t, J = 4.5 Hz, 2H), 3.40 (t, J = 5.1 Hz, 2H), 2.13 (b, 1H). ^{13}C NMR (151 MHz, Chloroform-d) δ 72.60, 70.87, 70.84, 70.77, 70.53, 70.21, 61.92, 50.83. HRMS (ESI+): Found: 242.1110 m/z, Calc: 242.1111 m/z for $[C_8H_{17}O_4N_3Na]^+$

15.Synthesis of Ald-C8-PEG

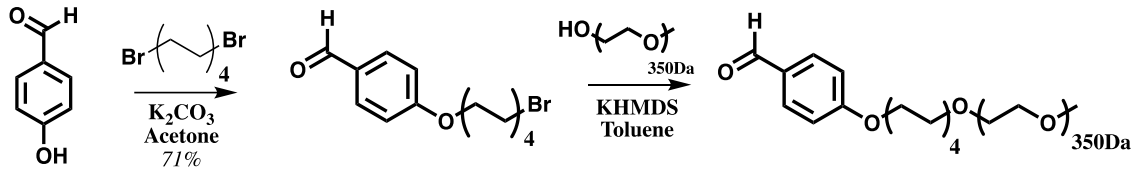

Scheme S2: *Synthetic scheme for Ald-C8-PEG.*

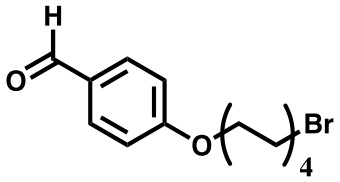

1

4-((8-bromooctyl)oxy)benzaldehyde (**1**): To a solution of 4-hydroxybenzaldehyde (2.4025 g, 19.7 mmol, 1 eq) in acetone (100 mL) was added 1,8-dibromooctane (11 mL, 16 g, 59.4 mmol, 3 eq) and anhydrous potassium carbonate (5.4064 g, 39.1 mmol, 2 eq) . The mixture was set to reflux at 70ºC for 13.5 hours, after which it was concentrated and resuspended in DCM (100 mL). The organic phase was washed with brine (100mL), dried with sodium sulfate, filtered and concentrated. The resulting crude was purified by flash chromatography (100% hexanes to 1:9 EtOAc:hexanes) to yield a colorless solid (4.3620 g, 13.93 mmol, 71 % yield). ^{1}H NMR (400 MHz, Chloroform-d) δ 9.87 (s, 1H), 7.82 (d, J = 8.8 Hz, 2H), 6.98 (d, J = 8.8 Hz, 2H), 4.03 (t, J = 6.5 Hz, 2H), 3.41 (t, J = 6.8 Hz, 2H), 2.04 – 1.74 (m, 4H), 1.56 – 1.30 (m, 8H). ^{13}C NMR (101 MHz, Chloroform-d) δ 190.96, 164.34, 132.13, 129.88, 114.86, 68.46, 34.12, 32.88, 29.27, 29.14, 28.79, 28.20, 26.01. HRMS (EI+): Found: 312.0722m/z, Calc: 312.0725m/z for $[C_{15}H_{21}O_2Br]^+$

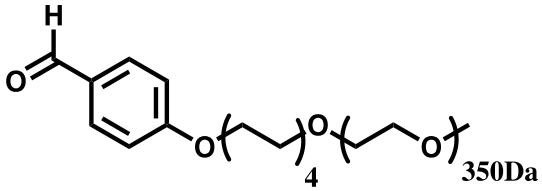

Ald-C8-PEG

*4-((8-(PEG$_{350Da}$)octyl))benzaldehyde (***Ald-C8-PEG)**: To a mixture of HO-PEG$_{350Da}$-OMe (2.124g, 6.07mmol, 0.95eq) in toluene (16mL) was added 4Å molecular sieves. The mixture was cooled to 0ºC under a nitrogen flow, and KHMDS (15% in toluene, 9.31mL, 1.21g, 6.07mmol, 0.95eq) was added dropwise. After stirring for 10 minutes, a mixture of aldehyde (2.003g, 6.36mmol, 1eq) in toluene (12mL) was added dropwise to the mixture. The reaction was then allowed to heat to room temperature overnight while stirring. The reaction was then quenched with sat. NH_4Cl, and extracted into DCM (3x100mL). The organic phases were dried with brine and Na_2SO_4, before purifying by silica column chromatography (DCM:MeOH; 1:0

to 95:5) to yield an orange-tinted oil (205.6mg, 0.35mmol, 6% yield). ^{1}H NMR (400 MHz, Chloroform-*d*) δ 9.88 (s, 1H), 7.82 (d, *J* = 8.8 Hz, 2H), 6.98 (d, *J* = 8.7 Hz, 2H), 4.03 (t, *J* = 6.5 Hz, 2H), 3.67-3.62 (m, 31H), 3.59 – 3.56 (m, 2H), 3.56-3.53 (m, 2H), 3.45 (t, *J* = 6.8 Hz, 2H), 3.38 (s, 3H), 1.84-1.76 (m, 2H), 1.63 – 1.54 (m, 2H), 1.50-1.41 (m, 2H), 1.38 – 1.30 (m, 6H). ^{13}C NMR (101 MHz, $CDCl_3$) δ 190.98, 164.40, 132.14, 114.89, 72.09, 71.62, 70.73, 70.22, 68.53, 59.19, 29.75, 29.52, 29.41, 29.18, 26.17, 26.05. HRMS (ESI+): Found: 639.3711m/z, Calc: 639.3715m/z for $[C_{32}H_{56}O_{11}Na]^{+}$

16.Synthesis of CS12-DITFAA

N3-PEG4-NHCOCF3 (**7**) was synthesized as previously reported[15].

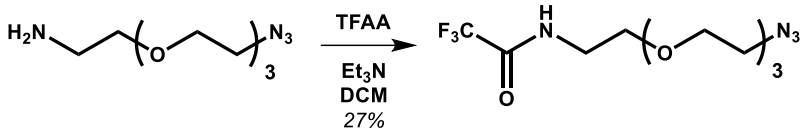

Scheme S3: *Synthetic scheme for the synthesis of* ***N_3-PEG4-NHCOCF$_3$.***

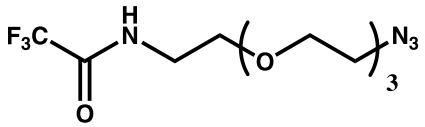

7

N-(2-(2-(2-(2-azidoethoxy)ethoxy)ethoxy)ethyl)-2,2,2-trifluoroacetamide ***(7):*** A mixture of 2-(2-(2-(2-azidoethoxy)ethoxy)ethoxy)ethan-1-amine (2g, 9.2mmol, 1eq) and TEA (1.55mL, 1.13g, 11.2mmol, 1.2eq) in DCM (20mL) was cooled to 0^{o}C under a flow of nitrogen. Then, TFAA (1.55mL, 2.3g, 11mmol, 1.2eq) was added dropwise, and the reaction was left to slowly cool to room temperature overnight. DCM (150mL) and DI H_2O (100mL) were added, and the organic phase was collected. The organic phase was added to sat. $NaHCO_3$ (100mL) and the organic phase was collected, and dried with Na_2SO_4 and concentrated. The crude product was purified by silica chromatography (MeOH:DCM from 2:98 to 5:95) to yield **7** as a colorless oil (784.8mg, 2.5mmol, 27% yield). The ^{1}H and ^{13}C NMR corresponded with that previously reported. ^{1}H NMR (400 MHz, Chloroform-*d*) δ 7.11 (s, 1H), 3.73 – 3.58 (m, 12H), 3.58 – 3.49 (m, 2H), 3.42 – 3.33 (m, 2H). 13C NMR (226 MHz, CDCl3) δ 157.36 (d, J = 37.0 Hz), 116.05 (d, J = 287.9 Hz), 70.84, 70.82, 70.72, 70.48, 70.21, 68.84, 50.81, 39.86. HRMS (ESI+): Found 337.1089m/z, Calc 337.1094m/z for $[C_{10}H_{17}O_4N_4F_3Na]^{+}$.

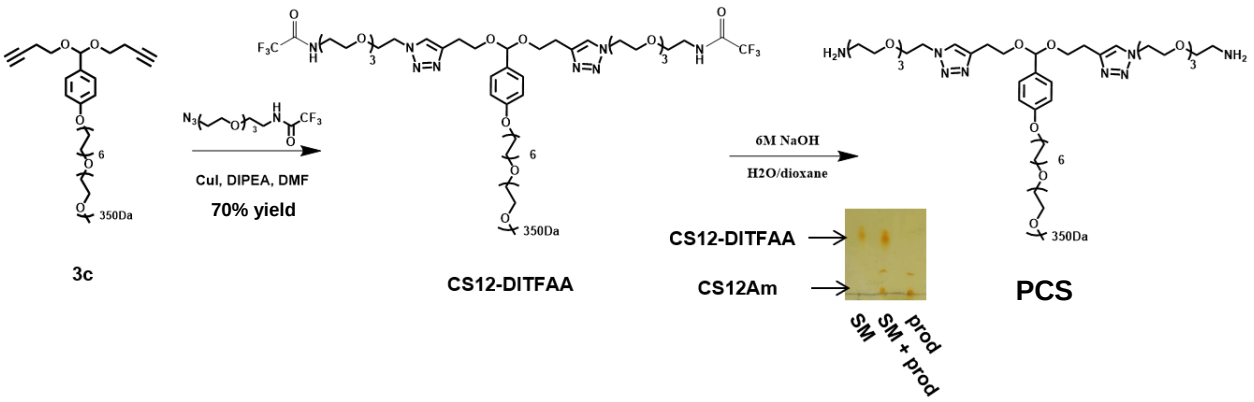

Scheme S4: *Synthetic scheme for PCS.*.

CS12-DITFAA: To a solution of **4c** (301.4mg, 0.4mmol, 1eq) in DMF (2mL) and DIPEA (209µL, 155mg, 1.2mmol, 3eq) was added **7** (499.8mg, 1.6mmol, 4eq) and CuI (15mg, 0.08mmol, 0.2eq). Nitrogen gas was bubbled through the reaction mixture for 30 minutes, and the reaction was set to stir at room temperature for 48 hours before DMF was removed throu gh co-evaporation with toluene (2 x 100mL). The crude product was purified by silica chromatography (MeOH:DCM:TEA from 2:98:0.2 to 5:95:0.2) to yield **CS12-DITFAA** as a clear oil (391mg, 0.28mmol, 70% yield). ^{1}H NMR (400 MHz, MeOD) δ 7.80 (s, 2H), 7.26 (d, J = 8.6 Hz, 2H), 6.86 (d, J = 8.7 Hz, 2H), 5.49 (s, 1H), 4.53 (t, J = 5.0 Hz, 4H), 3.96 (t, J = 6.5 Hz, 2H), 3.85 (t, J = 5.1 Hz, 4H), 3.77 – 3.42 (m, 57H), 3.35 (s, 3H), 2.94 (t, J = 6.5 Hz, 3H), 1.75 (q, J = 7.0 Hz, 2H), 1.56 (q, J = 6.8 Hz, 2H), 1.47 (s, 2H), 1.32 (s, 14H). ^{13}C NMR (226 MHz, MeOD) δ 160.75, 146.17, 131.86, 129.01, 124.81, 115.10, 103.05, 73.68, 72.99, 72.38, 71.65, 71.59, 71.57, 71.53, 71.51, 71.42, 71.38, 71.31, 71.19, 71.13, 70.44, 69.73, 69.03, 65.55, 59.10, 51.77, 51.31, 40.76, 40.72, 30.74, 30.70, 30.58, 30.52, 30.42, 27.23, 10.96. HRMS (ESI+): Found: 1357.6988m/z Calc: 1357.6952m/z for $[C_{60}H_{100}O_{18}N_8F_6Na]^+$.

17. TO-PEG4-N3 Synthesis

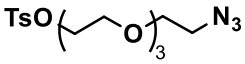

8

2-(2-(2-(2-azidoethoxy)ethoxy)ethoxy)ethyl 4-methylbenzenesulfonate (**8**): Compound **8** was synthesized according to previously reported procedures. Briefly, to a solution of **6** (2.55g, 11.6mmol, 1eq) in DCM (100mL) was added TsCl (5.6249g, 29.5mmol, 2.5eq) and TEA (4.1mL, 2.97g, 29.4mmol, 2.5eq). The reaction was allowed to stir at room temperature overnight. The solution was then added saturated NH4Cl (50mL), and the organic phase was collected. The organic phase was washed with brine (50mL), and the organic phase was further dried with Na2SO4 and concentrated by rotary evaporation. The resulting crude was purified by silica flash chromatography to yield **8** as a colorless oil (3.0558g, 8.2mmol, 71% yield). The NMR and HRMS data matched with that previously reported.

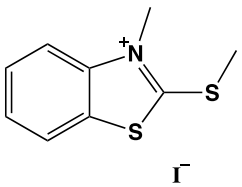

9

3-methyl-2-(methylthio)benzo[d]thiazol-3-ium iodide (**9**): To a round bottom flask containing 2-(methylthio)benzo[d]thiazole (0.5g, 2.76mmol, 1eq) was added iodomethane (515µL, 1.17g, 8.27mmol, 3eq), and the reaction was allowed to stir at 100°C overnight. The resulting mixture was filtered, and the solid was washed with cold diethyl ether. The residue was isolated to give **9** as an off-white fine powder (256.1mg, 0.79mmol, 29% yield). ^{1}H NMR (400 MHz, DMSO-d_6) δ 8.39 (d, J = 8.1 Hz, 1H), 8.20 (d, J = 8.4 Hz, 1H), 7.92 – 7.79 (m, 1H), 7.73 (t, J = 7.7 Hz, 1H), 4.11 (s, 3H), 3.12 (s, 3H). ^{13}C NMR (101 MHz, DMSO) δ 181.25, 142.54, 129.17, 128.26, 127.01, 124.00, 115.73, 36.51, 18.14. HRMS (ESI+): Found: 196.0249m/z Calc: 196.0249m/z for $[C_9H_{10}NS_2]^+$.

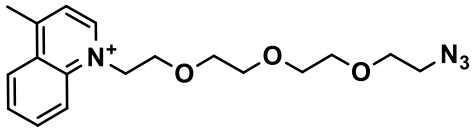

10

1-(2-(2-(2-(2-azidoethoxy)ethoxy)ethoxy)ethyl)-4-methylquinolin-1-ium iodide (**10**): To a solution of lepidine (2.6mL, 2.82g, 19.7mmol, 5eq) was added **8** (1.5009g, 4mmol, 1eq) in ethyl acetate (4mL), and the reaction was allowed to stir at 50°C overnight. The mixture was then concentrated, and directly purified by neutral alumina flash chromatography (2-4% MeOH in DCM) to yield **10** as a blue/purple oil (727mg, 2.1mmol, 53% yield). ^{1}H NMR (900 MHz, MeOD) δ 9.20 (d, J = 6.0 Hz, 1H), 8.58 (dd, J = 8.5, 1.3 Hz, 2H), 8.26 (ddd, J = 8.6, 6.9, 1.4 Hz, 1H), 8.11 – 8.03 (m, 1H), 7.98 (d, J = 6.0 Hz, 1H), 5.24 (t, J = 4.9 Hz, 2H), 4.11 – 4.03 (m, 2H), 3.63 – 3.58 (m, 4H), 3.55 – 3.50 (m, 4H), 3.50 – 3.48 (m, 2H), 3.34 (t, J = 4.9 Hz, 2H), 3.10 – 3.06 (m, 3H). ^{13}C NMR (226 MHz, MeOD) δ 161.06, 150.29, 138.92, 136.50, 130.98, 130.93, 128.28, 123.43, 120.26, 71.73, 71.56, 71.46, 71.02, 69.20, 58.39, 54.81, 51.75, 20.30. HRMS (ESI+): Found: 345.1919m/z Calc: 345.1921m/z for $[C_{18}H_{25}N_4O_3]^+$.

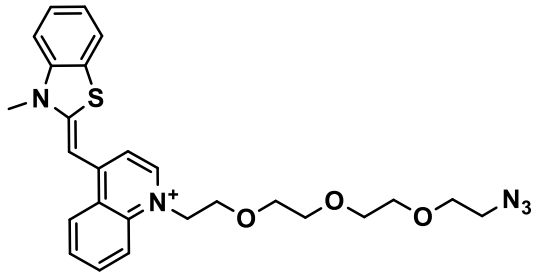

TO-PEG$_4$-N$_3$

(Z)-1-(2-(2-(2-(2-azidoethoxy)ethoxy)ethoxy)ethyl)-4-((3-methylbenzo[d]thiazol-2(3H)-ylidene)methyl)quinolin-1-ium iodide (**TO-PEG4-N3**): To a solution of **9** (99.8mg, 0.31mmol, 1.07eq) and **10** (99.6mg, 0.29mmol, 1eq) in EtOH (4mL) in a nitrogen-purged pressure tube was added TEA (120µL,). The reaction was allowed to stir at 60°C for two hours, and the reaction was then concentrated and purified directly by neutral alumina flash chromatography (0-2% MeOH in DCM) to yield **TO-PEG4-N3** as a red tar (89.6mg, 0.18mmol, 62% yield). ^{1}H NMR (900 MHz, MeOD) δ 8.68 (t, *J* = 8.0 Hz, 1H), 8.43 – 8.38 (m, 1H), 8.13 – 8.07 (m, 1H), 7.99 – 7.93 (m, 1H), 7.90 (t, *J* = 7.8 Hz, 1H), 7.79 – 7.73 (m, 1H), 7.66 (dd, *J* = 14.8, 8.2 Hz, 1H), 7.64 – 7.57 (m, 1H), 7.50 – 7.44 (m, 1H), 7.44 – 7.39 (m, 1H), 6.95 – 6.89 (m, 1H), 4.81 – 4.75 (m, 2H), 4.03 – 3.99 (m, 3H), 3.97 (t, *J* = 5.1 Hz, 2H), 3.64 – 3.59 (m, 2H), 3.58 – 3.54 (m, 4H), 3.52 – 3.48 (m, 4H), 3.28 (t, *J* = 4.9 Hz, 2H). ^{13}C NMR (226 MHz, MeOD) δ 159.23, 148.17, 143.21, 139.03, 136.03, 131.39, 126.54, 125.13, 123.70, 123.21, 122.95, 122.74, 120.73, 116.03, 110.76, 106.33, 86.26, 68.89, 68.68, 68.62, 68.53, 68.10, 66.45, 52.66, 48.75, 31.17. HRMS (ESI+): Found: 492.2058m/z Calc: 492.2064m/z for $[C_{26}H_{30}N_5O_3S]^+$.

18. Mass Spectrometry Data

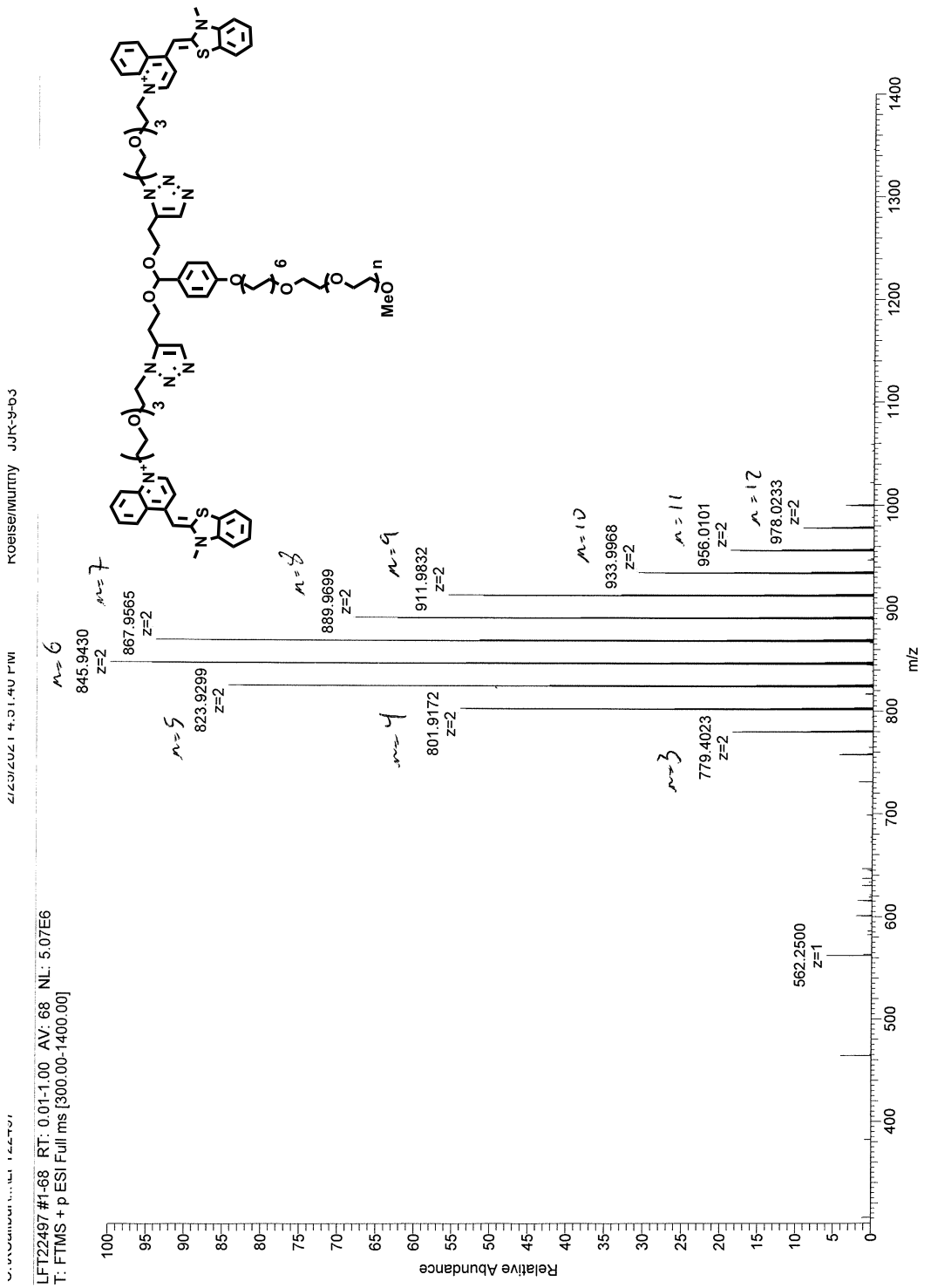

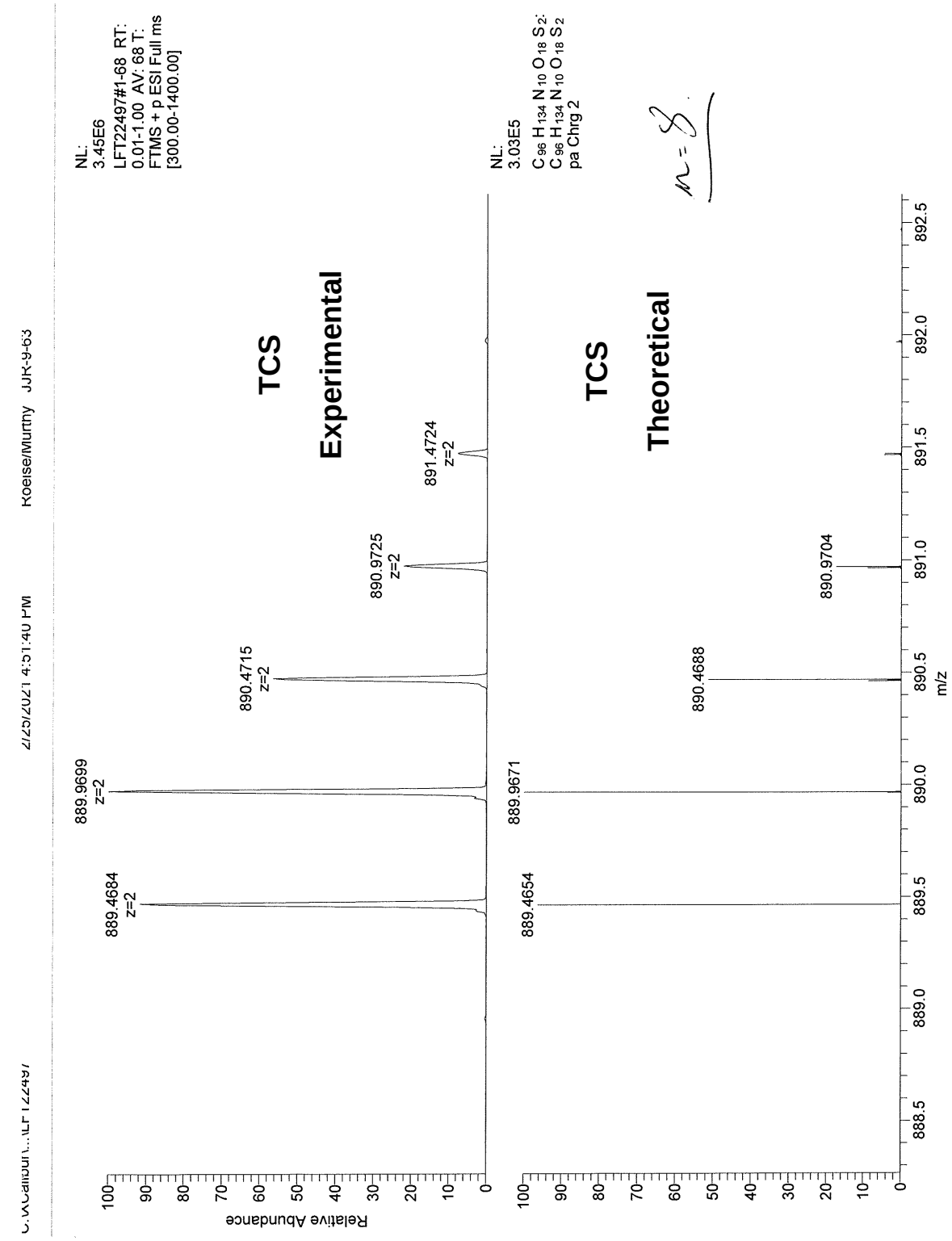
C:\Xcalibur\...\LFT22497
2/25/2021 4:51:40 PM
Koeise/Murthy JJR-9-63
NL:
3.45E6
LFT22497#1-68 RT:
0.01-1.00 AV: 68 T:
FTMS + p ESI Full ms
[300.00-1400.00]
TCS
Experimental
889.9699
z=2
889.4684
z=2
890.4715
z=2
890.9725
z=2
891.4724
z=2
NL:
3.03E5
C96 H134 N10 O18 S2:
C96 H134 N10 O18 S2
pa Chrg 2
TCS
Theoretical
889.9671
889.4654
890.4688
890.9704
Relative Abundance
m/z
n = 8

19. NMR Spectra

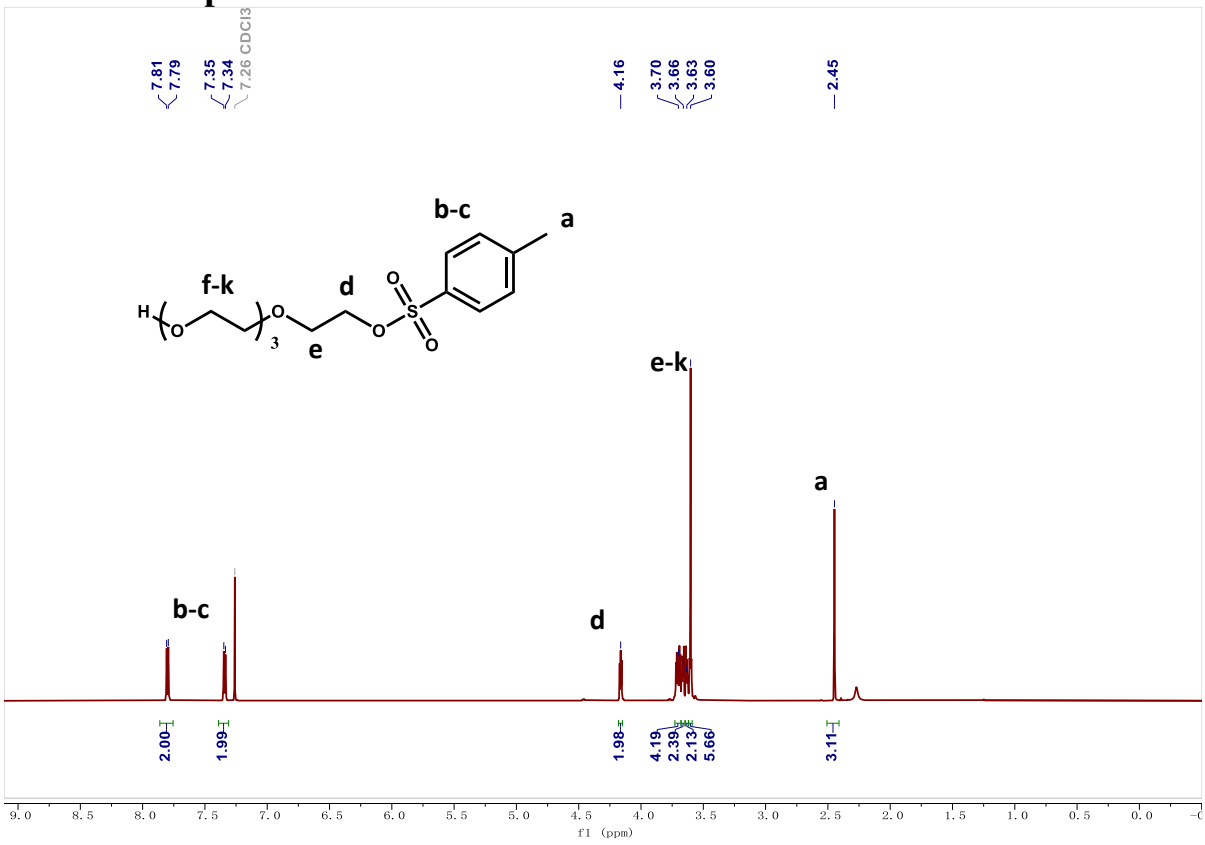

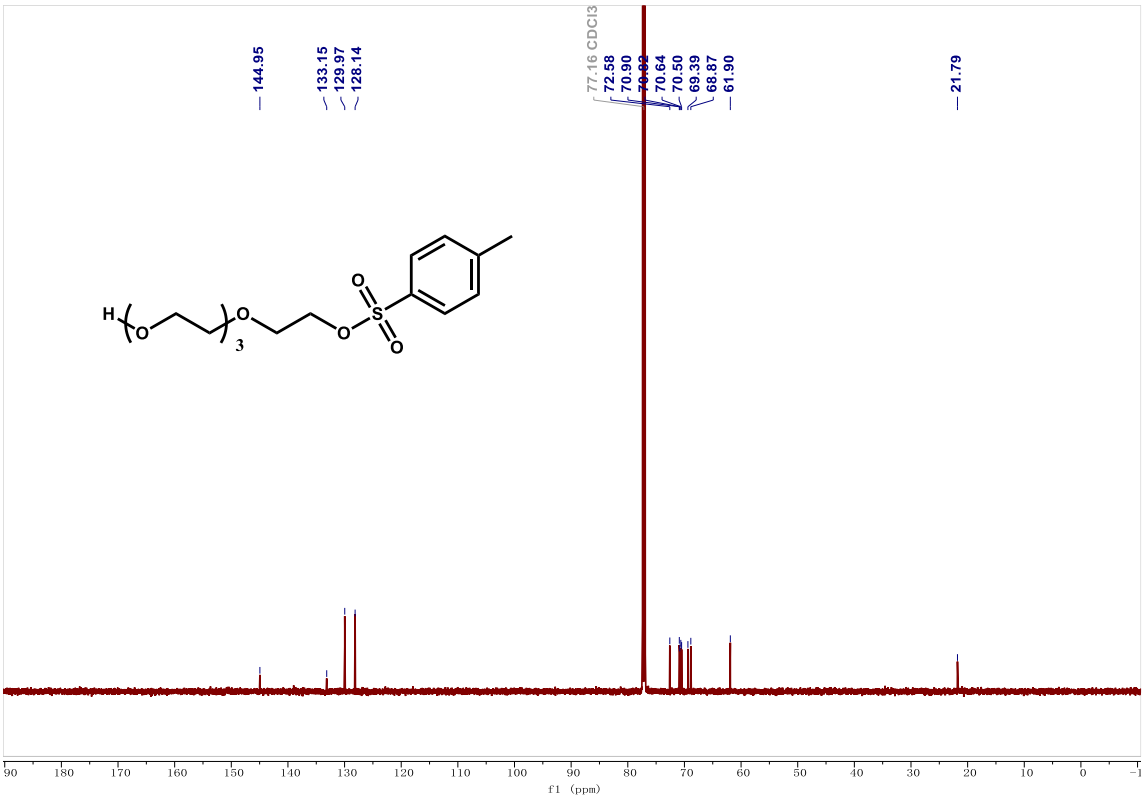

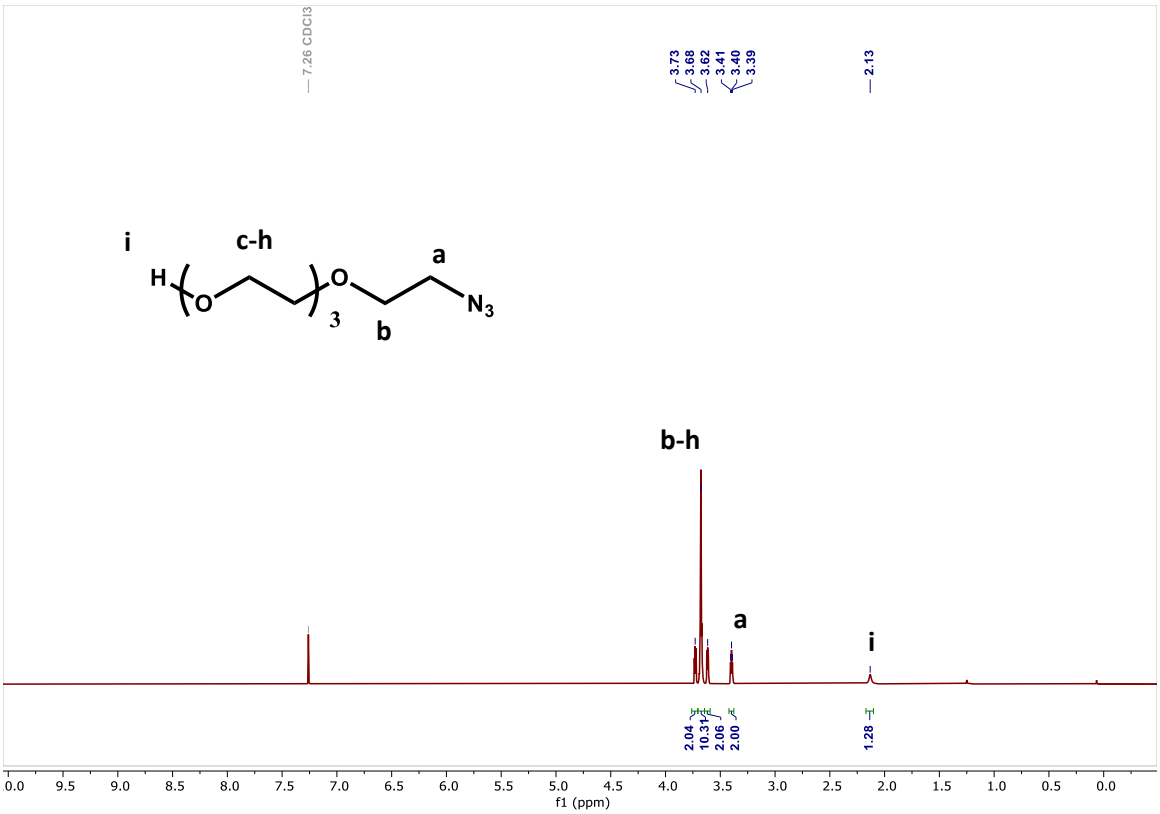
7.26 CDCl3
3.73
3.68
3.62
3.41
3.40
3.39
2.13
i
c-h
a
H
O
O
3
N3
b
b-h
a
i
2.04
10.31
2.06
2.00
1.28
f1 (ppm)

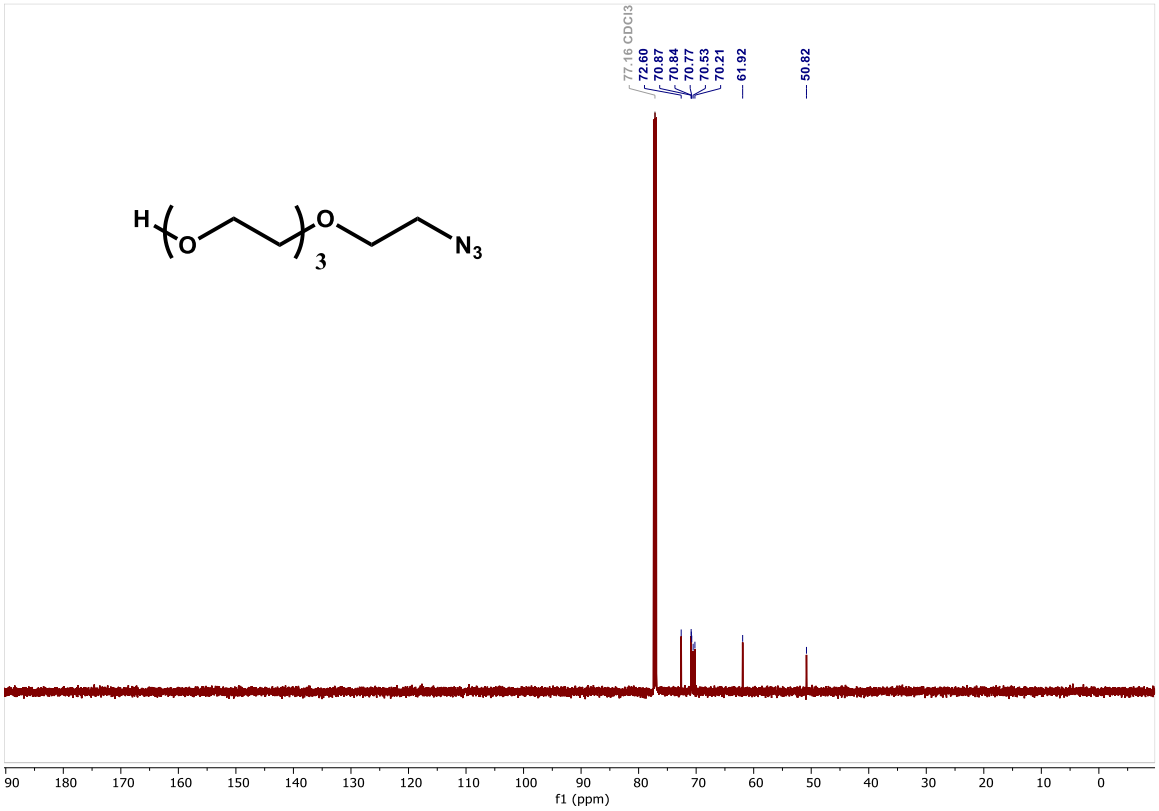
77.16 CDCl3
72.60
70.87
70.84
70.77
70.53
70.21
61.92
50.82
H
O
O
3
N3
f1 (ppm)

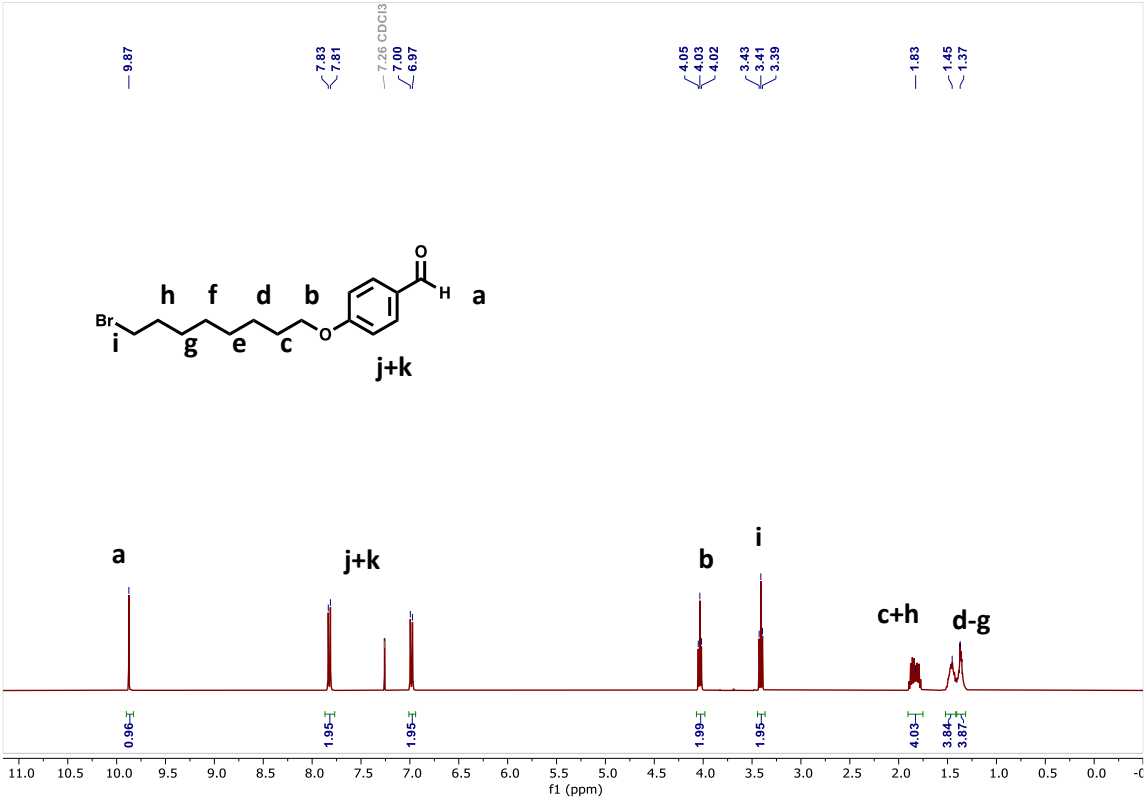
9.87
7.83
7.81
7.26 CDCl3
7.00
6.97
4.05
4.03
4.02
3.43
3.41
3.39
1.83
1.45
1.37
Br
O
H
h f d b a
i g e c
j+k
a
j+k
b
i
c+h
d-g
0.96
1.95
1.95
1.99
1.95
4.03
3.84
3.87
f1 (ppm)

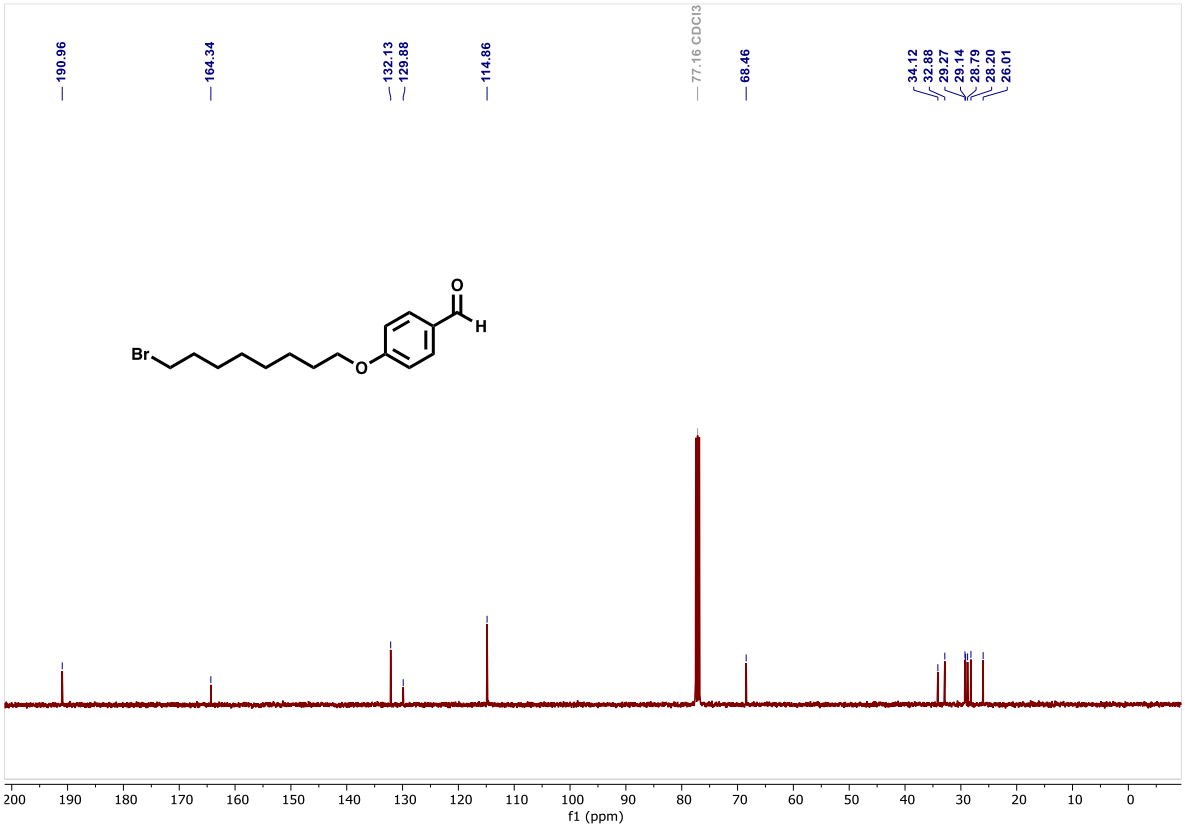
190.96
164.34
132.13
129.88
114.86
77.16 CDCl3
68.46
34.12
32.88
29.27
29.14
28.79
28.20
26.01
Br
O
H
f1 (ppm)

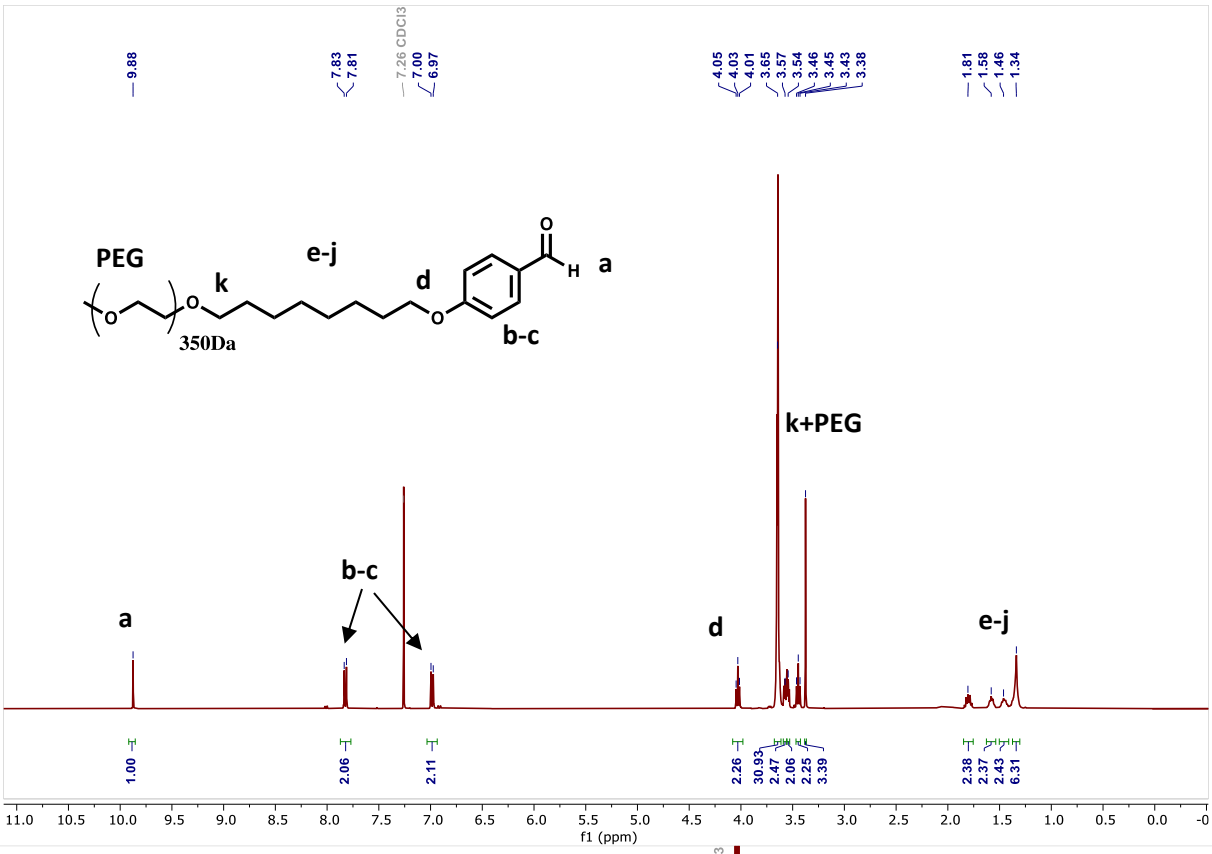
9.88
7.83
7.81
7.26 CDCl3
7.00
6.97
4.05
4.03
4.01
3.65
3.57
3.54
3.46
3.45
3.43
3.38
1.81
1.58
1.46
1.34
PEG
k
e-j
d
a
b-c
350Da
k+PEG
b-c
a
d
e-j
1.00
2.06
2.11
2.26
30.93
2.47
2.06
2.25
3.39
2.38
2.37
2.43
6.31
f1 (ppm)

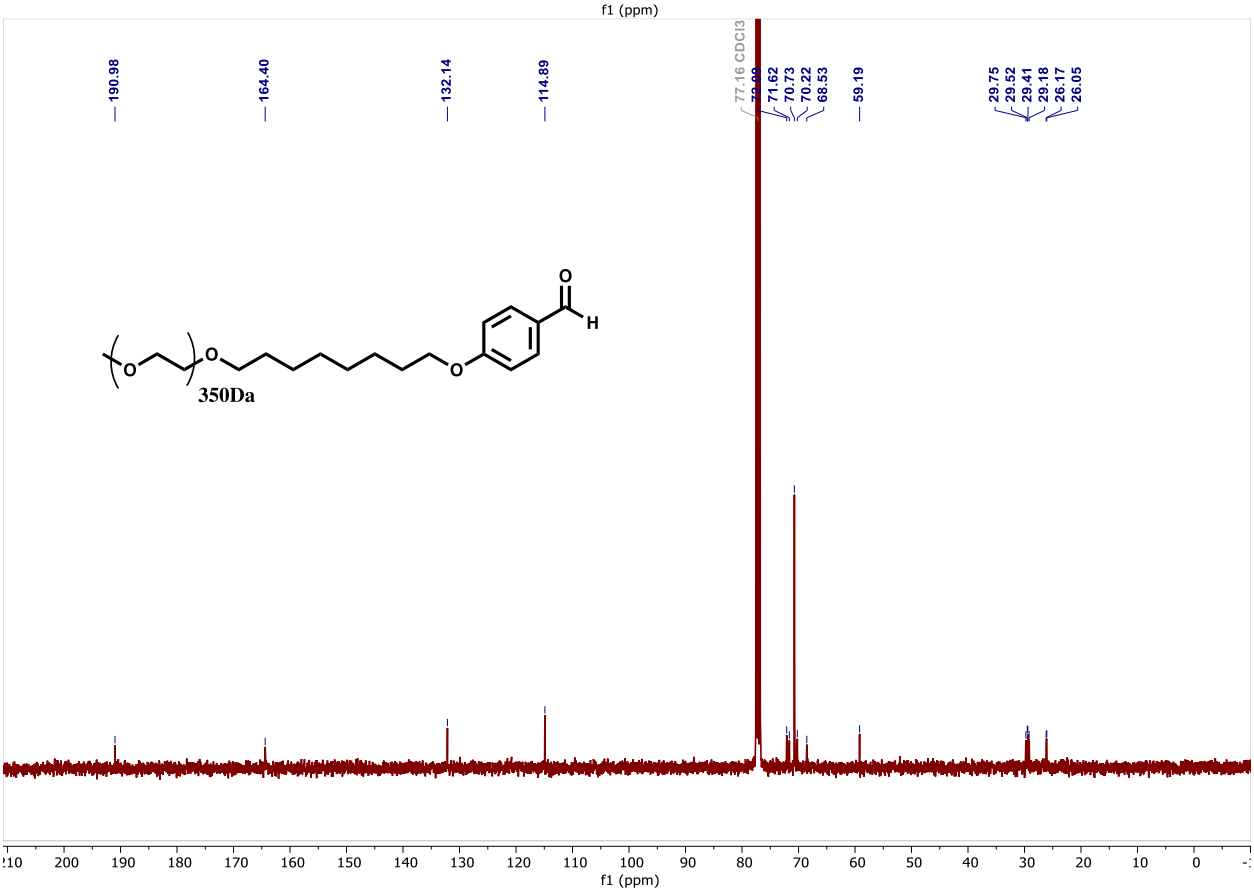
190.98
164.40
132.14
114.89
77.16 CDCl3
71.62
70.73
70.22
68.53
59.19
29.75
29.52
29.41
29.18
26.17
26.05
350Da
f1 (ppm)

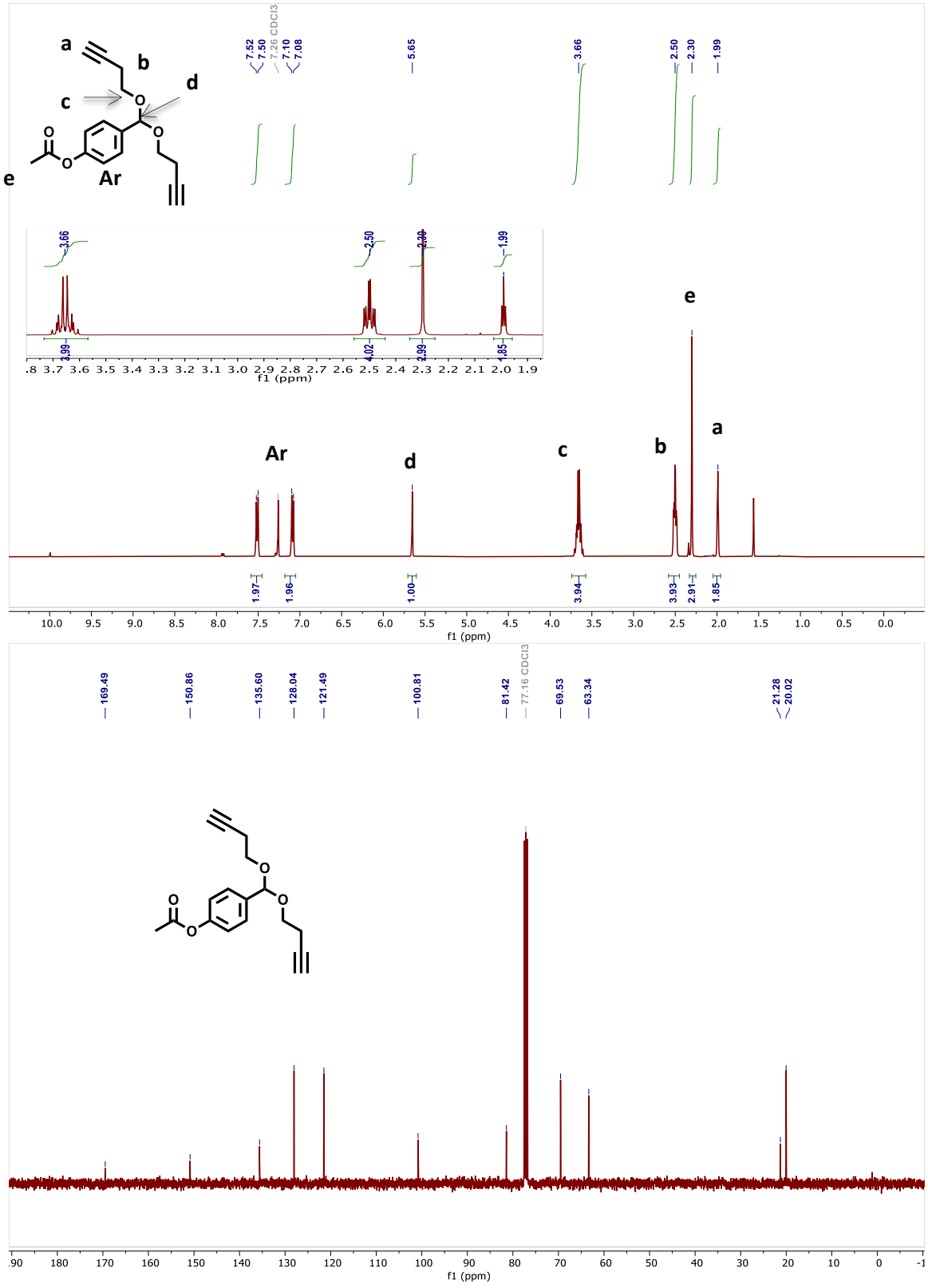
a
b
c
d
e
Ar
7.52
7.50
7.26 CDCl3
7.10
7.08
5.65
3.66
2.50
2.30
1.99
f1 (ppm)
Ar
d
c
b
a
e
1.97
1.96
1.00
3.94
3.93
2.91
1.85
f1 (ppm)
169.49
150.86
135.60
128.04
121.49
100.81
81.42
77.16 CDCl3
69.53
63.34
21.28
20.02
f1 (ppm)

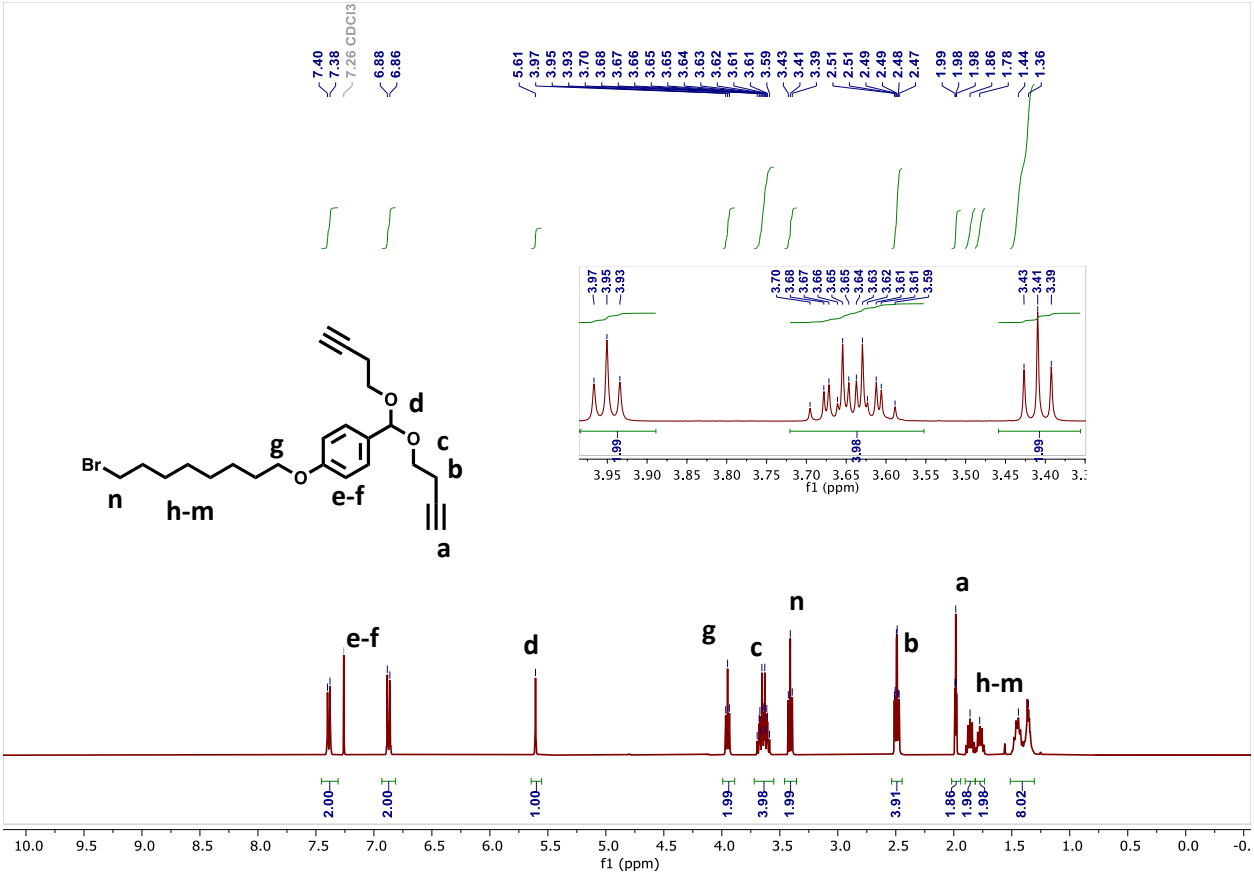
7.40
7.38
7.26 CDCl3
6.88
6.86
5.61
3.97
3.95
3.93
3.70
3.68
3.67
3.66
3.65
3.64
3.63
3.62
3.61
3.59
3.43
3.41
3.39
2.51
2.49
2.48
2.47
1.99
1.98
1.98
1.86
1.78
1.44
1.36
Br
n
h-m
g
e-f
d
c
b
a
e-f
d
g
c
n
b
a
h-m
2.00
2.00
1.00
1.99
3.98
1.99
3.91
1.86
1.98
1.98
8.02
f1 (ppm)

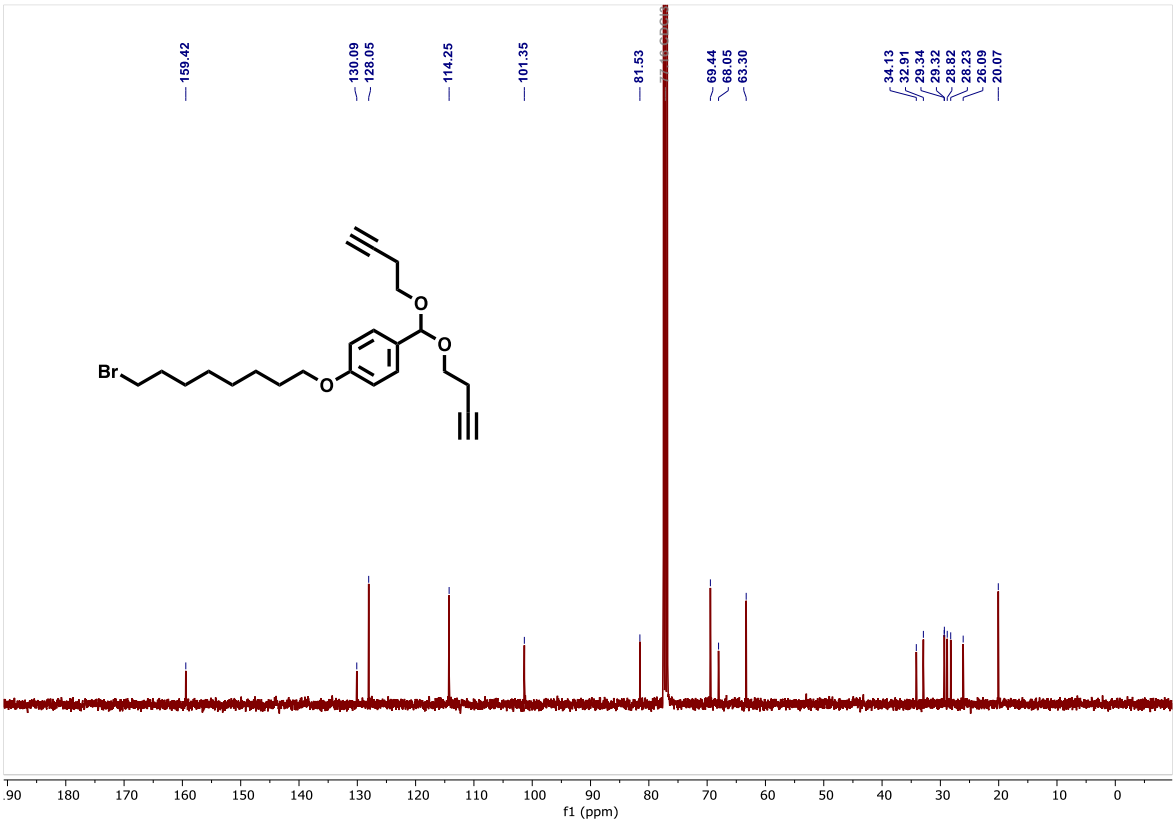
159.42
130.09
128.05
114.25
101.35
81.53
77.00
69.44
68.05
63.30
34.13
32.91
29.34
29.32
28.82
28.23
26.09
20.07
Br
f1 (ppm)

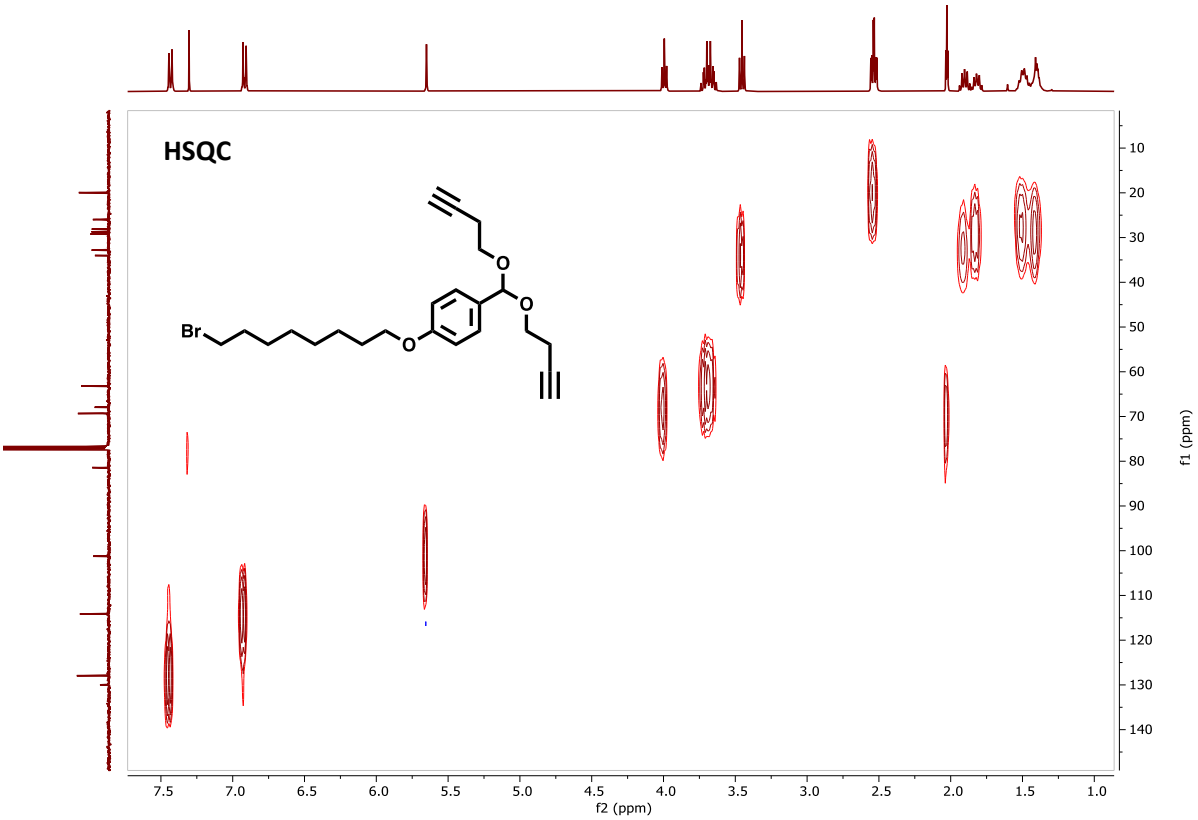
HSQC
Br
O
O
O
f2 (ppm)
f1 (ppm)

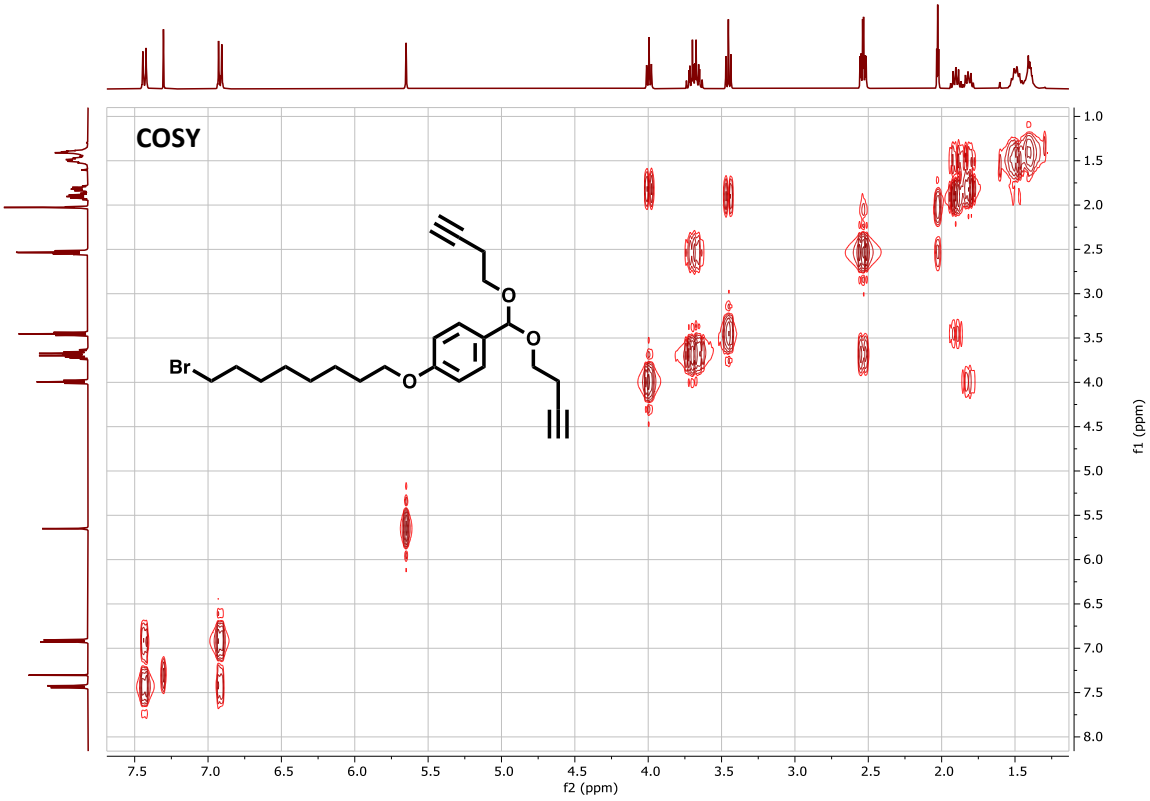
COSY
Br
O
O
O
f2 (ppm)
f1 (ppm)

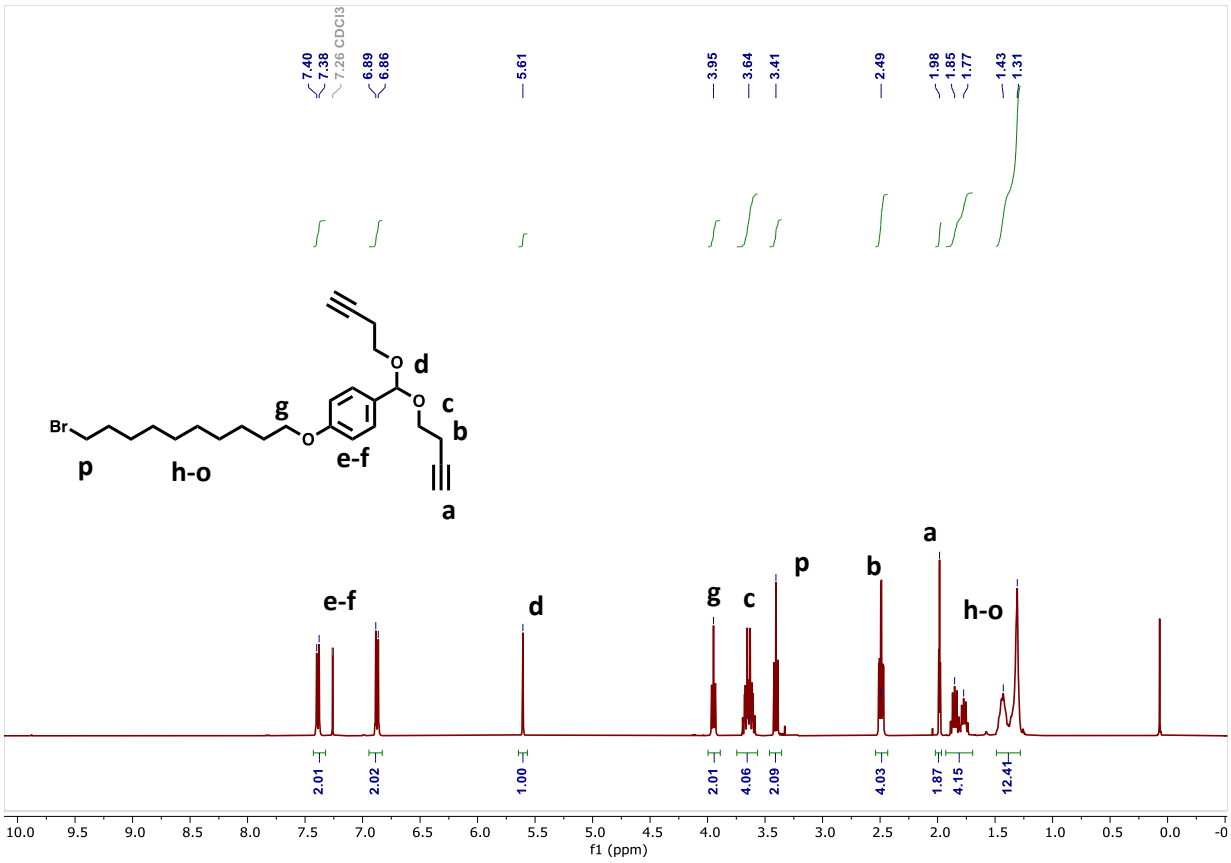
7.40
7.38
7.26 CDCl3
6.89
6.86
5.61
3.95
3.64
3.41
2.49
1.98
1.85
1.77
1.43
1.31
Br
p
h-o
g
e-f
d
c
b
a
2.01
2.02
1.00
2.01
4.06
2.09
4.03
1.87
4.15
12.41
f1 (ppm)

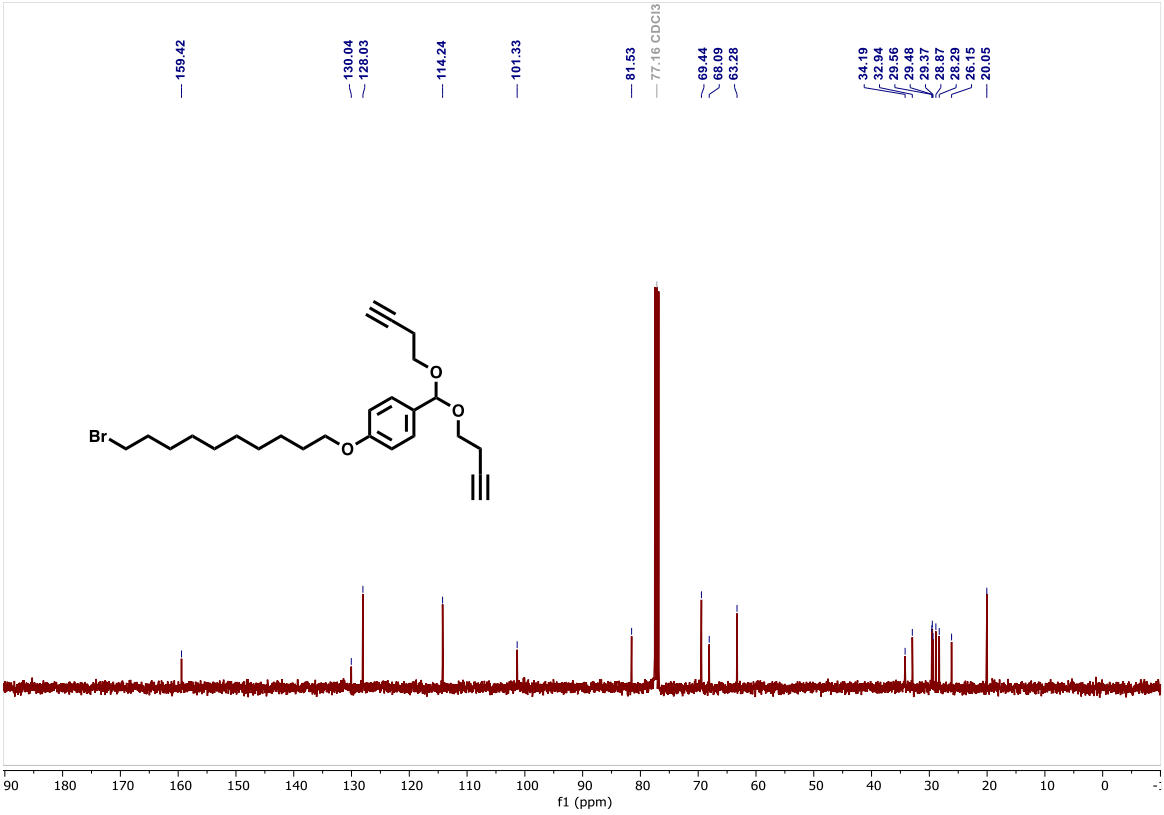
159.42
130.04
128.03
114.24
101.33
81.53
77.16 CDCl3
69.44
68.09
63.28
34.19
32.94
29.56
29.48
29.37
28.87
28.29
26.15
20.05
Br
f1 (ppm)

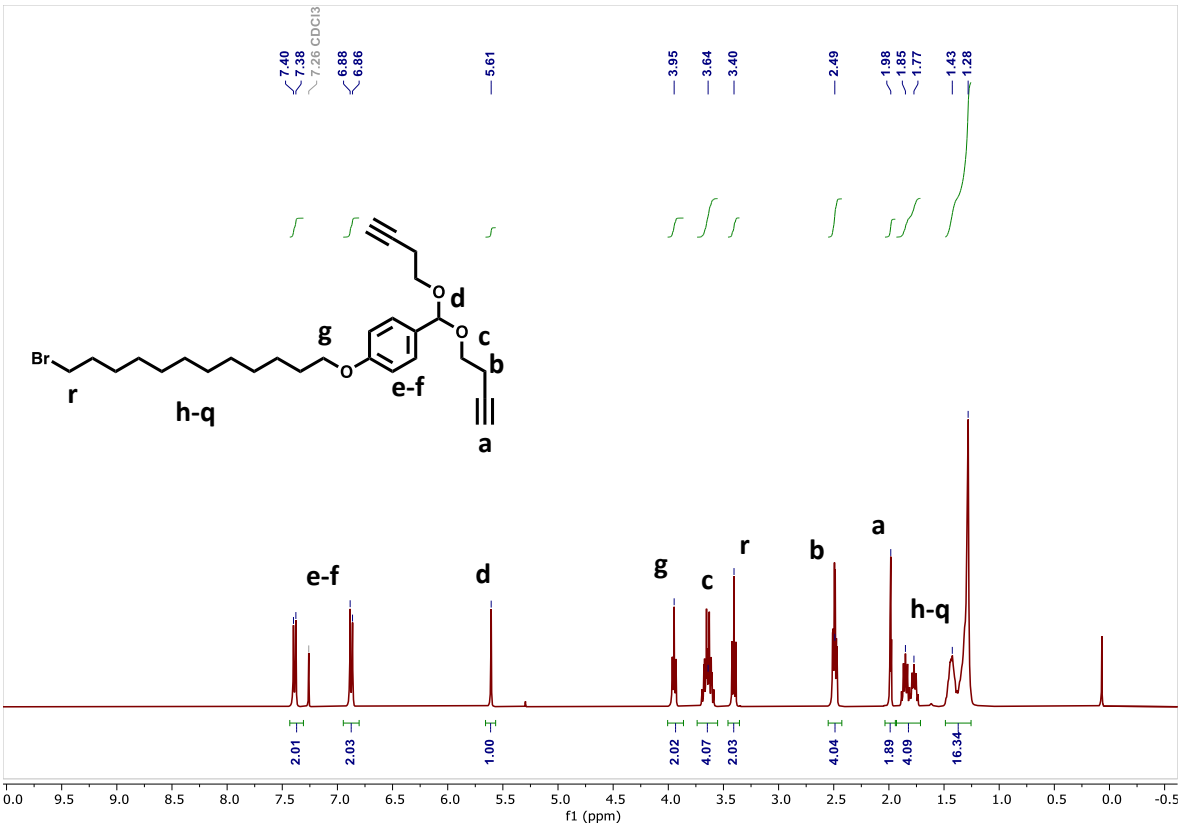
7.40
7.38
7.26 CDCl3
6.88
6.86
5.61
3.95
3.64
3.40
2.49
1.98
1.85
1.77
1.43
1.28
Br
r
h-q
g
e-f
d
O
c
b
a
e-f
d
g
c
r
b
a
h-q
2.01
2.03
1.00
2.02
4.07
2.03
4.04
1.89
4.09
16.34
f1 (ppm)

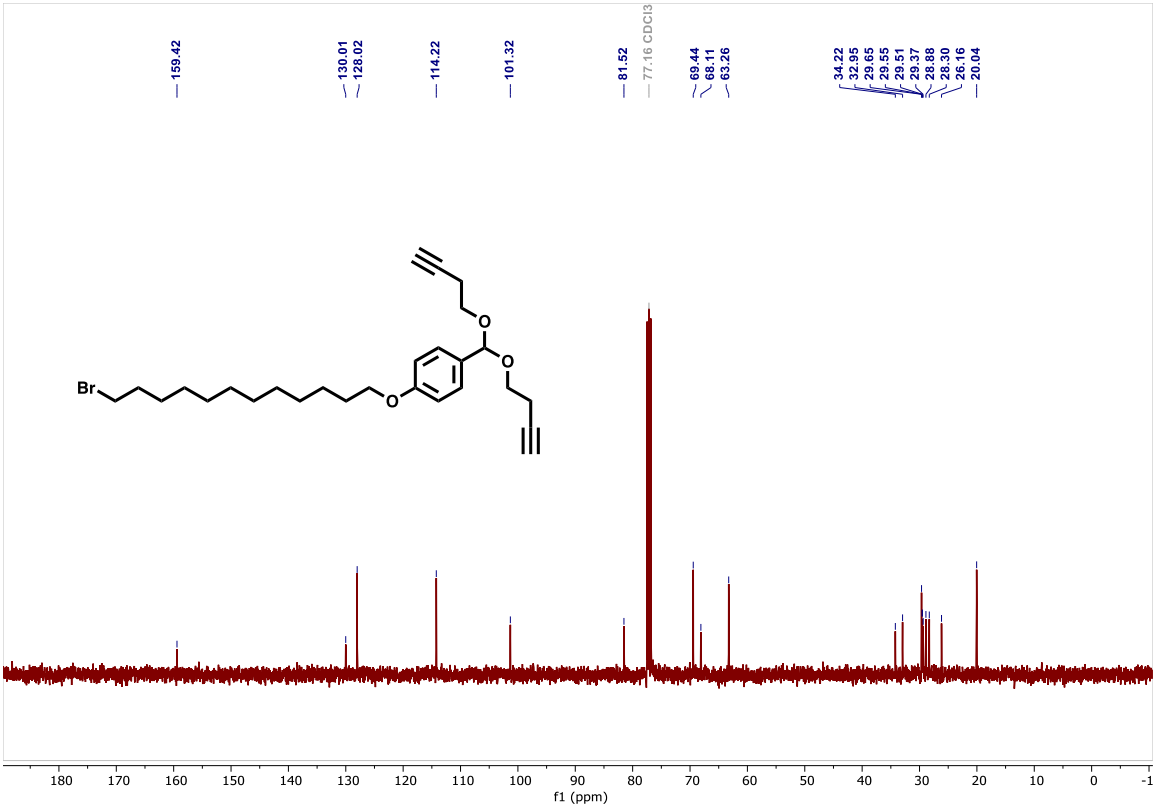
159.42
130.01
128.02
114.22
101.32
81.52
77.16 CDCl3
69.44
68.11
63.26
34.22
32.95
29.65
29.55
29.51
29.37
28.88
28.30
26.16
20.04
Br
O
f1 (ppm)

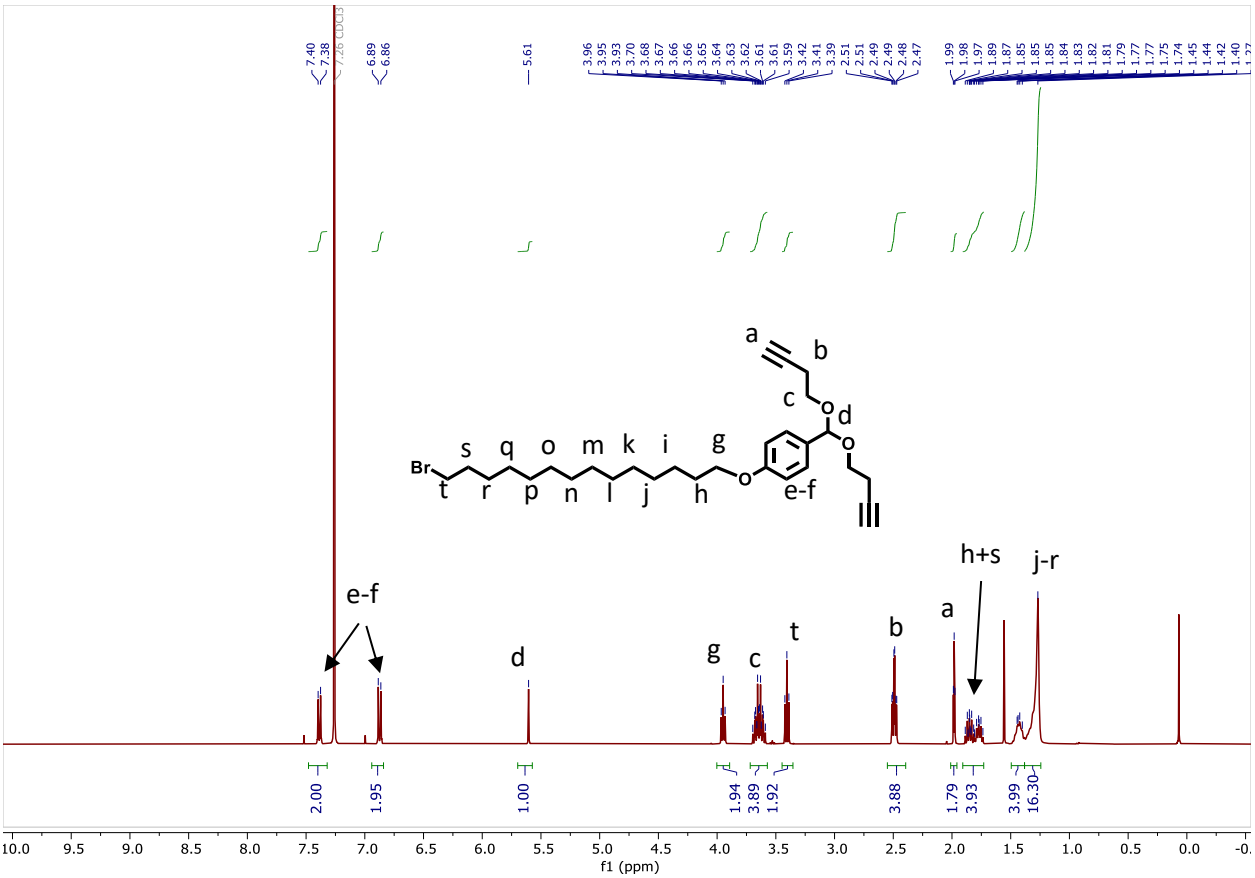
a
b
c
d
s q o m k i g
Br
t r p n l j h
e-f
e-f
d
g
c
t
b
a
h+s
j-r
2.00
1.95
1.00
1.94
3.89
1.92
3.88
1.79
3.93
3.99
16.30
f1 (ppm)

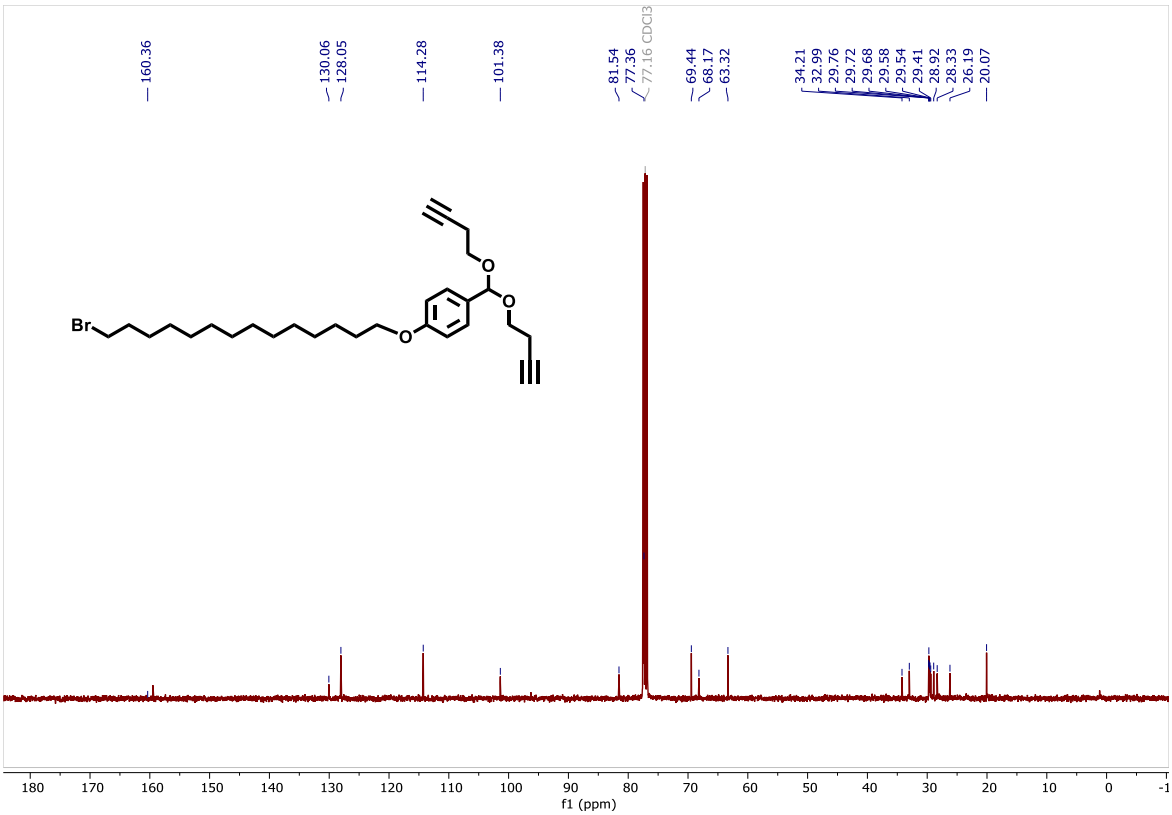
160.36
130.06
128.05
114.28
101.38
81.54
77.36
77.16 CDCl3
69.44
68.17
63.32
34.21
32.99
29.76
29.72
29.68
29.58
29.54
29.41
28.92
28.33
26.19
20.07
Br
O
O
O
f1 (ppm)

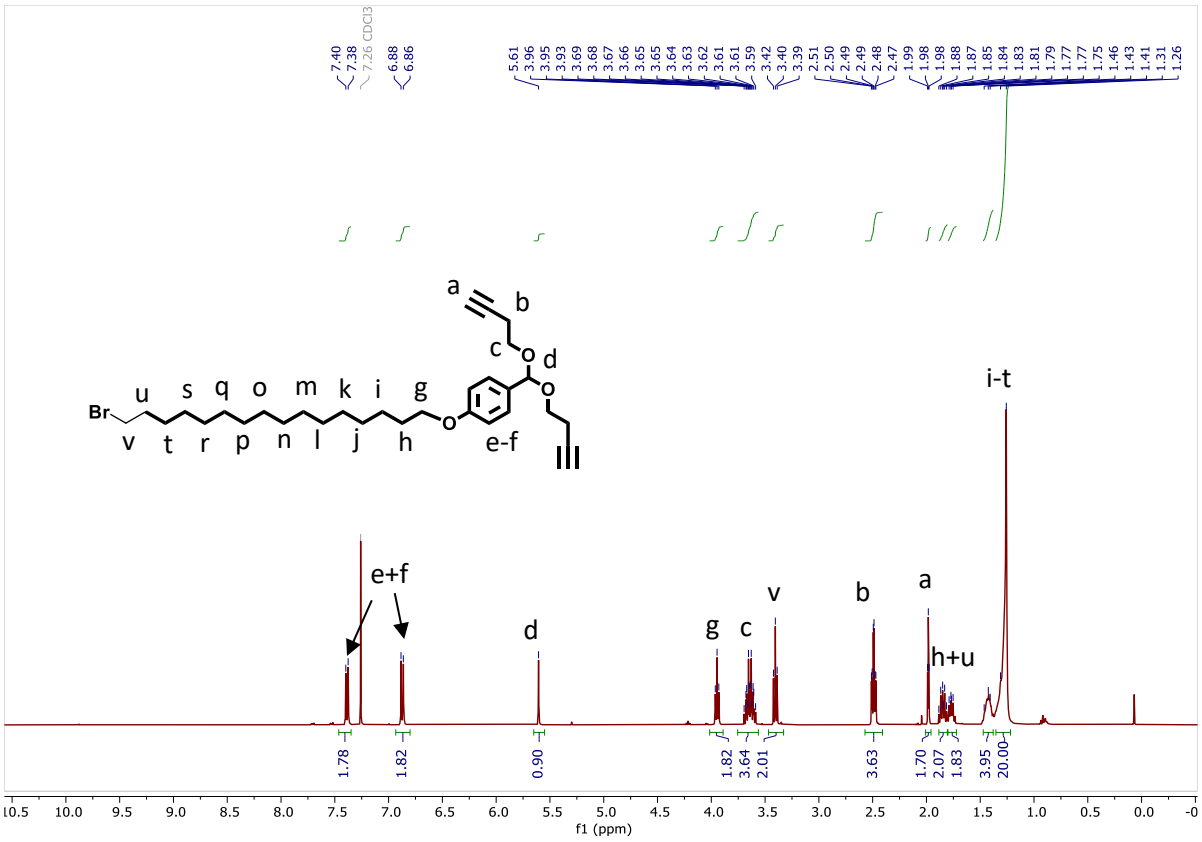
7.40
7.38
7.26 CDCl3
6.88
6.86
5.61
3.96
3.95
3.93
3.69
3.68
3.67
3.66
3.65
3.65
3.64
3.63
3.62
3.61
3.61
3.59
3.42
3.40
3.39
2.51
2.50
2.49
2.49
2.48
2.47
1.99
1.98
1.98
1.88
1.87
1.85
1.84
1.83
1.81
1.79
1.77
1.77
1.75
1.46
1.43
1.41
1.31
1.26
a
b
c
o
d
o
Br
u s q o m k i g
v t r p n l j h
o
e-f
i-t
e+f
d
g
c
v
b
a
h+u
1.78
1.82
0.90
1.82
3.64
2.01
3.63
1.70
2.07
1.83
3.95
20.00
f1 (ppm)

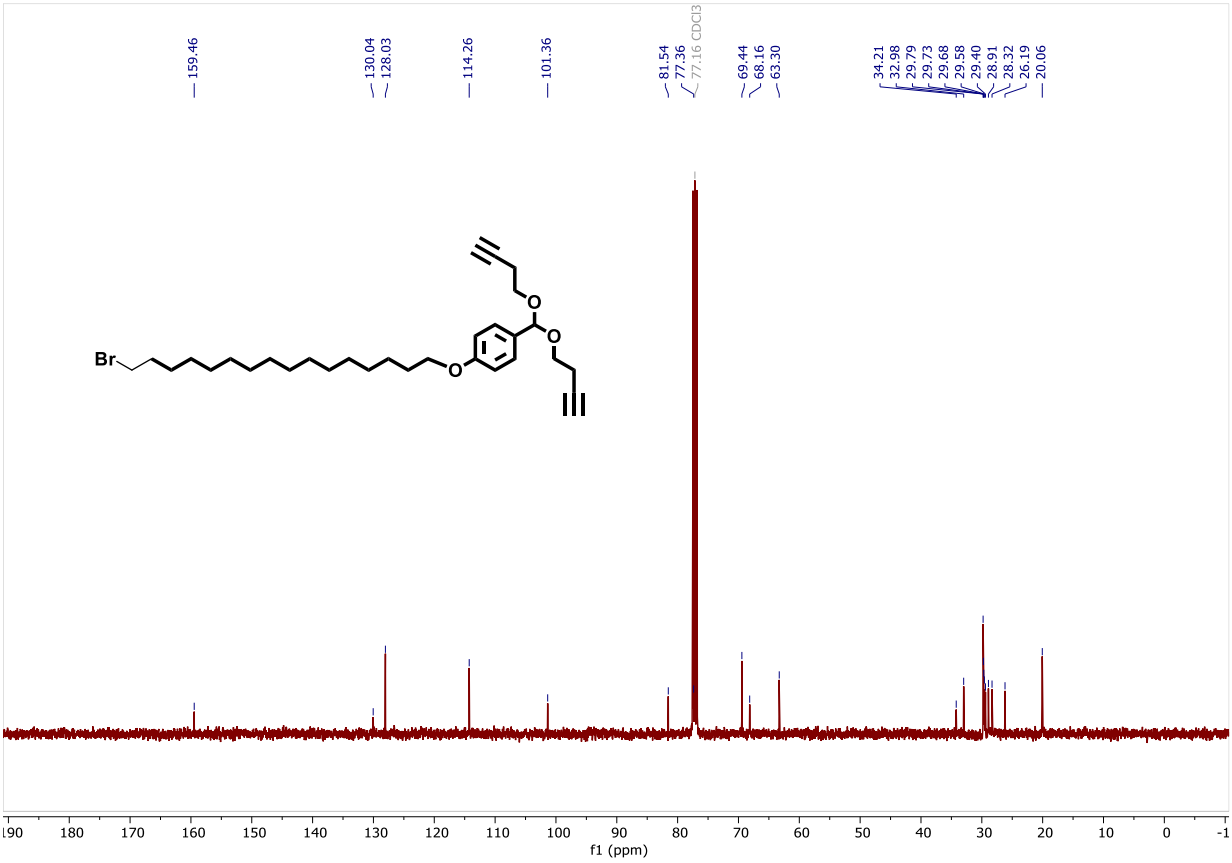
159.46
130.04
128.03
114.26
101.36
81.54
77.36
77.16 CDCl3
69.44
68.16
63.30
34.21
32.98
29.79
29.73
29.68
29.58
29.40
28.91
28.32
26.19
20.06
Br
o
o
o
f1 (ppm)

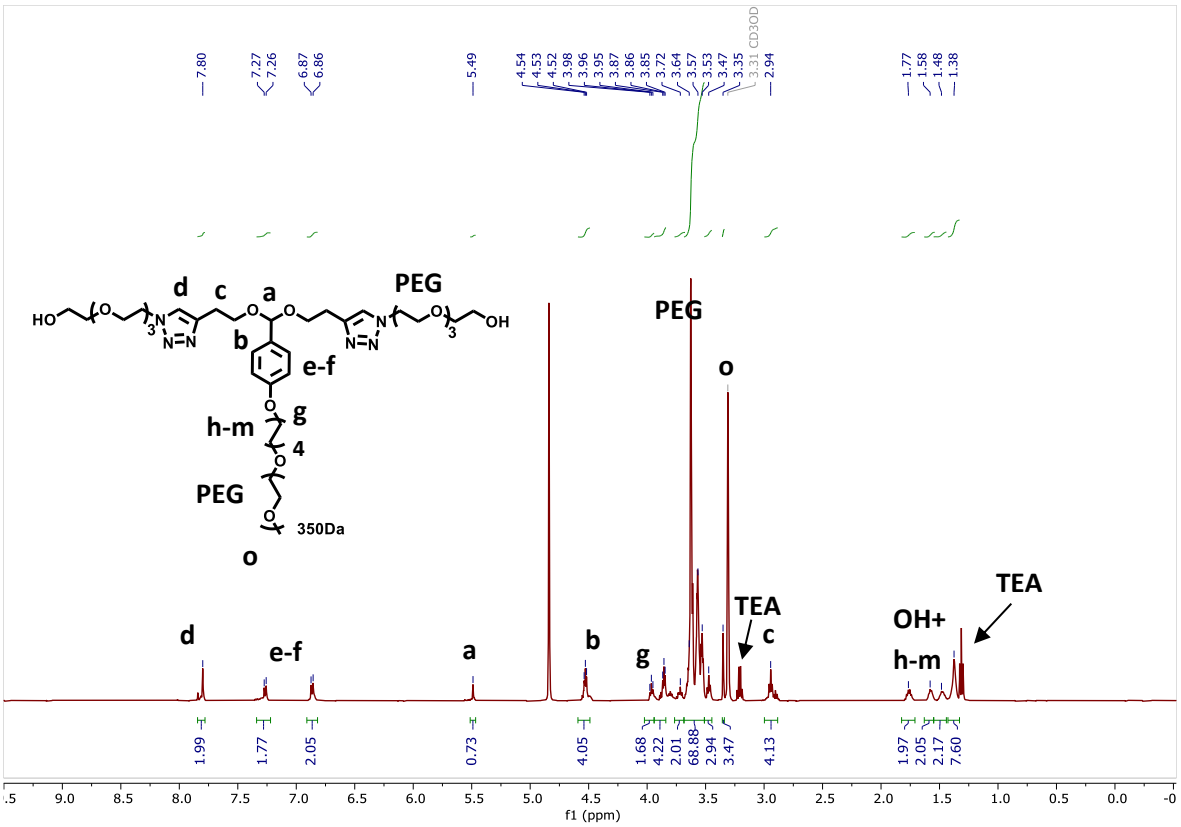
d
c
a
PEG
HO
OH
b
e-f
h-m
g
4
PEG
350Da
o
d
e-f
a
b
g
PEG
o
TEA
c
OH+
h-m
TEA
f1 (ppm)

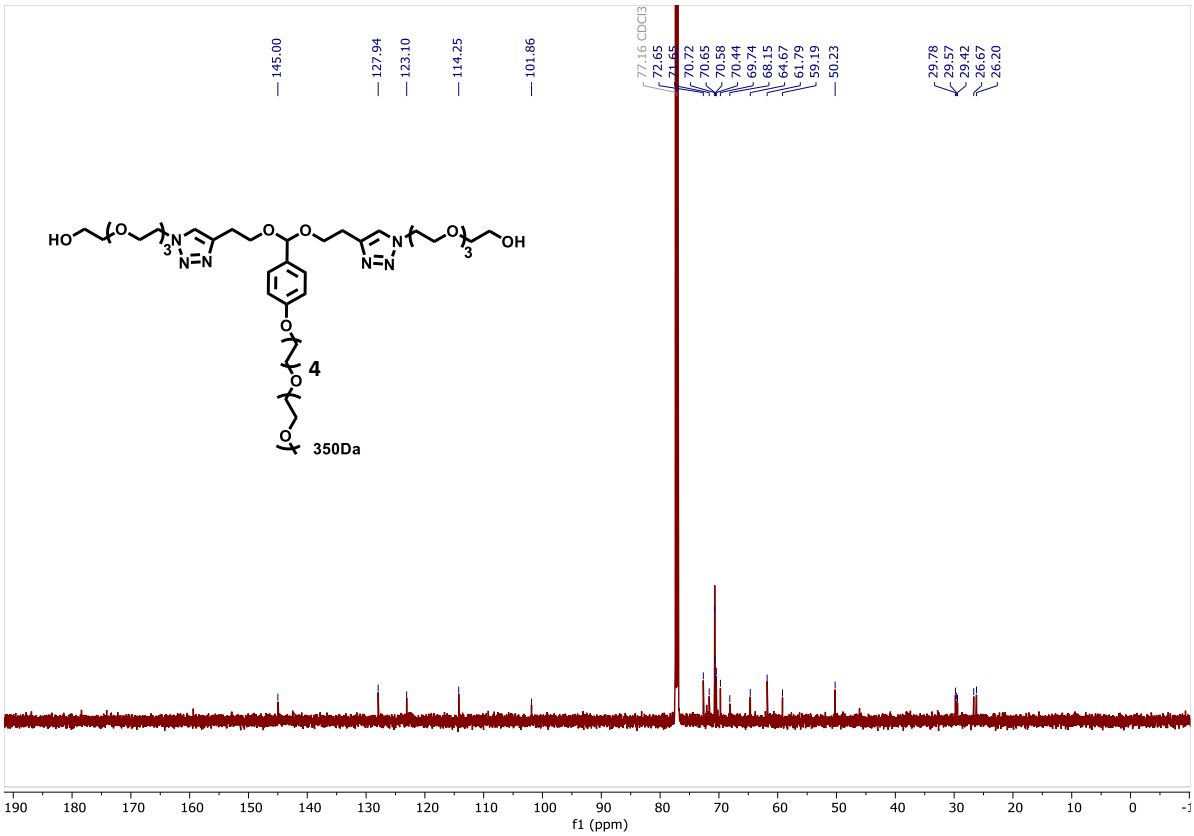
HO
OH
4
350Da
f1 (ppm)

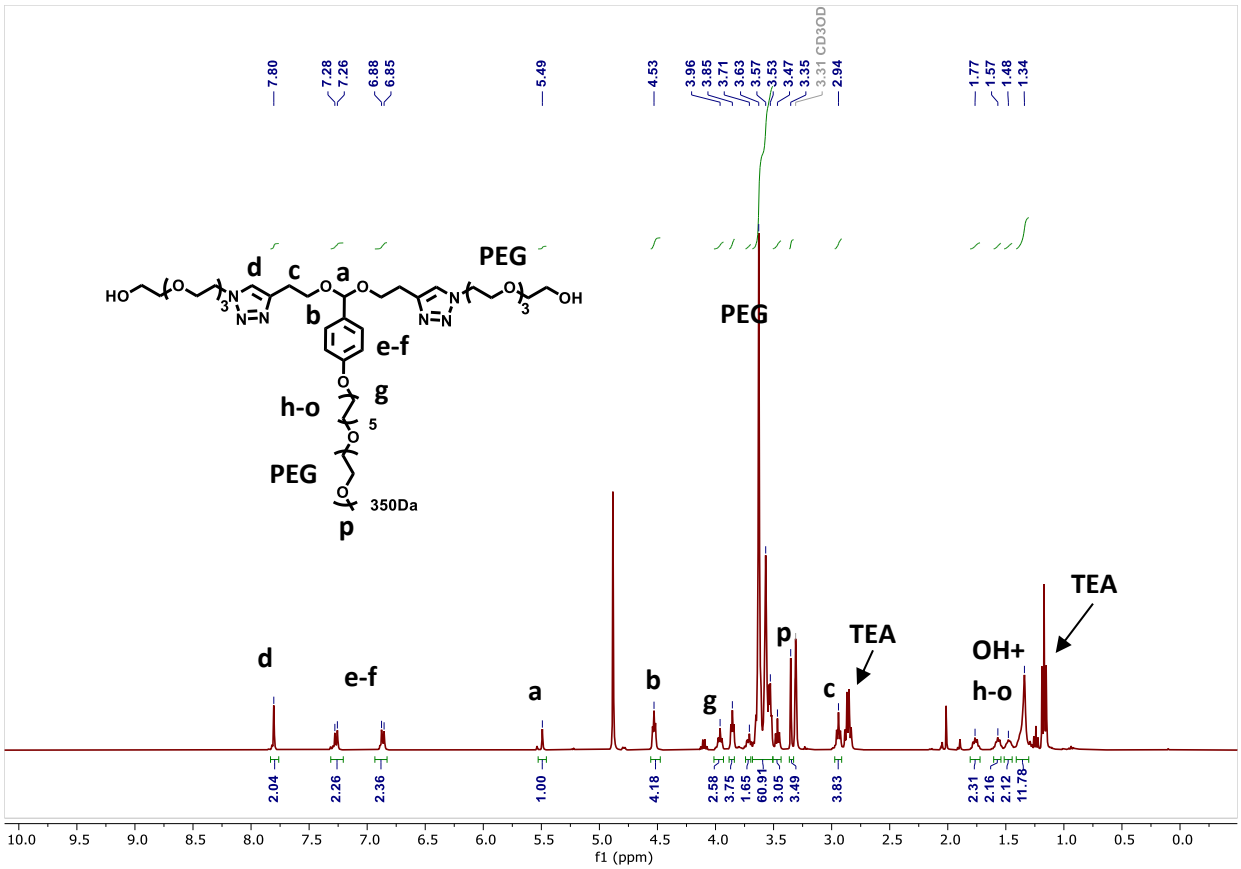
7.80
7.28
7.26
6.88
6.85
5.49
4.53
3.96
3.85
3.71
3.63
3.57
3.53
3.47
3.35
3.31 CD3OD
2.94
1.77
1.57
1.48
1.34
HO
OH
PEG
d
c
a
b
e-f
g
h-o
5
PEG
350Da
p
PEG
TEA
TEA
OH+
h-o
d
e-f
a
b
g
p
c
2.04
2.26
2.36
1.00
4.18
2.58
3.75
1.65
60.91
3.05
3.49
3.83
2.31
2.16
2.12
11.78
f1 (ppm)

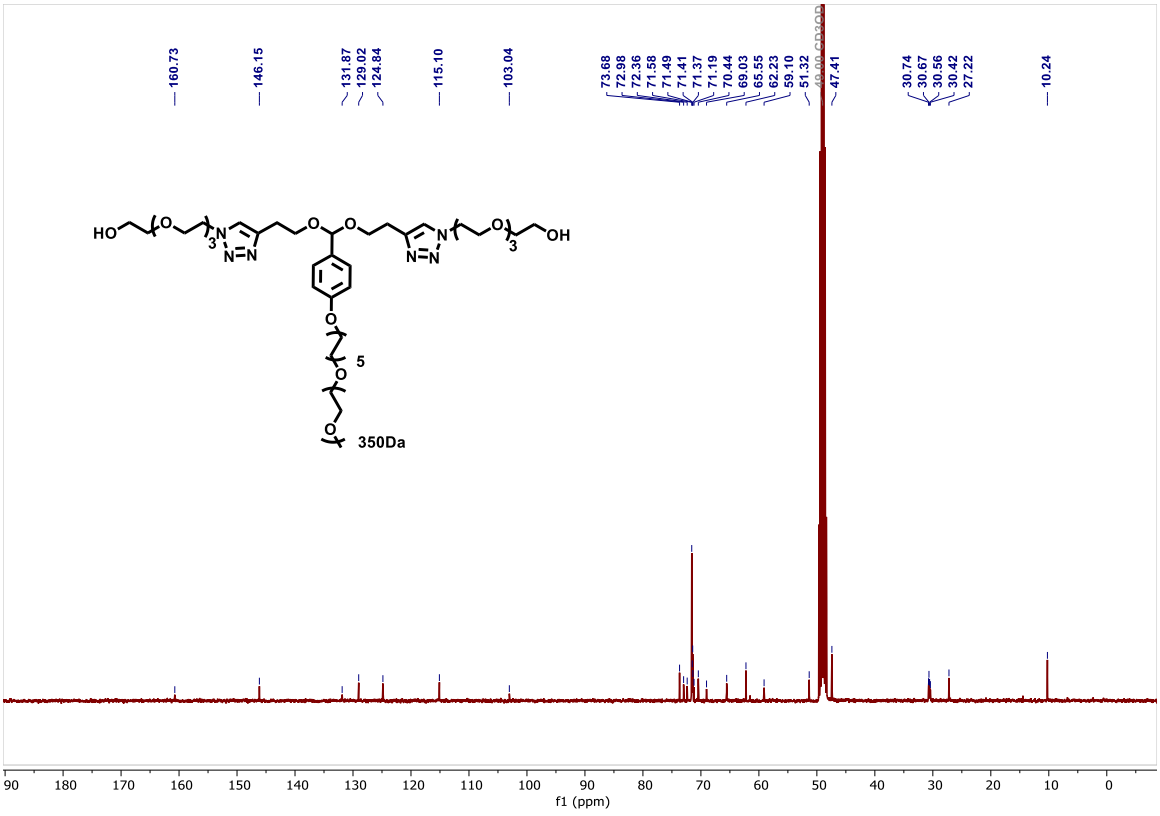
160.73
146.15
131.87
129.02
124.84
115.10
103.04
73.68
72.98
72.36
71.58
71.49
71.41
71.37
71.19
70.44
69.03
65.55
62.23
59.10
51.32
49.00 CD3OD
47.41
30.74
30.67
30.56
30.42
27.22
10.24
HO
OH
5
350Da
f1 (ppm)

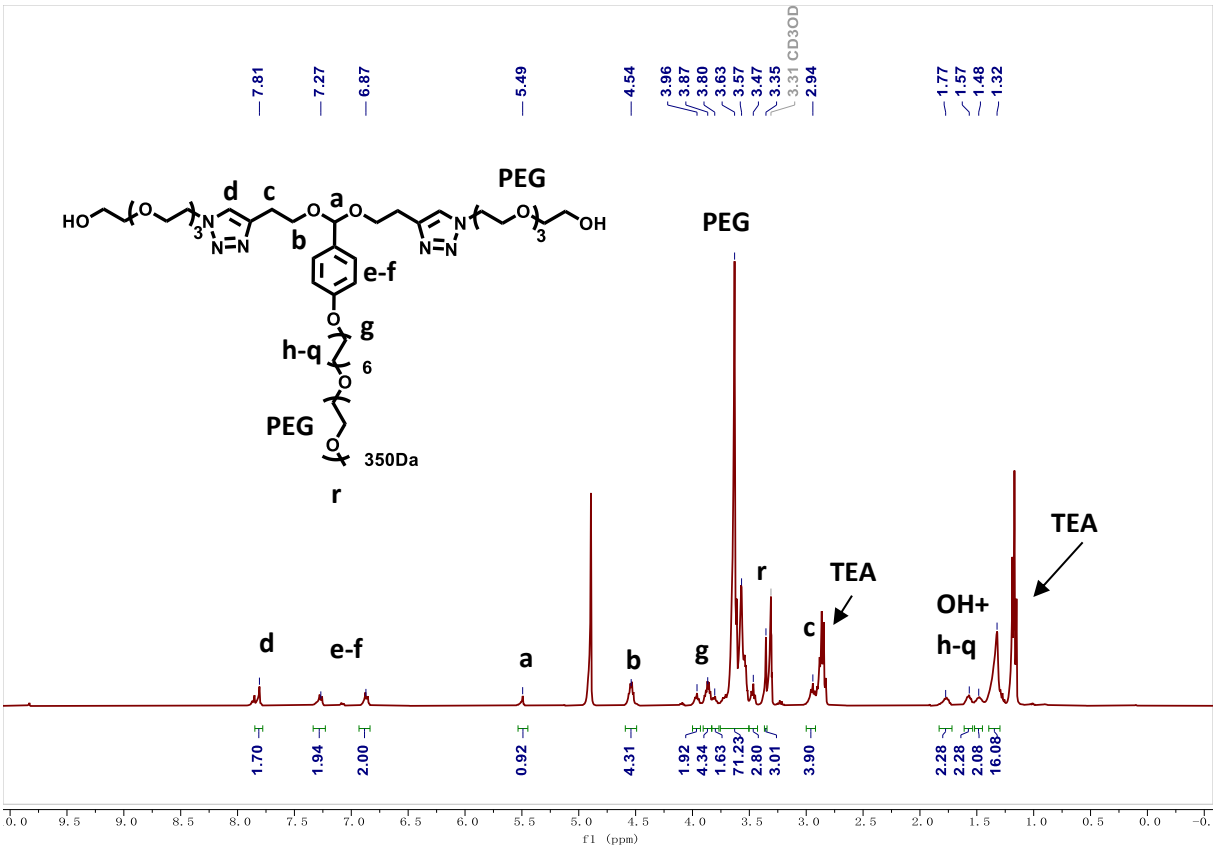
7.81
7.27
6.87
5.49
4.54
3.96
3.87
3.80
3.63
3.57
3.47
3.35
3.31 CD3OD
2.94
1.77
1.57
1.48
1.32
HO
PEG
OH
d
c
a
b
e-f
g
h-q
6
PEG
350Da
r
PEG
TEA
TEA
OH+
h-q
d
e-f
a
b
g
r
c
1.70
1.94
2.00
0.92
4.31
1.92
4.34
1.63
71.23
2.80
3.01
3.90
2.28
2.28
2.08
16.08
f1 (ppm)

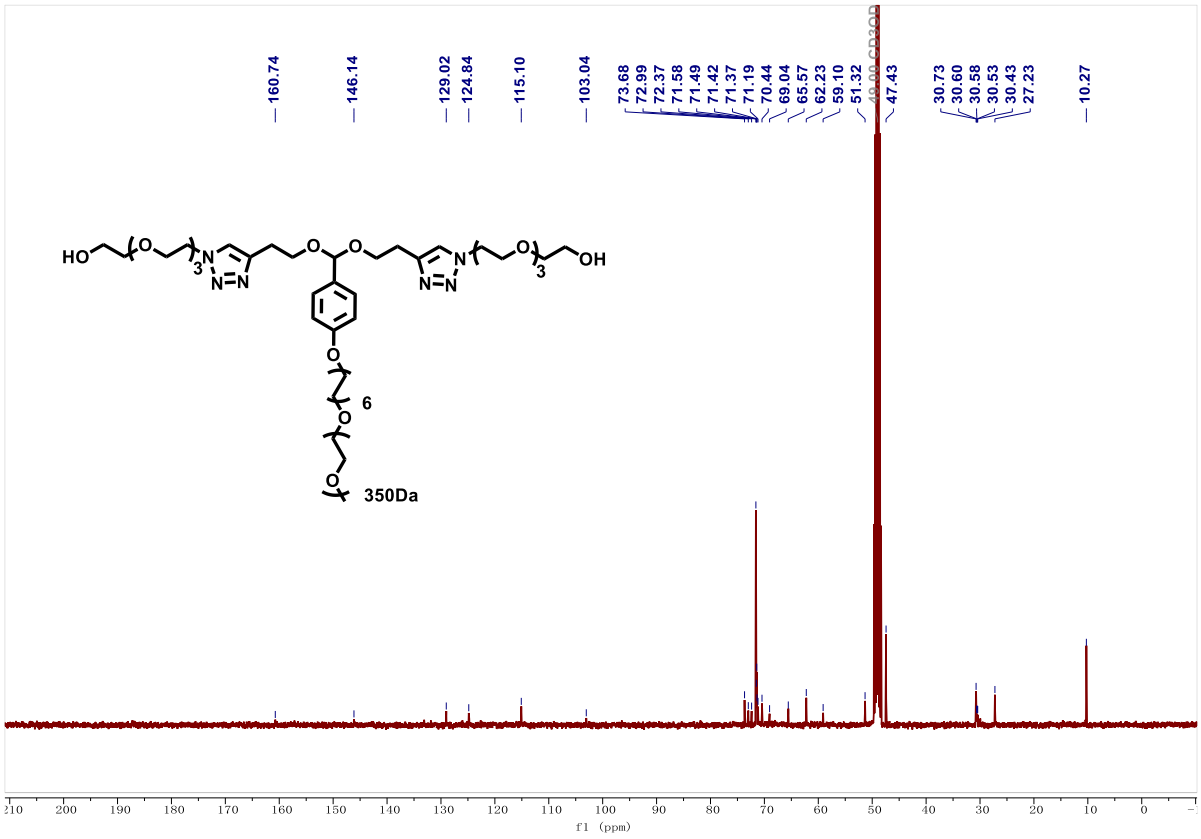
160.74
146.14
129.02
124.84
115.10
103.04
73.68
72.99
72.37
71.58
71.49
71.42
71.37
71.19
70.44
69.04
65.57
62.23
59.10
51.32
49.00 CD3OD
47.43
30.73
30.60
30.58
30.53
30.43
27.23
10.27
HO
OH
6
350Da
f1 (ppm)

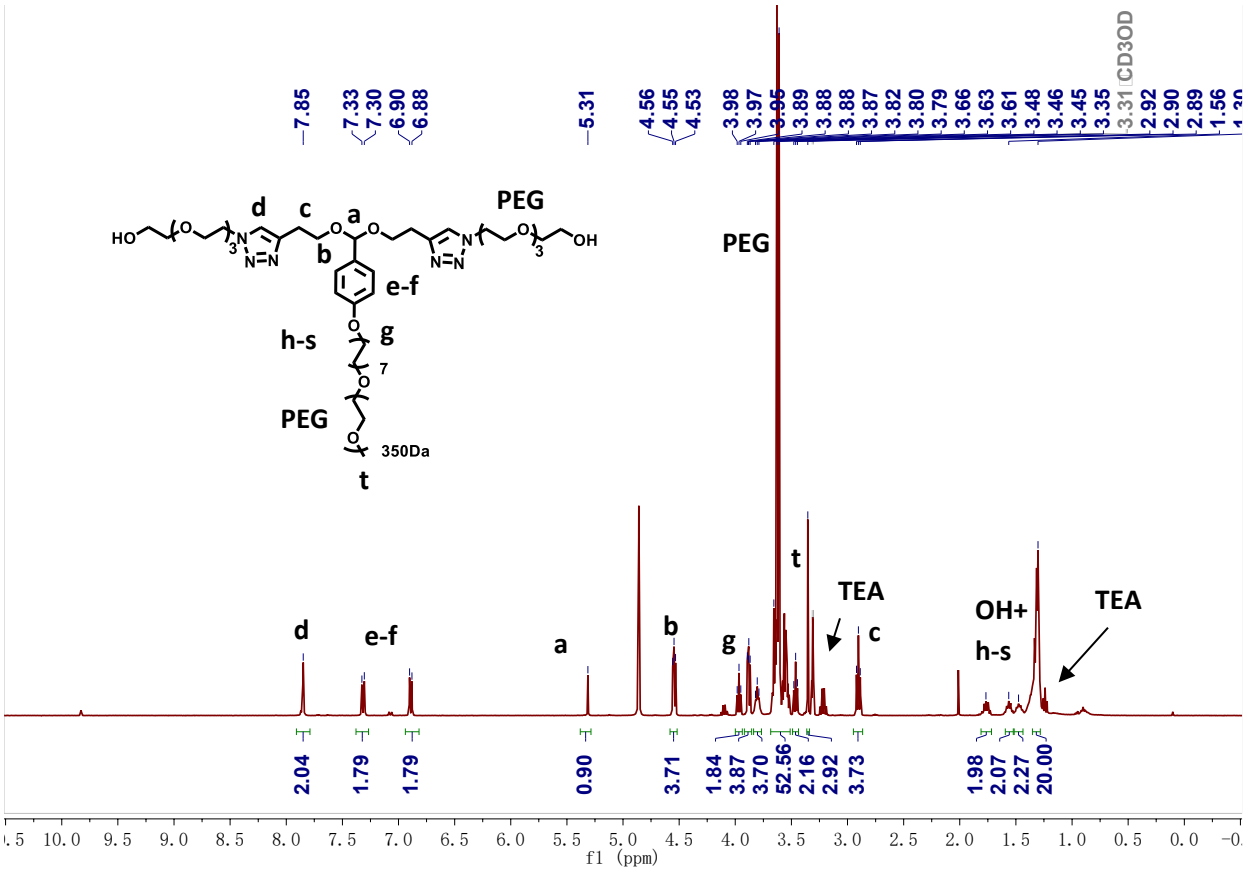
7.85
7.33
7.30
6.90
6.88
5.31
4.56
4.55
4.53
3.98
3.97
3.96
3.89
3.88
3.88
3.87
3.82
3.80
3.79
3.66
3.63
3.61
3.48
3.46
3.45
3.35
3.31 CD3OD
2.92
2.90
2.89
1.56
HO
OH
PEG
PEG
d
c
a
b
e-f
h-s
g
7
PEG
350Da
t
TEA
c
OH+
h-s
TEA
d
e-f
a
b
g
t
2.04
1.79
1.79
0.90
3.71
1.84
3.87
3.70
52.56
2.16
2.92
3.73
1.98
2.07
2.27
20.00
f1 (ppm)

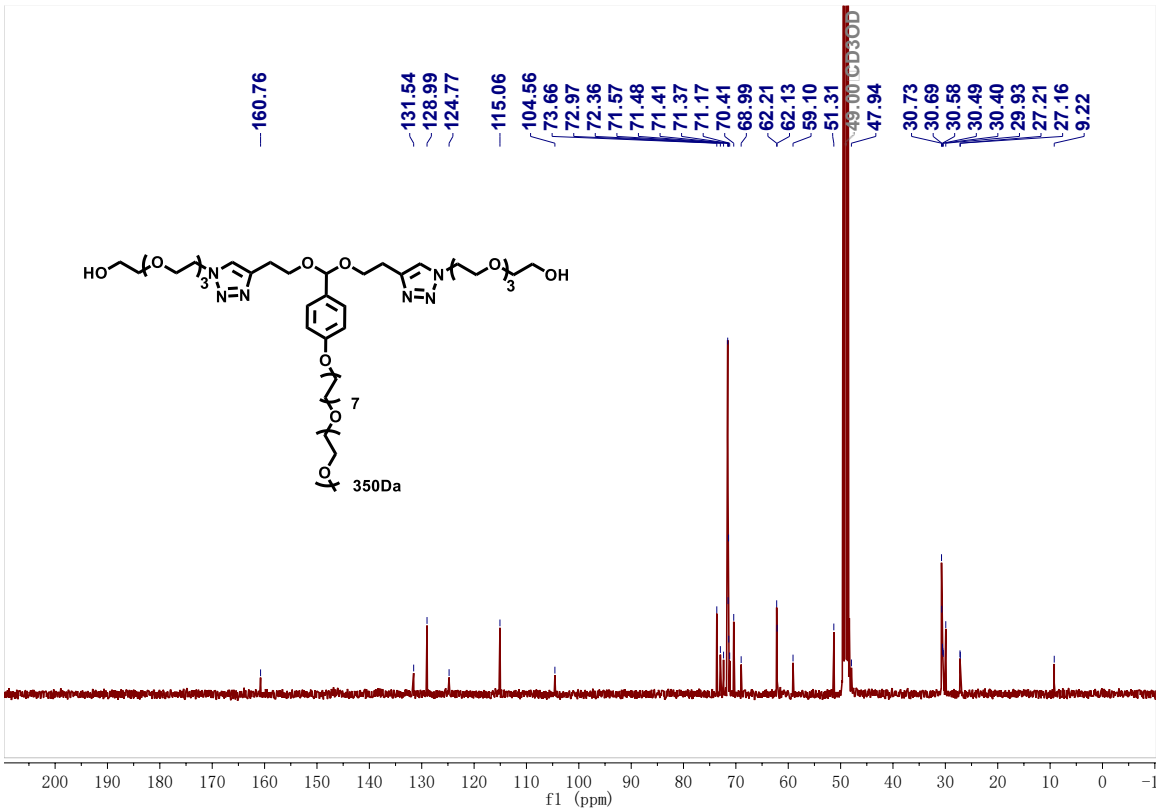
160.76
131.54
128.99
124.77
115.06
104.56
73.66
72.97
72.36
71.57
71.48
71.41
71.37
71.17
70.41
68.99
62.21
62.13
59.10
51.31
49.00 CD3OD
47.94
30.73
30.69
30.58
30.49
30.40
29.93
27.21
27.16
9.22
HO
OH
7
350Da
f1 (ppm)

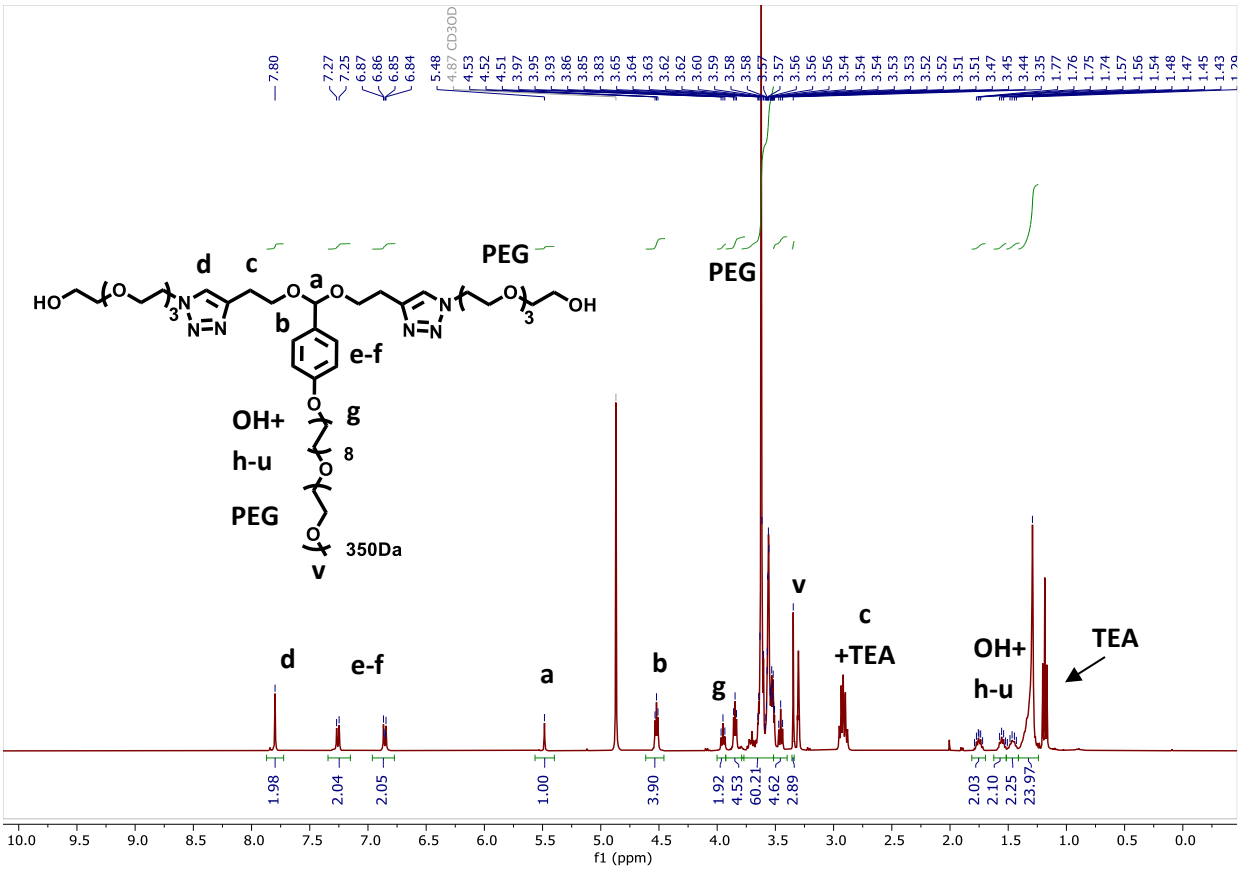
d
c
a
b
e-f
PEG
OH+
h-u
g
8
PEG
350Da
v
HO
OH
d
e-f
a
b
g
v
c
+TEA
OH+
h-u
TEA
1.98
2.04
2.05
1.00
3.90
1.92
4.53
60.21
4.62
2.89
2.03
2.10
2.25
23.97
f1 (ppm)

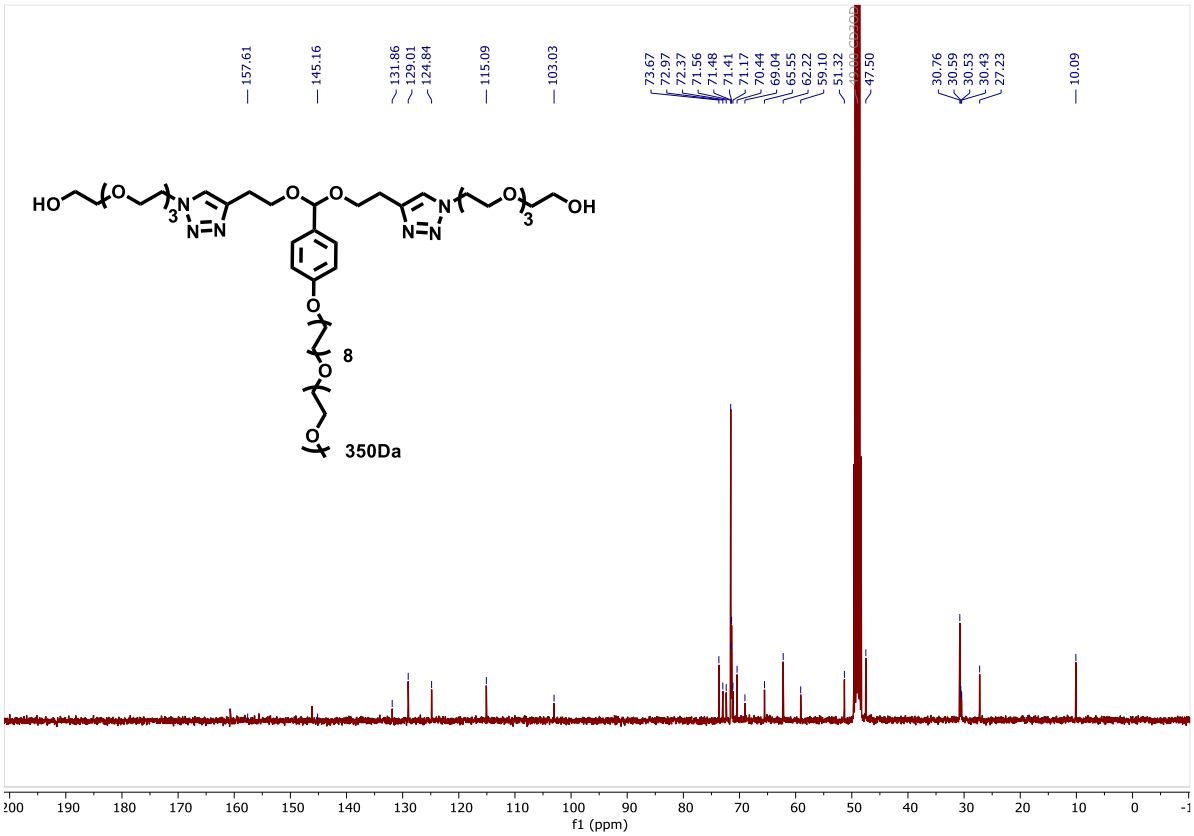
HO
OH
8
350Da
f1 (ppm)

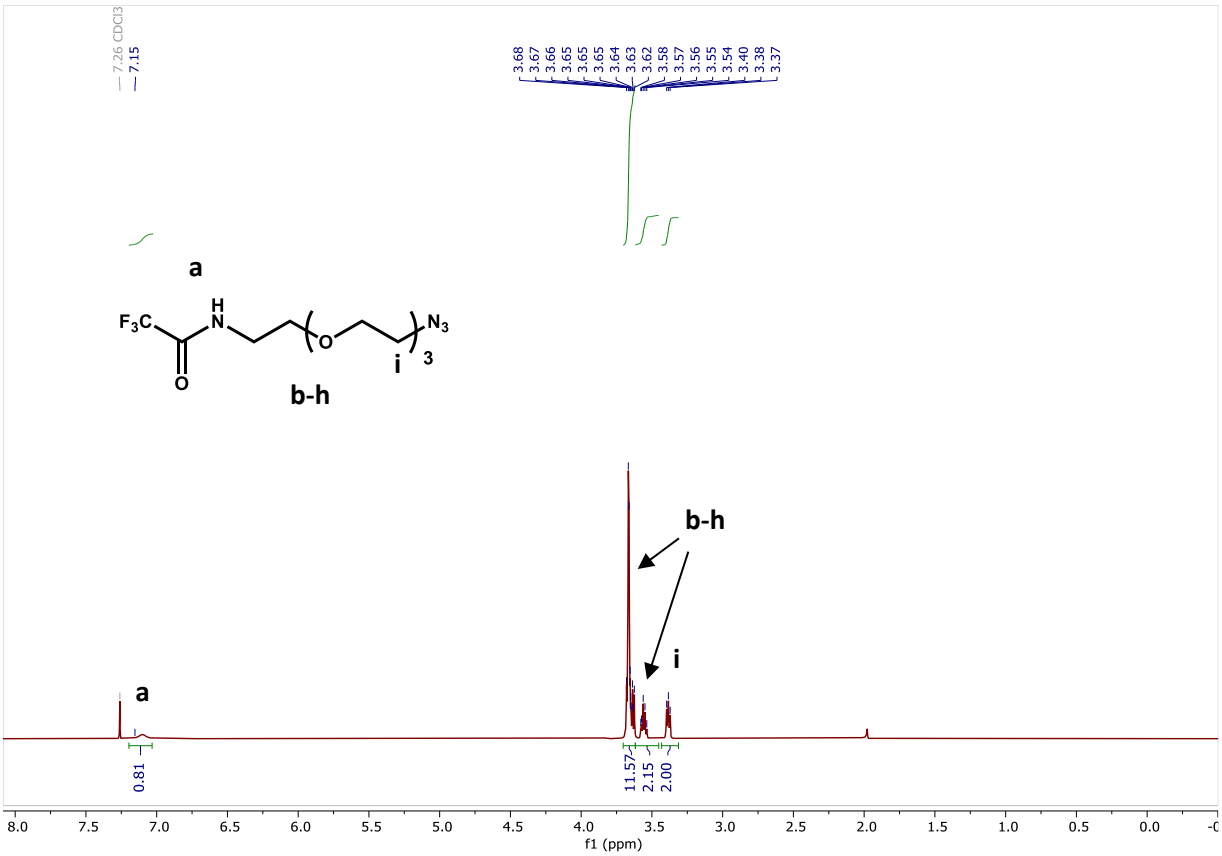
7.26 CDCl3
7.15
3.68
3.67
3.66
3.65
3.65
3.65
3.64
3.63
3.62
3.58
3.57
3.56
3.55
3.54
3.40
3.38
3.37
a
b-h
i
0.81
11.57
2.15
2.00
f1 (ppm)

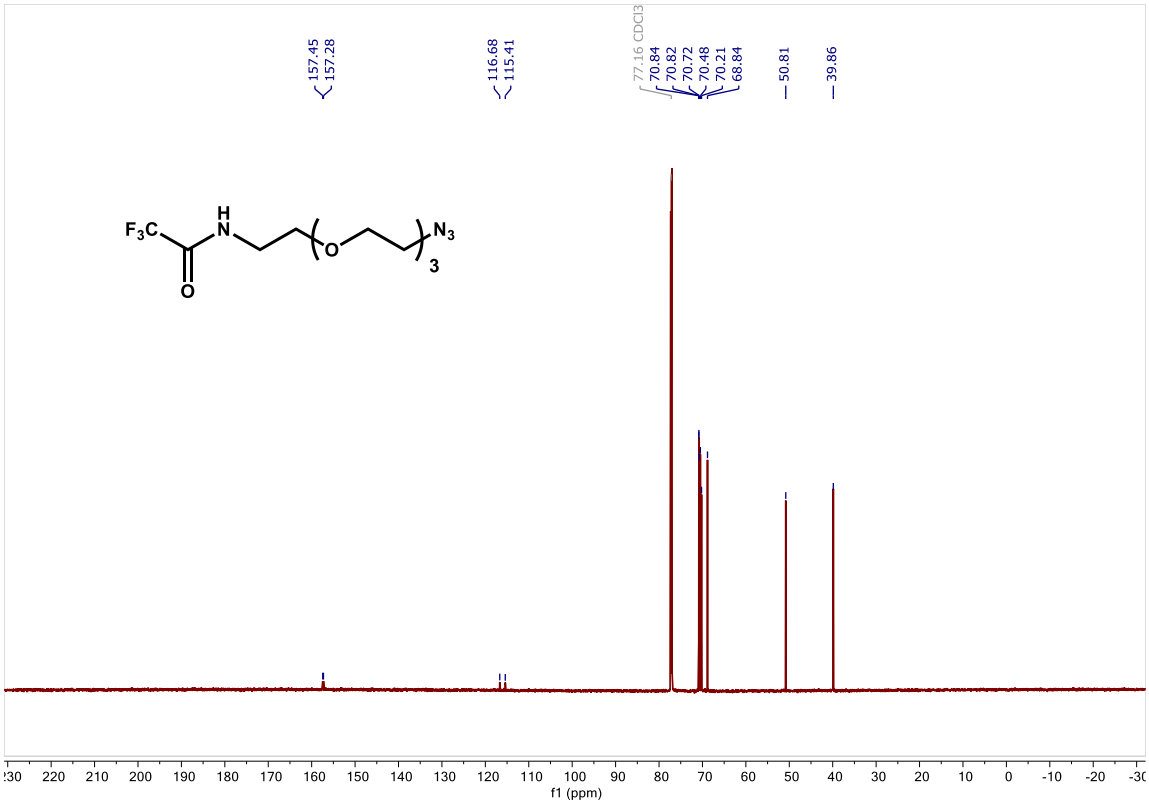
157.45
157.28
116.68
115.41
77.16 CDCl3
70.84
70.82
70.72
70.48
70.21
68.84
50.81
39.86
f1 (ppm)

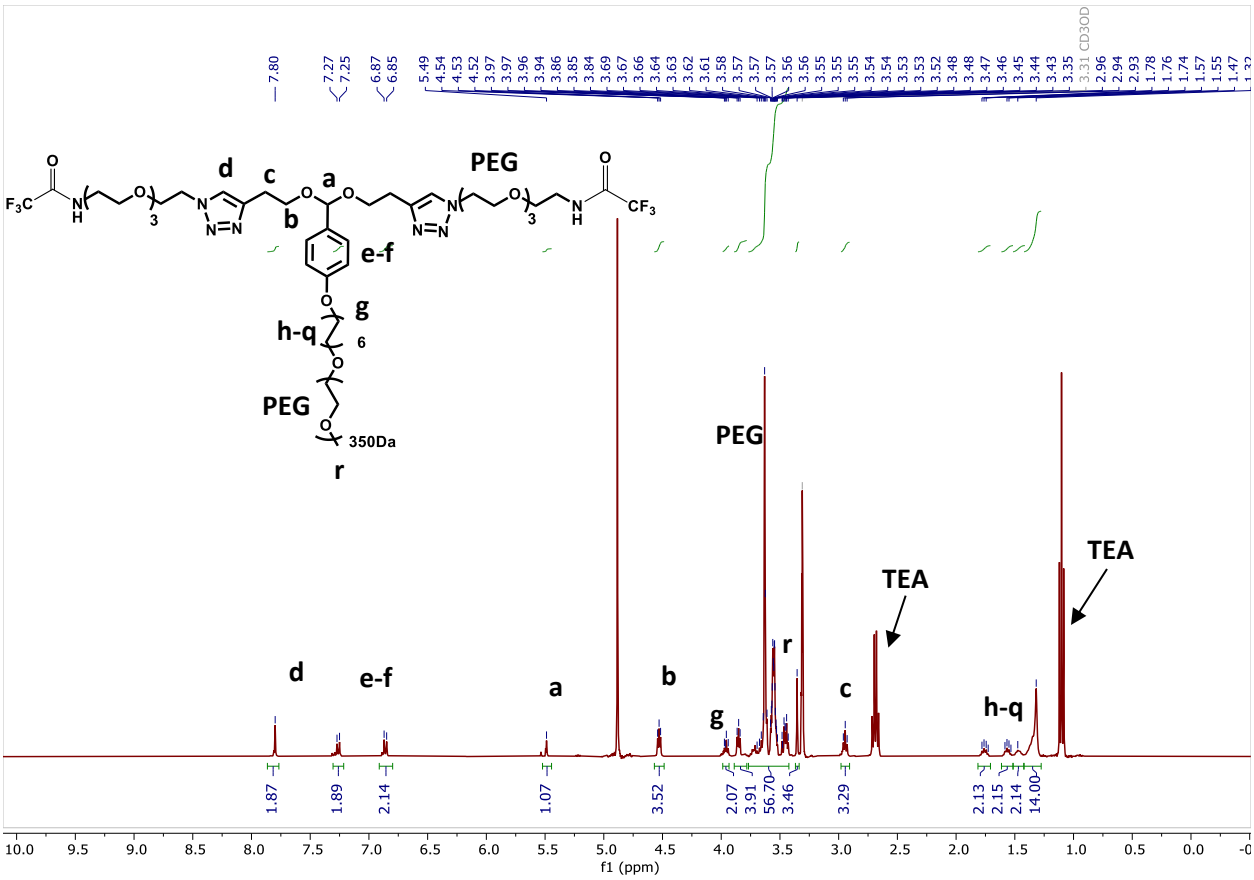
d
c
a
PEG
b
e-f
g
h-q
6
PEG
350Da
r
PEG
TEA
TEA
d
e-f
a
b
g
r
c
h-q
1.87
1.89
2.14
1.07
3.52
2.07
3.91
56.70
3.46
3.29
2.13
2.15
2.14
14.00
f1 (ppm)

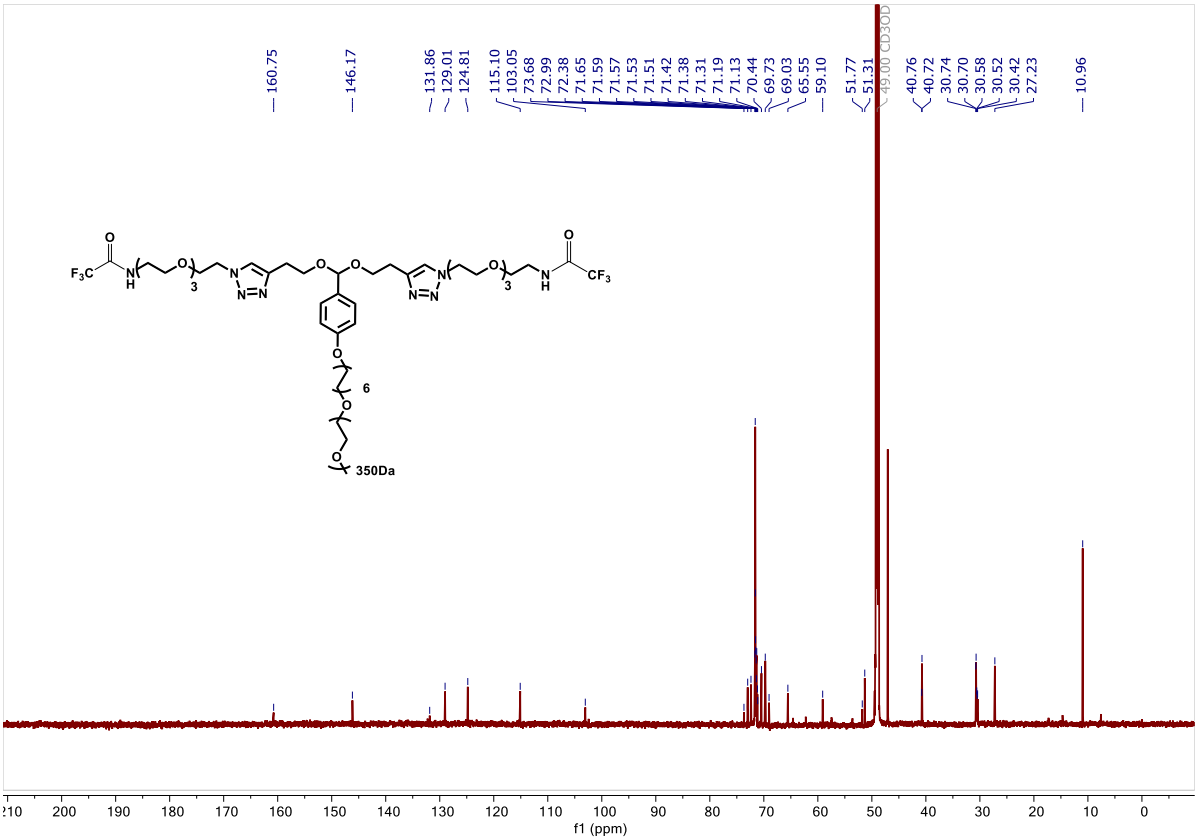
6
350Da
f1 (ppm)

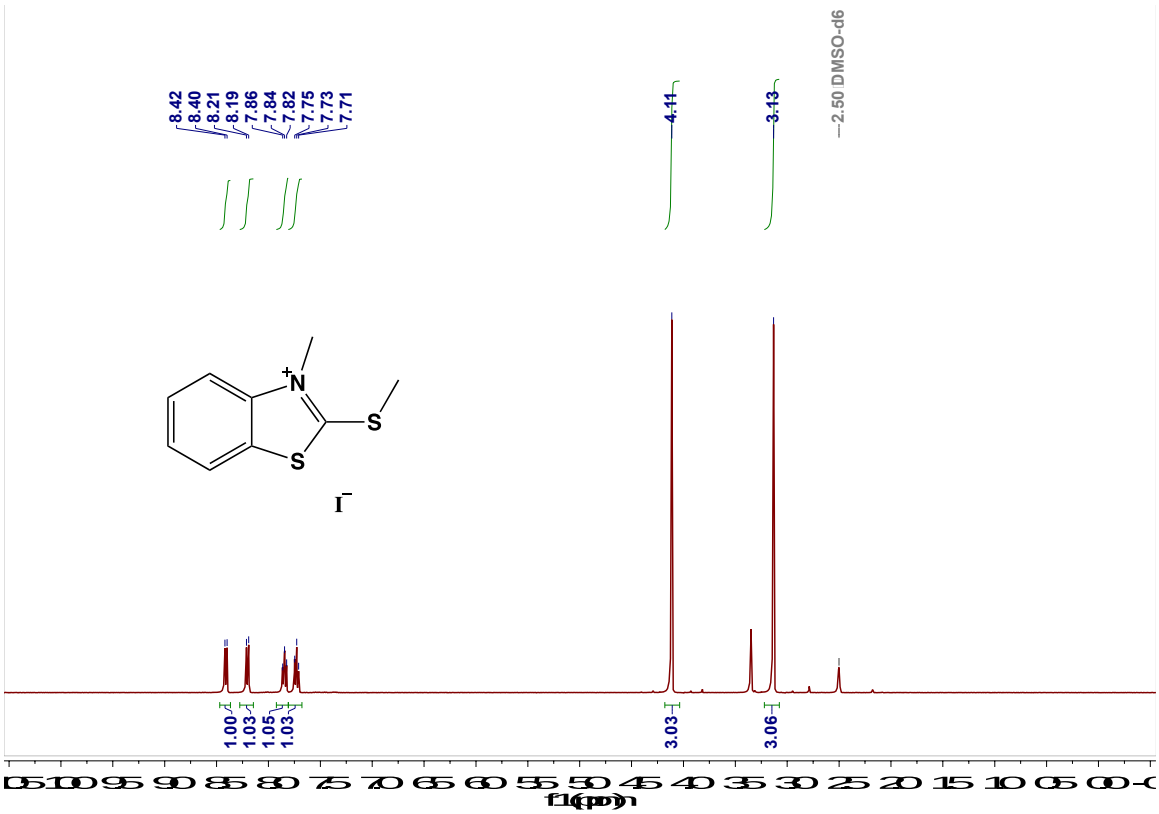
8.42
8.40
8.21
8.19
7.86
7.84
7.82
7.75
7.73
7.71
4.11
3.13
2.50 DMSO-d6
1.00
1.03
1.05
1.03
3.03
3.06
f1 (ppm)

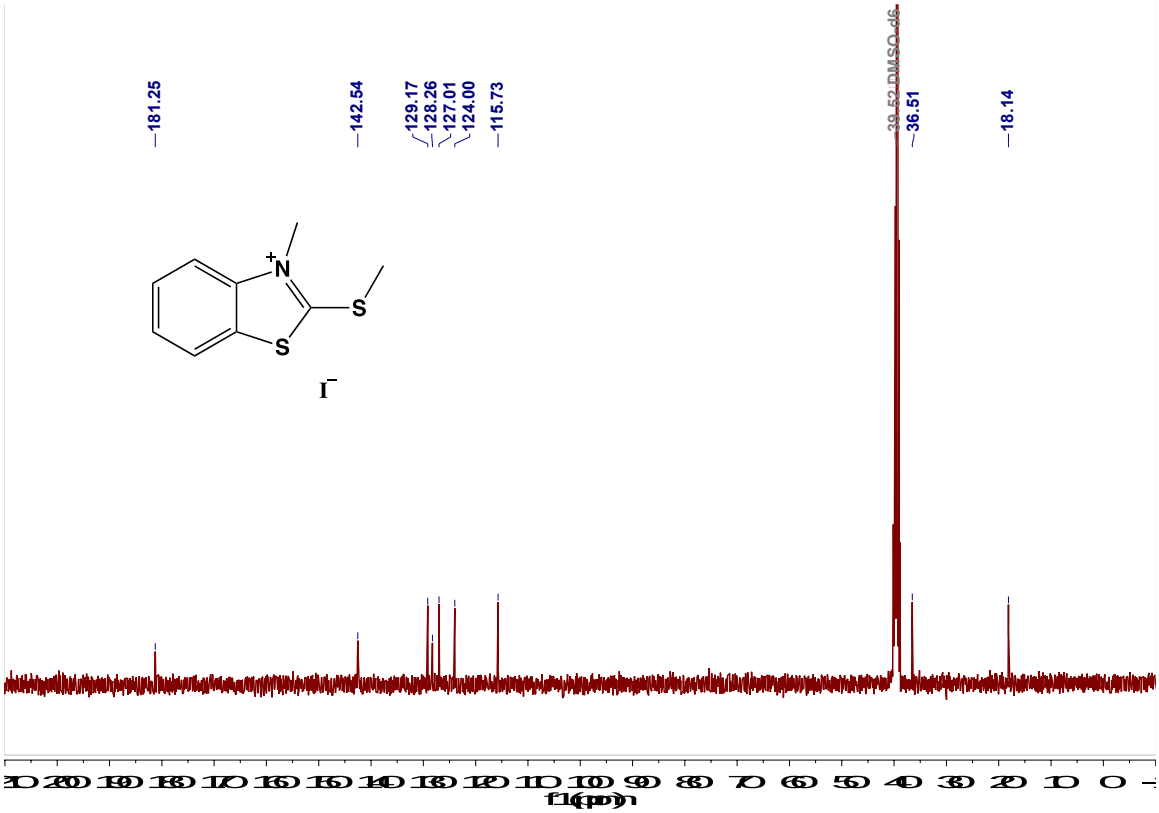
181.25
142.54
129.17
128.26
127.01
124.00
115.73
39.52 DMSO-d6
36.51
18.14
f1 (ppm)

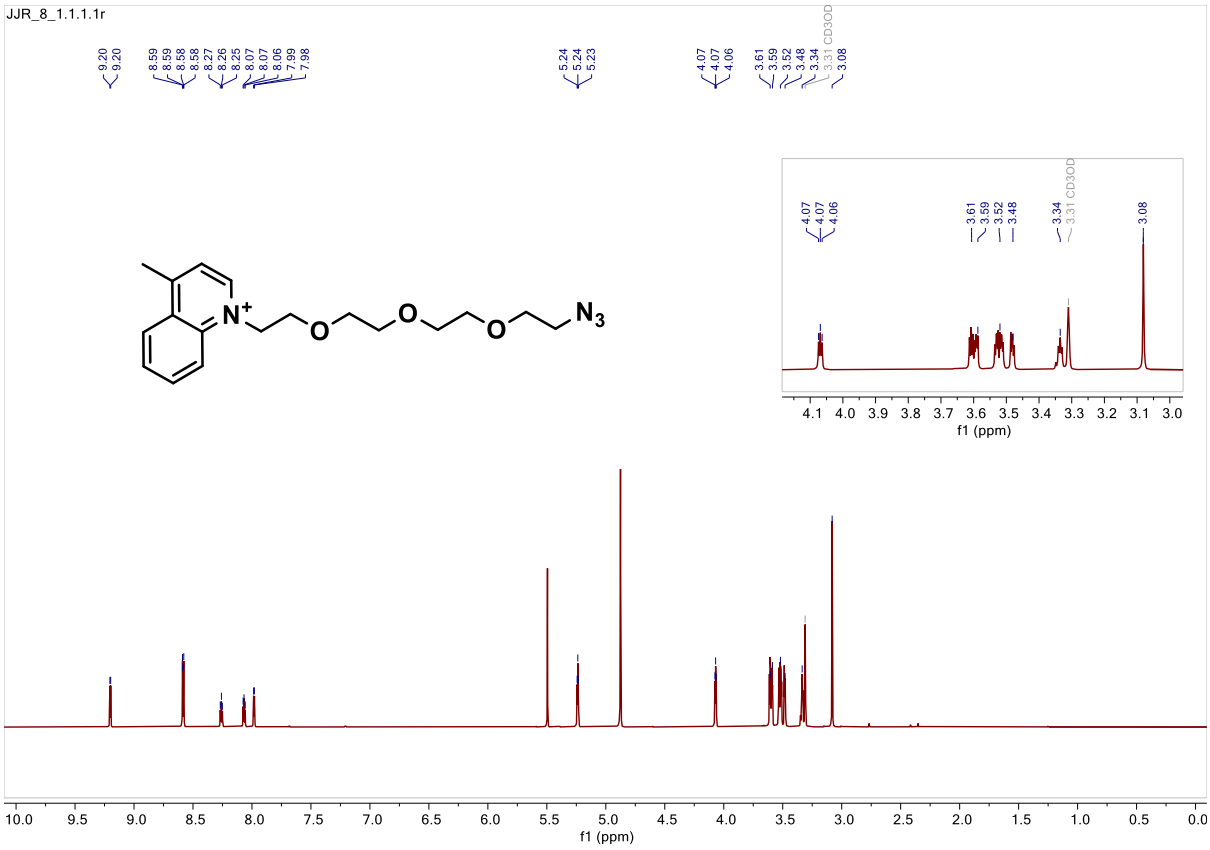
JJR_8_1.1.1.1r
9.20
9.20
8.59
8.59
8.58
8.58
8.27
8.26
8.25
8.07
8.07
8.06
7.99
7.98
5.24
5.24
5.23
4.07
4.07
4.06
3.61
3.59
3.52
3.48
3.34
3.31 CD3OD
3.08
N+
O
O
O
N3
f1 (ppm)

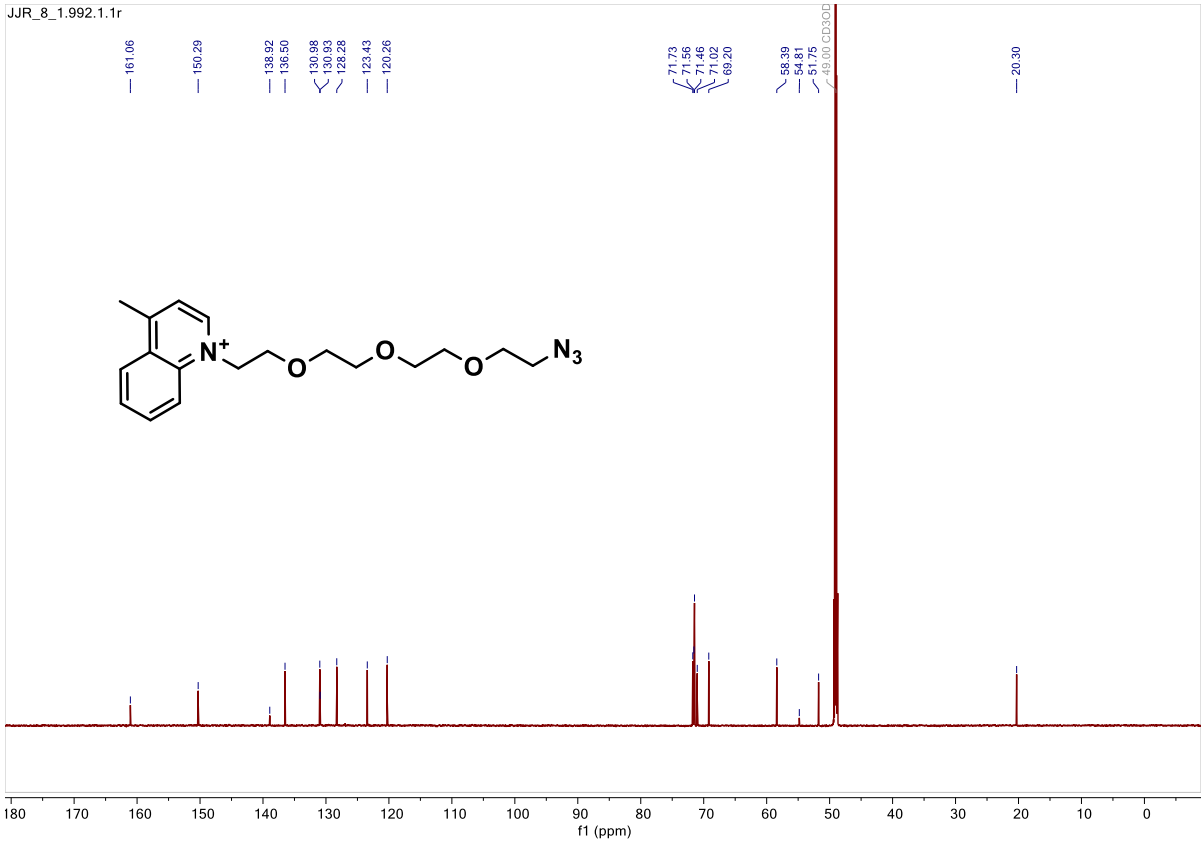
JJR_8_1.992.1.1r
161.06
150.29
138.92
136.50
130.98
130.93
128.28
123.43
120.26
71.73
71.56
71.46
71.02
69.20
58.39
54.81
51.75
49.00 CD3OD
20.30
N+
O
O
O
N3
f1 (ppm)

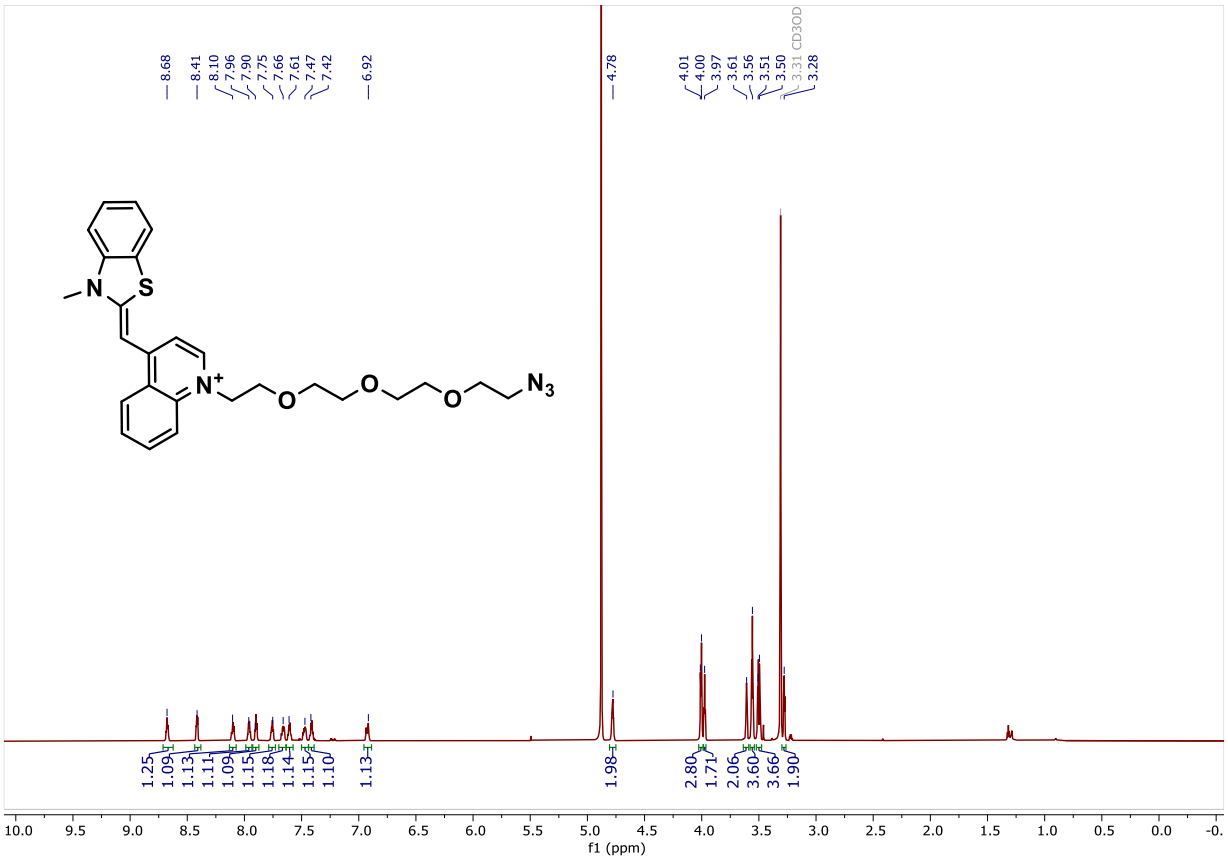
8.68
8.41
8.10
7.96
7.90
7.75
7.66
7.61
7.47
7.42
6.92
4.78
4.01
4.00
3.97
3.61
3.56
3.51
3.50
3.31 CD3OD
3.28
1.25
1.09
1.13
1.11
1.09
1.15
1.18
1.14
1.15
1.10
1.13
1.98
2.80
1.71
2.06
3.60
3.66
1.90
f1 (ppm)

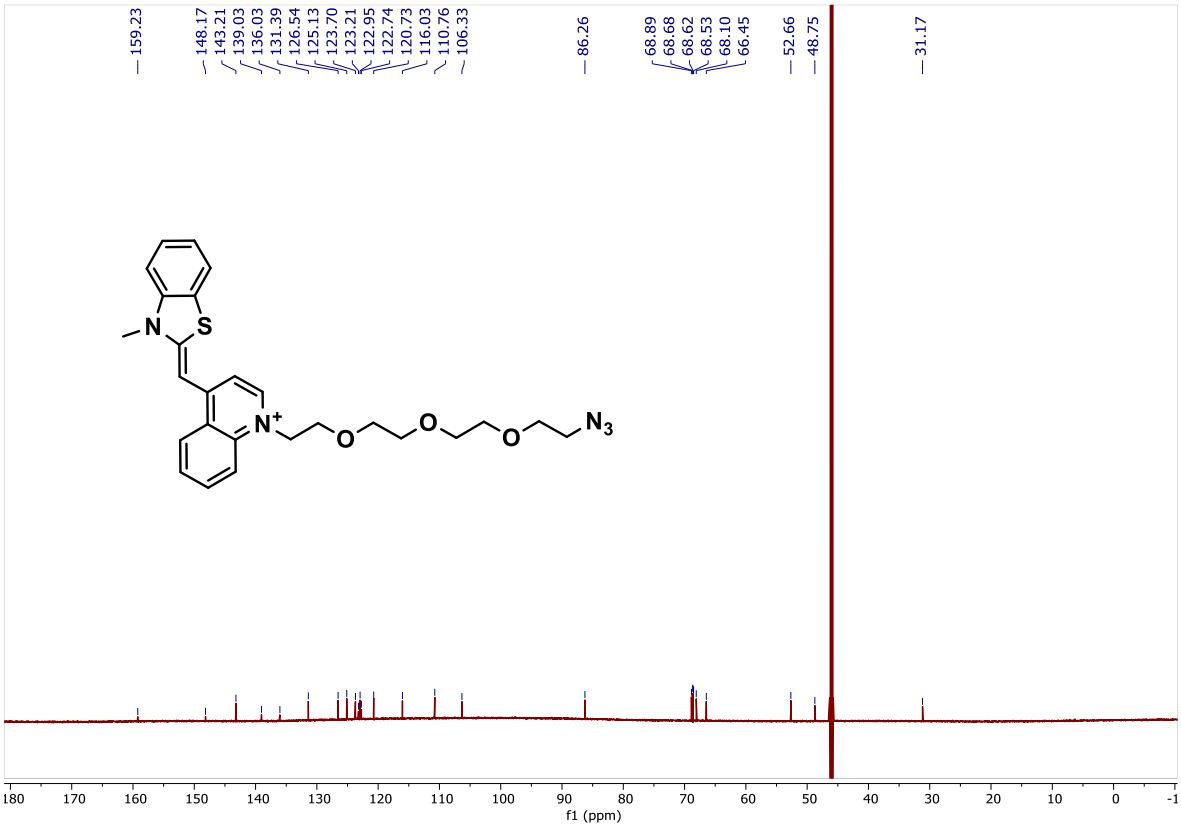
159.23
148.17
143.21
139.03
136.03
131.39
126.54
125.13
123.70
123.21
122.95
122.74
120.73
116.03
110.76
106.33
86.26
68.89
68.68
68.62
68.53
68.10
66.45
52.66
48.75
31.17
f1 (ppm)

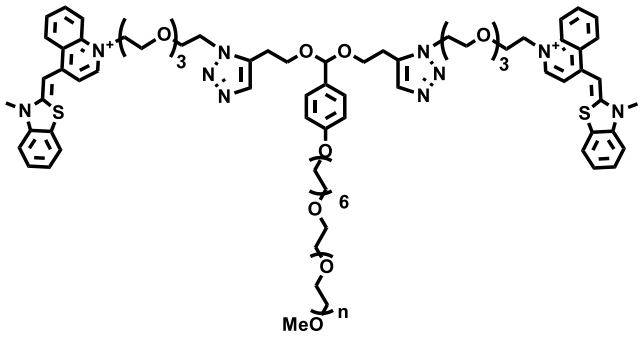

TCS

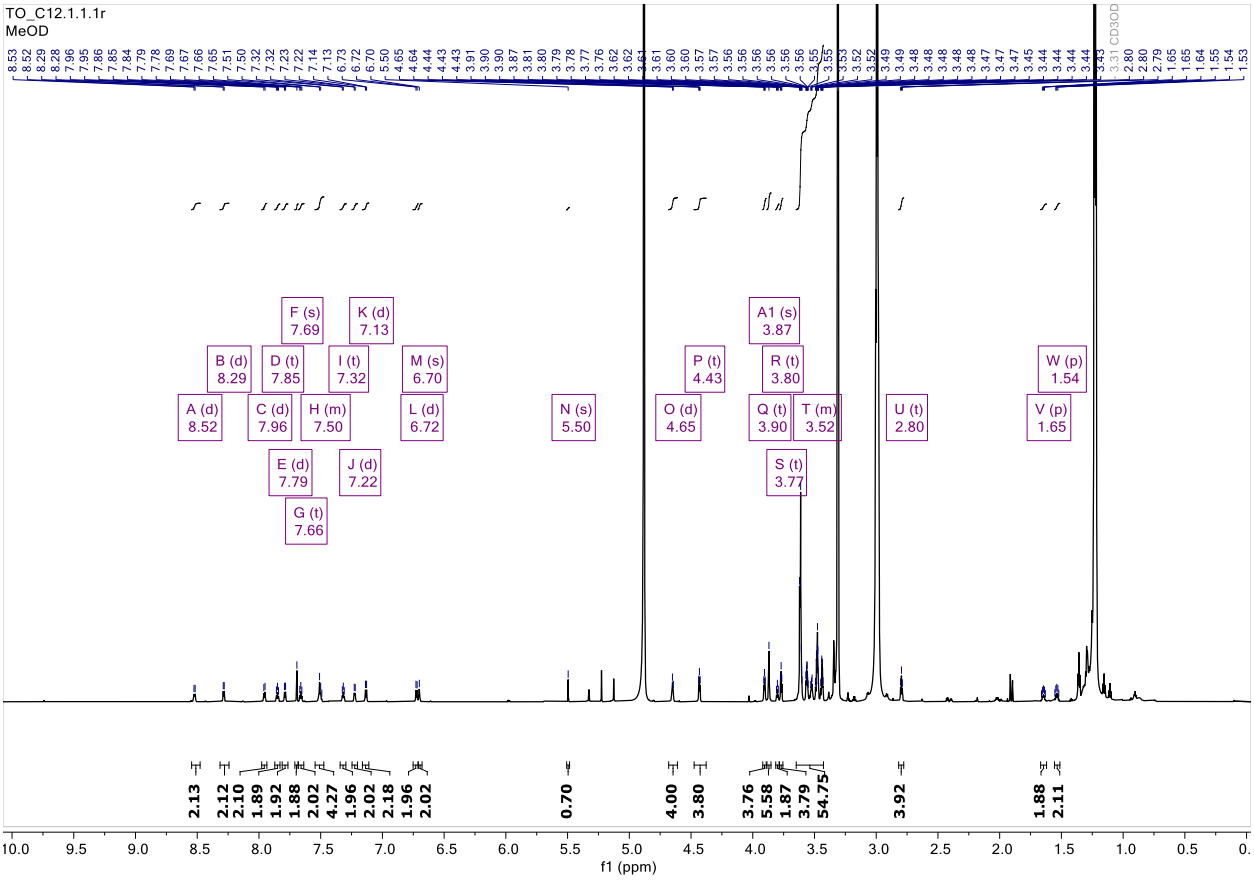
TO_C12.1.1.1r
MeOD
A (d) 8.52
B (d) 8.29
C (d) 7.96
D (t) 7.85
E (d) 7.79
F (s) 7.69
G (t) 7.66
H (m) 7.50
I (t) 7.32
J (d) 7.22
K (d) 7.13
L (d) 6.72
M (s) 6.70
N (s) 5.50
O (d) 4.65
P (t) 4.43
Q (t) 3.90
R (t) 3.80
S (t) 3.77
T (m) 3.52
U (t) 2.80
V (p) 1.65
W (p) 1.54
A1 (s) 3.87
f1 (ppm)

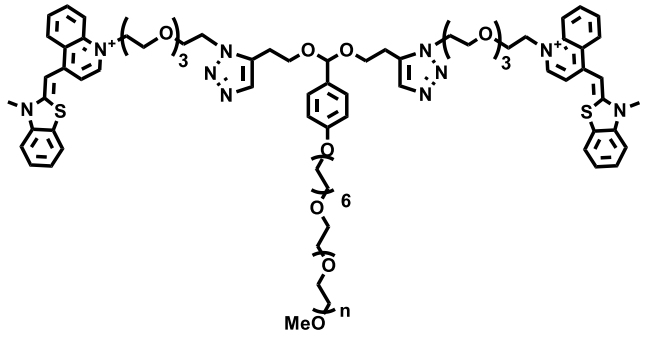

TCS

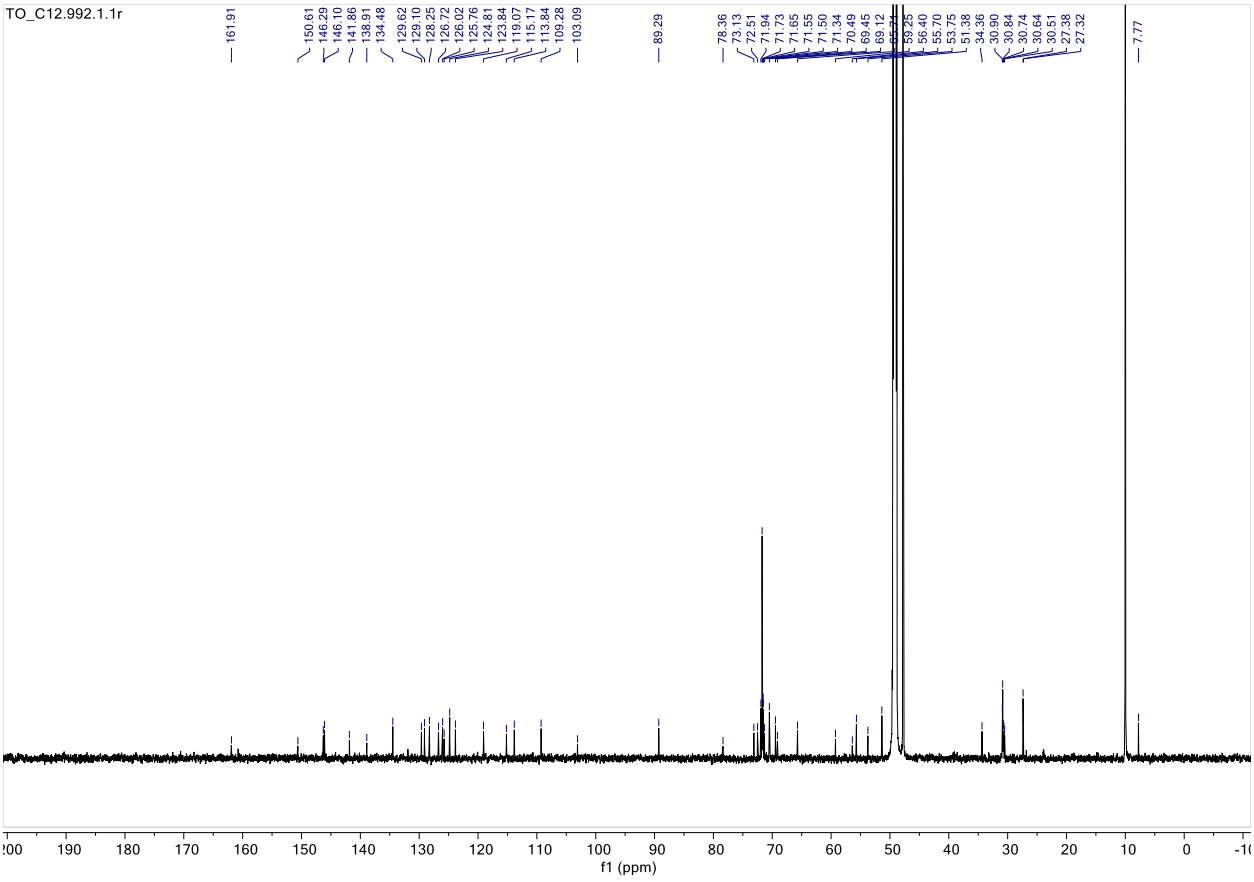
TO_C12.992.1.1r
161.91
150.61
146.29
146.10
141.86
138.91
134.48
129.62
129.10
128.25
126.72
126.02
125.76
124.81
123.84
119.07
115.17
113.84
109.28
103.09
89.29
78.36
73.13
72.51
71.94
71.73
71.65
71.55
71.50
71.34
70.49
69.45
69.12
59.25
56.40
55.70
53.75
51.38
34.36
30.90
30.84
30.74
30.64
30.51
27.38
27.32
7.77
190
180
170
160
150
140
130
120
110
100
90
80
70
60
50
40
30
20
10
0
f1 (ppm)

20. Citations

1 ChemAxon, *Marvin*, 2019.
2 K. Vanommeslaeghe, E. Hatcher, C. Acharya, S. Kundu, S. Zhong, J. Shim, E. Darian, O. Guvench, P. Lopes, I. Vorobyov and A. D. Mackerell, *J. Comput. Chem.*, 2010, **31**, 671–690.
3 W. Yu, X. He, K. Vanommeslaeghe and A. D. MacKerell, *J. Comput. Chem.*, 2012, **33**, 2451–2468.
4 K. Vanommeslaeghe and A. D. MacKerell, *J. Chem. Inf. Model.*, 2012, **52**, 3144–3154.
5 K. Vanommeslaeghe, E. P. Raman and A. D. MacKerell, *J. Chem. Inf. Model.*, 2012, **52**, 3155–3168.
6 N. M. O'Boyle, M. Banck, C. A. James, C. Morley, T. Vandermeersch and G. R. Hutchison, *J. Cheminformatics*, 2011, **3**, 33.
7 Schrödinger, LLC, *The PyMOL Molecular Graphics System*, 2019.
8 H. J. C. Berendsen, J. P. M. Postma, W. F. van Gunsteren, A. DiNola and J. R. Haak, *J. Chem. Phys.*, 1984, **81**, 3684–3690.
9 M. Parrinello and A. Rahman, *J. Appl. Phys*, 1981, **52**, 7182–7190.
10 W. Humphrey, A. Dalke and K. Schulten, *J. Mol. Graph.*, 1996, **14**, 33–38.
11 D. Vercauteren, R. E. Vandenbroucke, A. T. Jones, J. Rejman, J. Demeester, S. C. De Smedt, N. N. Sanders and K. Braeckmans, *Molecular Therapy*, 2010, **18**, 561–569.
12 G. J. Doherty and H. T. McMahon, *Annual Review of Biochemistry*, 2009, **78**, 857–902.
13 S. Cui, S. Zhang, H. Chen, B. Wang, Y. Zhao and D. Zhi, *ENG*, 2012, **04**, 172–175.
14 P. Lajoie and I. R. Nabi, *Journal of Cellular and Molecular Medicine*, 2007, **11**, 644–653.
15 J. ter Maat, R. Regeling, C. J. Ingham, C. A. G. M. Weijers, M. Giesbers, W. M. de Vos and H. Zuilhof, *Langmuir*, 2011, **27**, 13606–13617.